# N₂O isotopocule measurements using laser spectroscopy: analyzer characterization and intercomparison

Stephen J. Harris[1,2,*], Jesper Liisberg[3,*], Longlong Xia[4], Jing Wei[5], Kerstin Zeyer[5], Longfei Yu[5], Matti Barthel[6], Benjamin Wolf[4], Bryce F.J. Kelly[1], Dioni I. Cendón[2], Thomas Blunier[3], Johan Six[6], Joachim Mohn[5]

[1]School of Biological, Earth and Environmental Sciences, UNSW Sydney, NSW, Australia
[2]Australian Nuclear Science and Technology Organisation, Lucas Heights, NSW, Australia
[3]University of Copenhagen, Niels Bohr Institute, Copenhagen, Denmark
[4]Karlsruhe Institute of Technology, IMK-IFU, Garmisch-Partenkirchen, Germany
[5]Empa, Laboratory for Air Pollution/Environmental Technology, Dübendorf, Switzerland
[6]ETH Zürich, Department of Environmental Systems Science, Zürich, Switzerland

*Correspondence to*: Stephen J. Harris (s.j.harris@unsw.edu.au)
* These authors contributed equally to this work

**Abstract.** For the past two decades, the measurement of N₂O isotopocules – isotopically substituted molecules $^{14}N^{15}N^{16}O$, $^{15}N^{14}N^{16}O$ and $^{14}N^{14}N^{18}O$ of the main isotopic species $^{14}N^{14}N^{16}O$ – has been a promising technique for understanding N₂O production and consumption pathways. The coupling of non-cryogenic and tuneable light sources with different detection schemes, such as direct absorption quantum cascade laser absorption spectroscopy (QCLAS), cavity ring-down spectroscopy (CRDS) and off-axis integrated cavity output spectroscopy (OA-ICOS), has enabled the production of commercially-available and field-deployable N₂O isotopic analyzers. In contrast to traditional isotope-ratio mass-spectrometry (IRMS), these instruments are inherently selective for position-specific $^{15}N$ substitution and provide real-time data, with minimal or no sample pretreatment, which is highly attractive for process studies.

Here, we compared the performance of N₂O isotope laser spectrometers with the three most common detection schemes: OA-ICOS (N₂OIA-30e-EP, ABB-Los Gatos Research Inc.), CRDS (G5131-i, Picarro Inc.) and QCLAS (dual QCLAS and preconcentration (TREX)–mini QCLAS, Aerodyne Research Inc.). For each instrument, the precision, drift and repeatability of N₂O mole fraction [N₂O]

and isotope data were tested. The analyzers were then characterized for their dependence on [$N_2O$], gas matrix composition ($O_2$, Ar) and spectral interferences caused by $H_2O$, $CO_2$, $CH_4$ and CO to develop analyzer-specific correction functions. Subsequently, a simulated two end-member mixing experiment was used to compare the accuracy and repeatability of corrected and calibrated isotope measurements that could be acquired using the different laser spectrometers.

Our results show that $N_2O$ isotope laser spectrometer performance is governed by an interplay between instrumental precision, drift, matrix effects and spectral interferences. To retrieve compatible and accurate results, it is necessary to include appropriate reference materials following the identical treatment (IT) principle during every measurement. Remaining differences between sample and reference gas compositions have to be corrected by applying analyzer-specific correction algorithms. These matrix and trace gas correction equations vary considerably according to $N_2O$ mole fraction, complicating the procedure further. Thus, researchers should strive to minimize differences in composition between sample and reference gases. In closing, we provide a calibration workflow to guide researchers in the operation of $N_2O$ isotope laser spectrometers in order to acquire accurate $N_2O$ isotope analyses. We anticipate that this workflow will assist in applications where matrix and trace gas compositions vary considerably (e.g. laboratory incubations, $N_2O$ liberated from wastewater or groundwater), as well as extending to future analyzer models and instruments focusing on isotopic species of other molecules.

## 1 Introduction

Nitrous oxide ($N_2O$) is a long-lived greenhouse gas with a 100-year global warming potential nearly 300 times that of carbon dioxide ($CO_2$; Forster et al., 2007), and is the largest emission source of ozone-depleting nitrogen oxides in the stratosphere (Ravishankara et al., 2009). In 2019, the globally averaged [$N_2O$] reached approximately 332 ppb compared to the pre-industrial level of 270 ppb (NOAA/ESRL, 2019). While this increase is known to be linked primarily to increased fertilizer use in agriculture (Bouwman et al., 2002; Mosier et al., 1998; Tian et al., 2015), understanding the underlying microbial

processes producing and consuming $N_2O$ has proved more challenging, and individual source contributions from sectors such as agricultural soils, wastewater management and biomass burning to global bottom-up estimates of $N_2O$ emissions have large uncertainties (Denman et al., 2007). Stable isotopes are an effective tool for distinguishing $N_2O$ sources and determining production pathways, which is critical for developing appropriate mitigation strategies (Baggs, 2008; Ostrom and Ostrom, 2011; Toyoda et al., 2017).

The $N_2O$ molecule has an asymmetric linear structure (NNO), with the following most abundant isotopocules: $^{14}N^{15}N^{16}O$ ($^{15}N^\alpha$-$N_2O$); $^{15}N^{14}N^{16}O$ ($^{15}N^\beta$-$N_2O$); $^{14}N^{14}N^{18}O$ ($^{18}O$-$N_2O$); and $^{14}N^{14}N^{16}O$ (Yoshida and Toyoda, 2000). The terms $^{15}N^\alpha$ and $^{15}N^\beta$ refer to the respective central and terminal positions of nitrogen (N) atoms in the NNO molecule (Toyoda and Yoshida, 1999). Isotopic abundances are reported in δ-notation, where $\delta^{15}N = R(^{15}N/^{14}N)_{sample} / R(^{15}N/^{14}N)_{reference} - 1$ denotes the relative difference in per mil (‰) of the sample versus atmospheric $N_2$ (AIR-$N_2$). The isotope ratio $R(^{15}N/^{14}N)$ equals $x(^{15}N)/x(^{14}N)$, with x being the absolute abundance of $^{14}N$ and $^{15}N$, respectively. Similarly, Vienna Standard Mean Ocean Water (VSMOW) is the international isotope ratio scale for $\delta^{18}O$. In practice, the isotope δ value is calculated from measurement of isotopocule ratios of sample and reference gases, with the latter being defined on the AIR-$N_2$ and VSMOW scales. By extension, $\delta^{15}N^\alpha$ denotes the corresponding relative difference of isotope ratios for $^{14}N^{15}N^{16}O/^{14}N^{14}N^{16}O$, and $\delta^{15}N^\beta$ for $^{15}N^{14}N^{16}O/^{14}N^{14}N^{16}O$. The site-specific intramolecular distribution of $^{15}N$ within the $N_2O$ molecule is termed $^{15}N$-site preference (SP), and is defined as: $SP = \delta^{15}N^\alpha - \delta^{15}N^\beta$ (Yoshida and Toyoda, 2000). The term $\delta^{15}N^{bulk}$ is used to express the average $\delta^{15}N$ value, and is equivalent to $\delta^{15}N^{bulk} = (\delta^{15}N^\alpha + \delta^{15}N^\beta)/2$.

Extensive evidence has shown that SP, $\delta^{15}N^{bulk}$ and $\delta^{18}O$ can be used to differentiate $N_2O$ source processes and biogeochemical cycling (Decock and Six, 2013; Denk et al., 2017; Heil et al., 2014; Lewicka-Szczebak et al., 2014, 2015; Ostrom et al., 2007; Sutka et al., 2003, 2006; Toyoda et al., 2005, 2017; Wei et al., 2017). Isotopocule abundances have been measured in a wide range of environments, including the troposphere (Harris et al., 2014a; Röckmann and Levin, 2005; Toyoda et al., 2013), agricultural soils (Buchen et al., 2018; Ibraim et al., 2019; Köster et al., 2011; Mohn et al., 2012;

Ostrom et al., 2007; Park et al., 2011; Pérez et al., 2001, 2006; Toyoda et al., 2011; Verhoeven et al., 2018, 2019; Well et al., 2008, 2009; Wolf et al., 2015), mixed urban-agricultural environments (Harris et al., 2017), coal and waste combustion (Harris et al., 2014b; Ogawa and Yoshida, 2005), fossil fuel combustion (Toyoda et al., 2008), wastewater treatment (Harris et al., 2015a, b; Wunderlin et al., 2012,

5    2013), groundwater (Koba et al., 2009; Minamikawa et al., 2011; Nikolenko et al., 2019; Well et al., 2005, 2012), estuaries (Erler et al., 2015), mangrove forests (Murray et al., 2018), stratified water impounds (Yue et al., 2018), and firn air and ice cores (Bernard et al., 2006; Ishijima et al., 2007; Prokopiou et al., 2017). While some applications like laboratory incubation experiments allow for analysis of the isotopic signature of the pure source, most studies require analysis of the source diluted

10    in ambient air. This specifically applies to terrestrial ecosystem research, since $N_2O$ emitted from soils is immediately mixed with background atmospheric $N_2O$. To understand the importance of soil emissions for the global $N_2O$ budget, two end-member mixing models commonly interpreted using Keeling or Miller-Tans plots are frequently used to back-calculate the isotopic composition of $N_2O$ emitted from soils (Keeling, 1958; Miller and Tans, 2003).

$N_2O$ isotopocules can be analyzed by isotope-ratio mass spectrometry (IRMS) and mid-infrared (MIR) laser spectroscopic techniques. IRMS analysis of the $N_2O$ intramolecular $^{15}N$ distribution is based on quantification of the fragmented ($NO^+$, *m/z* 30 and 31) and molecular ($N_2O^+$, *m/z* 44, 45 and 46) ions to calculate isotope ratios for the entire molecule ($^{15}N/^{14}N$ and $^{18}O/^{16}O$) and the central ($N^\alpha$) and terminal

20    ($N^\beta$) N atom (Toyoda and Yoshida, 1999). The analysis of $N_2O$ SP by IRMS is complicated by the rearrangement of $N^\alpha$ and $N^\beta$ in the ion source, while analysis of $\delta^{15}N^{bulk}$ (45/44) involves correction for $NN^{17}O$ (mass 45). IRMS can achieve repeatability as good as 0.1 ‰ for $\delta^{15}N$, $\delta^{18}O$, $\delta^{15}N^\alpha$ and $\delta^{15}N^\beta$ (Potter et al., 2013; Röckmann and Levin, 2005), but an inter-laboratory comparison study showed substantial deviations in measurements of $N_2O$ isotopic composition, in particular for SP (up to

25    10 ‰) (Mohn et al., 2014). The advancement of mid-infrared laser spectroscopic techniques was enabled by the invention and availability of non-cryogenic light sources which have been coupled with different detection schemes such as direct absorption quantum cascade laser absorption spectroscopy (QCLAS; Aerodyne Research Inc. [ARI]; Wächter et al., 2008), cavity ring-down spectroscopy (CRDS;

Picarro Inc.) and off-axis integrated-cavity-output spectroscopy (OA-ICOS; ABB Los Gatos Research Inc.; Baer et al., 2002) to realize compact field-deployable analyzers. These instruments can analyze the $N_2O$ isotopic composition in gaseous mixtures (e.g. ambient air) in a flow-through mode, providing real-time data with minimal or no sample pretreatment, which is highly attractive to better resolve the

5   temporal complexity of $N_2O$ production and consumption processes (Decock and Six, 2013; Heil et al., 2014; Köster et al., 2013; Winther et al., 2018). Most importantly, MIR laser spectroscopy is selective for $^{17}O$, $^{18}O$ and position-specific $^{15}N$ substitution due to the existence of characteristic rotational-vibrational spectra (Rothman et al., 2005).

10   Despite the described inherent benefits of laser spectroscopy for $N_2O$ isotope analysis, applications remain challenging and are still scarce for four main reasons:

(1) two pure $N_2O$ isotopocule reference materials (USGS51, USGS52) have only recently been made available through the United States Geological Survey (USGS) with provisional values assigned by Tokyo Institute of Technology (Ostrom et al., 2018). The lack of $N_2O$ isotopocule reference materials

15   was identified as a major reason limiting inter-laboratory compatibility (Mohn et al., 2014);

(2) laser spectrometers are subject to drift effects, in particular under fluctuating environmental conditions, limiting their performance (Werle et al., 1993);

(3) changes in [$N_2O$] affect $N_2O$ isotope results when using the calibration approach (Griffith, 2018); and

20   (4) laser spectroscopic results are affected by mole fraction changes of atmospheric background gases ($N_2$, $O_2$, and Ar), herein called gas matrix effects, due to the difference of pressure-broadening coefficients (Nara et al., 2012), and potentially by spectral interferences from other atmospheric constituents ($H_2O$, $CO_2$, $CH_4$, CO, etc.), herein called trace gas effects, depending on the selected wavelength region. The latter is particularly pronounced for $N_2O$ due to its low atmospheric abundance

25   in comparison to other trace gases.

Several studies have described some of the above effects for $CO_2$ (Bowling et al., 2003, 2005; Griffis et al., 2004; Griffith et al., 2012; Friedrichs et al., 2010; Malowany et al., 2015; Pataki et al., 2006; Pang et

al., 2016; Rella et al., 2013; Vogel et al., 2013; Wen et al. 2013), $CH_4$ (Eyer et al., 2016; Griffith et al., 2012; Rella et al., 2013), and recently $N_2O$ isotope laser spectrometers (Erler et al., 2015; Harris et al., 2014; Ibraim et al., 2018; Wächter et al., 2008). However, a comprehensive and comparative characterization of the above effects for commercially-available $N_2O$ isotope analyzers is lacking.

Here, we present an intercomparison study of commercially-available $N_2O$ isotope laser spectrometers with the three most common detection schemes: (1) OA-ICOS ($N_2$OIA-30e-EP, ABB-Los Gatos Research Inc.); (2) CRDS (G5131-i, Picarro Inc.); (3) QCLAS (dual QCLAS and TREX–mini QCLAS, ARI). Performance characteristics including precision, repeatability, drift and dependence of isotope measurements on [$N_2O$] were determined. Instruments were tested for gas matrix effects ($O_2$, Ar) and spectral interferences from enhanced trace gas mole fractions ($CO_2$, $CH_4$, CO, $H_2O$) at various [$N_2O$] to develop analyzer-specific correction functions. The accuracy of different spectrometer designs was then assessed during a laboratory-controlled mixing experiment designed to simulate two end-member mixing, in which results were compared to calculated expected values, as well as to those acquired using IRMS ($\delta$ values) and gas chromatography (GC, $N_2O$ concentration). In closing, we provide a calibration workflow that will assist researchers in the operation of $N_2O$ and other trace gas isotope laser spectrometers in order to acquire accurate isotope analyses.

## 2 Materials and Methods

### 2.1 Analytical techniques

20 Operational details of the laser spectrometers tested in this study, including wavenumber regions, line positions and line strengths of $N_2O$, are provided in Table 1. In Fig. 1, selected $N_2O$ rotational lines are shown in combination with the absorption lines of the atmospheric most abundant IR-active trace gases ($H_2O$, $CO_2$, $CH_4$, CO and $O_3$) within the different wavenumber regions used by the analyzers. Fig. 1 can be used to rationalize possible spectral interferences within different wavenumber regions.

**Table 1.** Overview on the wavelength regions, line positions and line strengths of $N_2O$ isotopocules, and key operating parameters for each laser spectrometer tested in this study.

| Detection scheme (model; manufacturer) | $N_2O$ range [ppb] | Wavenumber region (cm⁻¹) | Isotopocules | Line positions (cm⁻¹) / Line strength [cm⁻¹/(molecule cm⁻²)] | Flow rate (cm³ min⁻¹) | Cell temperature (°C) | Cell pressure (hPa) | Internal plumbing volume (cm³) | Effective volume at NTP (cm³) | Measurement frequency (seconds) | References |
|---|---|---|---|---|---|---|---|---|---|---|---|
| OA-ICOS I (N₂OIA-30e-EP; ABB Los Gatos Research Inc.) | 300 – 100000 | 2192.1 – 2192.5 | $^{14}N^{14}N^{16}O$<br><br>$^{14}N^{15}N^{16}O$<br>$^{15}N^{14}N^{16}O$<br>$^{14}N^{14}N^{18}O$ | 2192.40 / $4.919\cdot10^{-20}$<br>2192.44 / $4.919\cdot10^{-20}$<br>2192.48 / $3.375\cdot10^{-19}$<br>2192.31 / $3.31\cdot10^{-21}$<br>2192.33 / $2.968\cdot10^{-21}$<br>2192.13 / $1.113\cdot10^{-21}$ | 60 | 43.6 | 61 | 930 | 60.50 | 1.00 | Baer et al. (2002) ABB-Los Gatos Research Inc. (2019) |
| CRDS I & II (G5131-i; Picarro Inc.) | 300 – 1500 | 2195.7 – 2196.3 | $^{14}N^{14}N^{16}O$<br><br>$^{14}N^{15}N^{16}O$<br>$^{15}N^{14}N^{16}O$<br>$^{14}N^{14}N^{18}O$ | 2196.21 / $5.161\cdot10^{-20}$<br>2196.24 / $5.161\cdot10^{-20}$<br>2195.76 / $2.734\cdot10^{-21}$<br>2195.80 / $2.197\cdot10^{-21}$<br>2195.95 / $1.431\cdot10^{-21}$ | 25.2 (CRDS I) 12.5 (CRDS II) | 40.2 | 100 | 40 | 4.22 | 3.41 (CRDS I) 2.54 (CRDS II) | Picarro Inc. (2019) |
| QCLAS I, II & III (CW-QC-TILDAS-SC-D; Aerodyne Research Inc.) | 300 – 90000 | 2187.7 – 2188.15 and 2203.1 – 2203.4 | $^{14}N^{14}N^{16}O$<br>$^{14}N^{15}N^{16}O$<br>$^{15}N^{14}N^{16}O$<br>$^{14}N^{14}N^{18}O$ | 2188.04 / $2.601\cdot10^{-21}$<br>2187.94 / $3.294\cdot10^{-21}$<br>2187.85 / $3.274\cdot10^{-21}$<br>2203.28 / $1.794\cdot10^{-21}$ | 130[a] | 20[a] | 53.3[a] | 2100 | 104[a] | 1.00[a] | Nelson (2008) Wächter et al. (2008) |
| TREX-QCLAS I (Modified CW-QC-TILDAS-76-CS; Aerodyne Research Inc.) | 300 – 1500[a,b] | 2203.1 – 2203.4[a] | $^{14}N^{14}N^{16}O$<br><br>$^{14}N^{15}N^{16}O$<br>$^{15}N^{14}N^{16}O$<br>$^{14}N^{14}N^{18}O$ | 2203.10 / $2.710\cdot10^{-21}$<br>2203.11 / $1.435\cdot10^{-21}$<br>2203.36 / $9.798\cdot10^{-22}$<br>2203.20 / $7.016\cdot10^{-22}$<br>2203.28 / $1.794\cdot10^{-21}$ | -[b] | 20[a] | 35.6[a] | 620 | 20[a] | 1.00[a] | Ibraim et al. (2018) |

[a] Dual QC-TILDAS and mini QC-TILDAS are flexible spectrometer platforms, which can be used with different parameter settings. The indicated numbers were chosen for the described experiments.

[b] The mini QC-TILDAS spectrometer is used in combination with a preconcentration device (Ibraim et al., 2018), the indicated $N_2O$ concentration range is prior to preconcentration.

[c] The preconcentration – mini QC-TILDAS system is used in a repetitive batch cycle without a continuous sample gas flow (Ibraim et al., 2018, 2019).
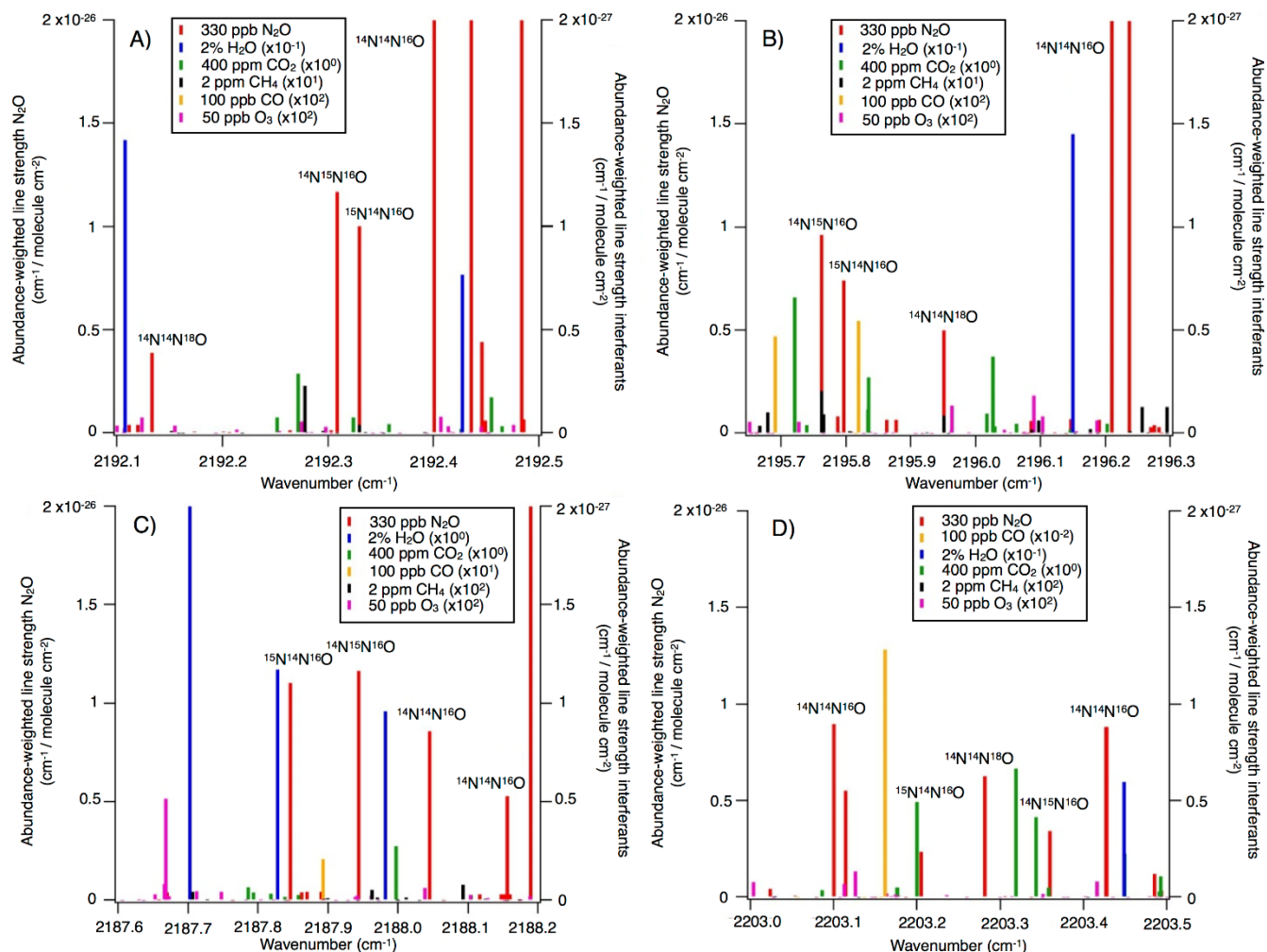
**Fig. 1.** N₂O isotopocule absorption line positions in the wavenumber regions selected for A) OA-ICOS; B) CRDS; and C & D) QCLAS techniques. Regions of possible spectral overlap from interfering trace gases such as $H_2O$, $CO_2$, $CH_4$ and CO are shown.

### 2.1.1 OA-ICOS (ABB-Los Gatos Research Inc.)

The N₂OIA-30e-EP (model 914-0027, ABB-Los Gatos Research Inc., USA) tested in this study was provided by the University of New South Wales (UNSW Sydney, Australia), and is herein referred to as OA-ICOS I (Table 1). The instrument employs the OA-ICOS technique integrated with a QCL (Baer et al., 2002). In short, the QCL beam is directed off axis into the cavity cell with highly-reflective mirrors, providing an optical path of several kilometers. For further details on the OA-ICOS technique, the

reader is referred to the webpage of ABB-Los Gatos Research Inc. (ABB-Los Gatos Research Inc., 2019).

The specific analyzer tested here was manufactured in June 2014, and has had no hardware
5    modifications since then. It is also important to note that a more recent $N_2OIA$-30e-EP model (model 914-0060) is available, that in addition quantifies $\delta^{17}O$. We are unaware of any study measuring $N_2O$ isotopocules at natural abundance and ambient mole fractions with the $N_2OIA$-30e-EP. The only studies published so far reporting $N_2O$ isotope data apply the $N_2OIA$-30e-EP either at elevated $[N_2O]$ in a standardized gas matrix or using $^{15}N$ labelling, including Soto et al. (2015), Li et al. (2016), Kong et al.
10   (2017), Brase et al. (2017), Wassenaar et al. (2018) and Nikolenko et al. (2019).

### 2.1.2 CRDS (Picarro Inc.)

Two G5131-i analyzers (Picarro Inc., USA) were used in this study: a 2015 model (referred to as CRDS I, delivered September 2015) provided by the Niels Bohr Institute, University of Copenhagen, Denmark; and a 2018 model (referred to as CRDS II, delivered June 2018) provided by Karlsruhe
15   Institute of Technology, Germany (Table 1). In CRDS, the beam of a single-frequency continuous wave (cw) laser diode enters a three-mirror cavity with an effective pathlength of several km to support a continuous traveling light wave. A photodetector measures the decay of light in the cavity after the cw laser diode is shut off to retrieve the mole fraction of $N_2O$ isotopocules. For more details we refer the reader to the webpage of Picarro Inc. (Picarro Inc., 2019).

Importantly, the manufacturer-installed flow-restrictors were replaced in both analyzer models, as we noted reduced flow rates due to clogging during initial reconnaissance testing. In CRDS I, a capillary (inner diameter (ID): 150 μm, length: 81 mm, flow: 25.2 $cm^3$ $min^{-1}$) was installed, while CRDS II was equipped with a critical orifice (ID: 75 μm, flow: 12.5 $cm^3$ $min^{-1}$). Both restrictors were tested and
25   confirmed leak-proof. Both analyzers had manufacturer-installed permeation driers located prior to the inlet of the cavity, which were not altered for this study. In December 2017, CRDS I received a

software and hardware update as per the manufacturer's recommendations. The CRDS II did not receive any software or hardware upgrades as it was acquired immediately prior to testing.

To the best of our knowledge, the work presented in Lee et al. (2017) and Ji and Grundle (2019) are the only published uses of G5131-i models. A prior model (the G5101-i), which employs a different spectral region and does not offer the capability for $\delta^{18}O$ was used by Peng et al. (2014), Erler et al. (2015), Li et al. (2015), Lebegue et al. (2016) and Winther et al. (2018).

### 2.1.3 QCLAS (Aerodyne Research Inc.)

Three QCLAS instruments (ARI, USA; CW-QC-TILDAS-SC-D) were used in this study. One instrument (QCLAS I), purchased in 2013, was provided by Karlsruhe Institute of Technology, Germany and two instruments, purchased in 2014 (QCLAS II) and 2016 (QCLAS III), were supplied by ETH Zürich, Switzerland (Table 1).

All instruments were dual QCL spectrometers, equipped with mirror optics guiding the two laser beams through an optical anchor point to assure precise coincidence of the beams at the detector. On the way to the detector, the laser beams are coupled into an astigmatic multipass cell with a volume of approx. 2100 cm³ in which the beams interact with the sample air. The multiple passes through the absorption cell result in an absorption path length of approx. 204 m. The cell pressure can be selected by the user and was set to 53.3 mbar as a trade-off between line separation and sensitivity. This set point is automatically maintained by the TDLWintel software (Version 1.14.89 ARI, MA, USA), which compensates for variations in vacuum pump speed by closing or opening a throttle valve at the outlet of the absorption cell.

QCLAS instruments offer great liberty to the user as the system can also be operated with different parameter settings, e.g. selection of spectral lines for quantification, wavenumber calibration, sample flow rate, pressure etc. Thereby different applications can be realized, from high flow eddy covariance studies or high mole fraction process studies to high-precision measurements coupled to a customized

inlet system. QCLAS I was operated as a single laser instrument using laser one, to optimize spectral resolution of the frequency sweeps. It is important to note the mixing ratios returned by the instrument are solely based on fundamental spectroscopic constants (Rothman et al., 2005), so that corrections such as the dependence of isotope ratios on [$N_2O$] have to be implemented by the user in the post processing.

To our knowledge, QCLAS instruments have so far predominately been used for determination of $N_2O$ isotopic composition in combination with preconcentration (see below) or at enhanced mole fractions (Harris et al., 2015; Heil et al. 2014; Köster et al., 2013), except for Yamamoto et al. (2014) who had used a QCLAS (CW-QC-TILDAS-SC-S-N2OISO; ARI, USA) with one laser (2189 cm$^{-1}$) in

10  combination with a closed chamber system. Spectrometer raw data were corrected for drift applying a reference gas every hour and dependence on [$N_2O$].

### 2.1.4 TREX-QCLAS

A compact mini QCLAS device (CW-QC-TILDAS-76-CS; ARI, USA) coupled with a preconcentration system, called trace gas extractor (TREX) was provided by Empa, Switzerland. The spectrometer

15  comprises a continuous-wave mid-infrared quantum cascade laser source emitting at 2203 cm$^{-1}$ and an astigmatic multipass absorption cell with a path length of 76 m and a volume of approximately 620 cm$^3$ (Ibraim et al., 2018) (Table 1). The TREX unit was designed and manufactured at Empa and is used to separate the $N_2O$ from the sample gas prior to QCLAS analysis. Thereby, the initial [$N_2O$] is increased by a factor of 200 – 300, other trace gases are removed and the gas matrix is set to standardized

20  conditions. Before entering the TREX device, CO is oxidized to $CO_2$ using a metal catalyst (Sofnocat 423, Molecular Products Limited, GB). Water and $CO_2$ in sample gases were removed by a permeation dryer (PermaPure Inc., USA) in combination with a sodium hydroxide (NaOH) / magnesium perchlorate ($Mg(ClO_4)_2$) trap (Ascarite: 6 g, 10–35 mesh, Sigma Aldrich, Switzerland, bracketed by $Mg(ClO_4)_2$, $2 \times 1.5$ g, Alfa Aesar, Germany). Thereafter, $N_2O$ is adsorbed on a HayeSepD (Sigma

25  Aldrich, Switzerland) filled trap, cooled down to $125.1 \pm 0.1$ K by attaching it to a copper baseplate mounted on a high-power Stirling cryo-cooler (CryoTel GT, Sunpower Inc., USA). $N_2O$ adsorption requires $5.080 \pm 0.011$ L of gas to have passed through the adsorption trap. For $N_2O$ desorption, the trap

is decoupled from the copper baseplate, while slowly heating it to 275 K with a heat foil (diameter 62.2 mm, 100 W, HK5549, Minco Products Inc., USA). Desorbed $N_2O$ is purged with 1–5 $cm^3$ $min^{-1}$ of synthetic air into the QCLAS cell for analysis. By controlling the flow rate and trapping time, the $[N_2O]$ in the QCLAS cell can be adjusted to 60–80 ppm at a cell pressure of 35.6 ± 0.04 mbar. A custom-written LabVIEW program (Version 18.0.1, National Instruments Corp., USA) allows remote control and automatic operation of the TREX. So far, the TREX-QLCAS system has been successfully applied to determine $N_2O$ emission, as well as $N_2O$ isotopic signatures from various ecosystems (e.g. Mohn et al., 2012; Harris et al., 2014; Wolf et al., 2015; Ibraim et al., 2019).

### 2.1.5 GC-IRMS

IRMS analyses were conducted at ETH Zürich using a gas preparation unit (Trace Gas, Elementar, Manchester, UK) coupled to an IsoPrime100 IRMS (Elementar, Manchester, UK). $[N_2O]$ analysis using gas chromatography was also performed at ETH Zürich (456-GC, Scion Instruments, Livingston, UK). GC-IRMS analyses were conducted as part of experiments described further in Section 2.4.8. Further analytical details are provided in Supplementary Material 1.

## 2.2 Sample and reference gases

### 2.2.1 Matrix and interference test gases

Table 2 provides $O_2$, Ar and trace gas mole fractions of matrix gases and interference test gases used during testing. The four matrix gases comprised: synthetic air (matrix a, Messer Schweiz AG, Switzerland); synthetic air with Ar (matrix b, Carbagas AG, Switzerland); synthetic air with Ar, $CO_2$, $CH_4$ and CO at near-ambient mole fractions (matrix c, Carbagas AG, Switzerland); and high purity nitrogen gas ($N_2$, Messer Schweiz AG, Switzerland). Matrix gases were analyzed in the WMO GAW World Calibration Center at Empa (WCC Empa) for $CO_2$, $CH_4$, $H_2O$ (G1301, Picarro Inc., USA), and $N_2O$ and CO (CW-QC-TILDAS-76-CS; ARI, USA) against standards of the National Oceanic and Atmospheric Administration/Earth System Research Laboratory/Global Monitoring Division (NOAA/ESRL/GMD). The $[N_2O]$ in all matrix gases and $N_2$ were below 0.3 ppb. The three gas

mixtures used for testing of spectral interferences contained higher mole fractions of either $CO_2$, $CH_4$ or CO in matrix gas b (Carbagas AG, Switzerland), which prevented spectroscopic analysis of other trace substances.

**Table 2.** $O_2$, Ar content and trace gas concentrations for matrix and interference test gases. Trace gas concentrations of matrix gases were analyzed by WMO GAW WCC Empa against standards of the NOAA/ESRL/GMD. For trace gas concentrations of interference test gases manufacturer specifications are given. Reported $O_2$ and Ar contents are according to manufacturer specifications. The given uncertainty is the uncertainty stated by the manufacturer or the standard deviation for analysis of n cylinders of the same specification.

| Gas | Abbreviation | $O_2$ [a) [%] | Ar [a) [%] | $CO_2$ [b) [ppm] | $CH_4$ [b) [ppb] | CO [b) [ppb] | $N_2O$ [b) [ppb] | n |
|---|---|---|---|---|---|---|---|---|
| Matrix gases | | | | | | | | |
| Synthetic air | matrix a | 20.5±0.5 | - | < 1 | < 25 | < 200 | < 0.25 | 4 |
| Synthetic air + Ar | matrix b | 20.95±0.2 | 0.95±0.01 | < 0.5 | < 15 | < 150 | < 0.15 | 3 |
| Synthetic air + Ar +$CO_2$ + $CH_4$ + CO | matrix c | 20.95±0.4 | 0.95±0.02 | 397±3 | 2004±20 | 195±3 | < 0.15 | 9 |
| Nitrogen (6.0) | $N_2$ | < 0.00003 | < 0.0001 | < 0.2 | < 1 | < 1 | < 0.05 | 2 |
| | | $O_2$ [a) [%] | Ar [a) [%] | $CO_2$ [a) [%] | $CH_4$ [a) [ppm] | CO [a) [ppm] | $N_2O$ [a) [ppb] | n |
| Interference test gases | | | | | | | | |
| $CO_2$ in synthetic air + Ar | $CO_2$ in matrix b | 21.06±0.2 | 0.94±0.01 | 4.02±0.04 | n.a. | n.a. | n.a. | - |
| $CH_4$ in synthetic air + Ar | $CH_4$ in matrix b | 20.79±0.4 | 0.96±0.02 | n.a. | 199±4 | n.a. | n.a. | - |
| CO in synthetic air + Ar | CO in matrix b | 20.95±0.4 | 0.95±0.02 | n.a. | n.a. | 20.6±0.4 | n.a. | - |

[a) manufacturer specifications
[b) analyzed at WMO GAW WCC Empa
n.a. not analyzed due to very high concentration of one trace substance, which affects spectroscopic analysis of other species

### 2.2.2 Reference gases (S1, S2) and pressurized air (PA1, PA2)

Preparation of pure and diluted reference gases

Two reference gases (S1, S2) with different $N_2O$ isotopic composition were used in this study. Pure $N_2O$ reference gases were produced from high purity $N_2O$ (Linde, Germany) decanted into evacuated Luxfer aluminum cylinders (S1: P3333N, S2: P3338N) with ROTAREX valves (Matar, Italy) to a final pressure of maximum 45 bar to avoid condensation. Reference gas 1 (S1) was high purity $N_2O$ only. For reference gas 2 (S2), high purity $N_2O$ was supplemented with defined amounts of isotopically pure (>98%) $^{14}N^{15}NO$ (NLM-1045-PK), $^{15}N^{14}NO$ (NLM-1044-PK) (Cambridge Isotope Laboratories, USA)

and $NN^{18}O$ using a ten-port two-position valve (EH2C10WEPH with 20 mL sample loop, Valco Instruments Inc., Switzerland). Since $NN^{18}O$ was not commercially available, it was synthesized using the following procedure: (1) $^{18}O$ exchange of $HNO_3$ (1.8 mL, Sigma Aldrich) with 97% $H_2^{18}O$ (5 mL, Medical Isotopes Inc.) under reflux for 24 hours; (2) condensation of $NH_3$ and reaction controlled by $LN_2$; and (3) thermal decomposition of $NH_4NO_3$ in batches of 1 g in 150 mL glass bulbs with breakseal (Glasbläserei Möller AG, Switzerland) to produce $NN^{18}O$. The isotopic enrichment was analyzed after dilution in $N_2$ (99.9999 %, Messer Schweiz AG) with a Vision 1000C quadrupole mass spectrometer (QMS) equipped with a customized ambient pressure inlet (MKS Instruments, UK). Triplicate analysis provided the following composition: $36.25 \pm 0.10$ % of $NN^{16}O$ and $63.75 \pm 0.76$ % of $NN^{18}O$.

High [$N_2O$] reference gases (S1-a$_{90ppm}$, S1-b$_{90ppm}$, S1-c$_{90ppm}$, S2-a$_{90ppm}$) with a target mole fraction of 90 ppm were prepared in different matrix gases (a, b, c) using a two-step procedure. First, defined volumes of S1 and S2 were dosed into Luxfer aluminum cylinders (ROTAREX valve, Matar, Italy) filled with matrix gas (a, b and c) to ambient pressure using $N_2O$ calibrated MFCs (Vögtlin Instruments GmbH, Switzerland). Second, the $N_2O$ was gravimetrically diluted (ICS429, Mettler Toledo GmbH, Switzerland) with matrix gas to the target mole fraction. Ambient [$N_2O$] reference gases (S1-c$_{330ppb}$, S2-c$_{330ppb}$) with a target mole fraction of 330 ppb were prepared by dosing S1-c$_{90ppm}$ or S2-c$_{90ppm}$ into evacuated cylinders with a calibrated MFC, followed by gravimetric dilution with matrix c.

Analysis of reference gases and pressurized air

Table 3 details the trace gas mole fractions and $N_2O$ isotopic composition of high and ambient [$N_2O$] reference gases, as well as commercial pressurized air (PA1 and PA2) used during testing. Trace gas mole fractions of high [$N_2O$] reference gases were acquired from the trace gas levels in the respective matrix gases (Table 2), while ambient [$N_2O$] reference gases and target as well as background gases were analyzed by WCC Empa. The isotopic composition of high [$N_2O$] isotope reference gases in synthetic air (S1-a$_{90ppm}$, S2-a$_{90ppm}$) was analyzed in relation to $N_2O$ isotope standards (for S1-a$_{90ppm}$: Cal1 and Cal2; for S2-a$_{90ppm}$: Cal3 and Cal2) in an identical gas matrix (matrix a) by laser spectroscopy (CW-QC-TILDAS-200; ARI, Billerica, USA). The applied standards (Cal1–3) have previously been

measured by Sakae Toyoda at Tokyo Institute of Technology: Cal1 ($\delta^{15}N^{\alpha} = 2.06 \pm 0.05$ ‰, $\delta^{15}N^{\beta} = 1.98 \pm 0.20$ ‰, $\delta^{18}O = 36.12 \pm 0.32$ ‰); Cal2 ($\delta^{15}N^{\alpha} = -48.59 \pm 0.25$ ‰, $\delta^{15}N^{\beta} = -46.11 \pm 0.43$ ‰, $\delta^{18}O = 27.37 \pm 0.11$ ‰); and Cal3 ($\delta^{15}N^{\alpha} = 25.73 \pm 0.24$ ‰, $\delta^{15}N^{\beta} = 25.44 \pm 0.36$ ‰, $\delta^{18}O = 35.86 \pm 0.22$ ‰).

**Table 3.** Trace gas concentrations and $N_2O$ isotopic composition of high and ambient $N_2O$ concentration reference gases, and pressurized air. Trace gas concentrations of high concentration reference gases were retrieved from the composition of matrix gases used for their production (see Table 1), trace gas concentrations in ambient concentration reference gases and pressurized air were analyzed by WMO GAW WCC Empa against standards of the NOAA/ESRL/GMD. The $N_2O$ isotopic composition was quantified by laser spectroscopy (QCLAS) and preconcentration - laser spectroscopy (TREX-QCLAS) against reference gases previously analyzed by Tokyo Institute of Technology.

| Gas | $CO_2$ [ppm] | $CH_4$ [ppb] | CO [ppb] | $N_2O$ [ppb] | $\delta^{15}N^{\alpha}$ vs AIR-$N_2$ [‰] | $\delta^{15}N^{\beta}$ vs AIR-$N_2$ [‰] | $\delta^{18}O$ vs VSMOW [‰] |
|---|---|---|---|---|---|---|---|
| High $N_2O$ concentration reference gases | | | | | | | |
| S1-a$_{90ppm}$ | < 1 | < 25 | < 200 | ~90000 | 0.54±0.17 | 1.15±0.06 | 39.46±0.01 |
| S1-b$_{90ppm}$ | < 0.5 | < 15 | < 150 | ~90000 | 0.54±0.17 | 1.15±0.06 | 39.46±0.01 |
| S1-c$_{90ppm}$ | 397±3 | 2004±20 | 195±3 | ~90000 | 0.54±0.17 | 1.15±0.06 | 39.46±0.01 |
| S2-a$_{90ppm}$ | < 1 | < 25 | < 200 | ~90000 | 51.43±0.06 | 55.14±0.09 | 100.09±0.03 |
| S2-c$_{90ppm}$ | 397±3 | 2004±20 | 195±3 | ~90000 | 51.43±0.06 | 55.14±0.09 | 100.09±0.03 |
| Ambient $N_2O$ concentration reference gases | | | | | | | |
| S1-c$_{330ppb}$ | 399.78±0.04 | 2022±0.2 | 195±0.3 | 327.45±0.06 | 0.92±0.39 | 1.44±0.25 | 39.12±0.18 |
| S2-c$_{330ppb}$ | 398.62±0.04 | 2020±0.2 | 193±0.3 | 323.97±0.06 | 52.38±0.10 | 55.61±0.12 | 99.59±0.03 |
| High $N_2O$ concentration source gas (SG) for two-end member mixing experiments (Sect. 2.4.8) | | | | | | | |
| SG1-a$_{90ppm}$ | < 1 | < 25 | < 200 | ~90000 | -24.35±0.32 | -22.94±0.33 | 31.79±0.12 |
| SG2-a$_{90ppm}$ | < 1 | < 25 | < 200 | ~90000 | 51.43±0.06 | 55.14±0.09 | 100.09±0.03 |
| Pressurized air | | | | | | | |
| Pressurized air (PA1) | 200.55±0.07 | 2582±0.2 | 187±0.2 | 326.51±0.06 | 15.83±0.03 | -3.39±0.14 | 44.66±0.02 |
| Pressurized air (PA2) | 437.99±0.36 | 2957±0.3 | 275±0.4 | 333.50±0.09 | 15.81±0.07 | -3.31±0.004 | 44.72±0.04 |

For high mole fraction reference gases in matrix b and c (S1-b$_{90ppm}$, S1-c$_{90ppm}$, S2-c$_{90ppm}$), the δ values acquired for S1-a$_{90ppm}$ and S2-a$_{90ppm}$ were applied. The absence of significant difference (< 1 ‰) in $N_2O$ isotopic composition between S1-b$_{90ppm}$ and S1-c$_{90ppm}$ in relation to S1-a$_{90ppm}$ (and S2-c$_{90ppm}$ to S2-a$_{90ppm}$) was assured by first statically diluting S1-b$_{90ppm}$, S1-c$_{90ppm}$ and S2-c$_{90ppm}$ to ambient $N_2O$ mole

fractions with synthetic air. This was followed by analysis using TREX-QCLAS (as described in Sect. 2.1.4) against the same standards used for S1-a$_{90ppm}$, S2-a$_{90ppm}$ isotope analysis.

Ambient mole fraction N$_2$O isotope reference gases (S1-c$_{330ppb}$, S2-c$_{330ppb}$) and PA1 and PA2 were analyzed by TREX-QCLAS (Sect. 2.1.4). The following N$_2$O isotope standards (values assigned by Tokyo Institute of Technology) were used: Cal1 and Cal2 for S1-c$_{330ppm}$; Cal3 and Cal2 for S2-c$_{330ppm}$; Cal4 ($\delta^{15}N^{\alpha}$ = 16.29 ± 0.07 ‰, $\delta^{15}N^{\beta}$ = -2.59 ± 0.06 ‰, $\delta^{18}O$ = 39.37 ± 0.04 ‰) and Cal5 ($\delta^{15}N^{\alpha}$ = -51.09 ± 0.07 ‰, $\delta^{15}N^{\beta}$ = -48.12 ± 0.04 ‰, $\delta^{18}O$ = 30.81 ± 0.03 ‰) for PA1 and PA2.

## 2.3 Laboratory setup, measurement procedures and data processing

### 2.3.1 Laboratory setup

All experiments were performed at the Laboratory for Air Pollution / Environmental Technology, Empa, Switzerland during June 2018 and February 2019. The laboratory was air conditioned to 295 K (± 1 K), with ± 0.5 K diel variations (Saveris 2, Testo AG, Switzerland), with the exception of a short period (7$^{th}$ to 8$^{th}$ July 2018), where the air conditioning was deactivated to test the temperature dependence of analyzers. Experiments were performed simultaneously for all analyzers, with the exception of the TREX-QCLAS, which requires an extensive measurement protocol and additional time to trap and measure N$_2$O (Ibraim et al., 2018) and thus could not be integrated concurrently with the other analyzers.

Fig. 2 shows a generalized experimental setup used for all experiments. Additional information for specific experiments is given in Section 2.4, and individual experimental setups are depicted in Supplementary Material 2. Gas flows were controlled using a set of mass flow controllers (MFC, model high-performance, Vögtlin Instruments GmbH, Switzerland) integrated into a MFC control unit (Contrec AG, Switzerland). All MFCs were calibrated by the manufacturer for whole air, which according to Vögtlin Instruments is valid for pure N$_2$ and pure O$_2$ as well. Operational ranges of applied MFCs ranged from 0–25 cm$^3$ min$^{-1}$ to 0–5000 cm$^3$ min$^{-1}$, and had reported uncertainties of 0.3 % of

their maximum flow and 0.5 % of actual flow. To reduce the uncertainty of the flow regulation, the MFC with the smallest maximum flow range available was selected. The sum of dosed gas flows was always higher than the sum of gas consumption by analyzers, with the overflow exhausted to room air. Gas lines between gas cylinders and MFCs, as well as between MFCs and analyzers, were 1/8" stainless steel tubing (type 304, Supelco, Sigma-Aldrich Chemie GmbH, Switzerland). Manual two-way (SS-1RS4 or SS-6H-MM, Swagelok, Switzerland) or three-way valves (SS-42GXS6MM, Swagelok, Switzerland) were used to separate or combine gas flows.
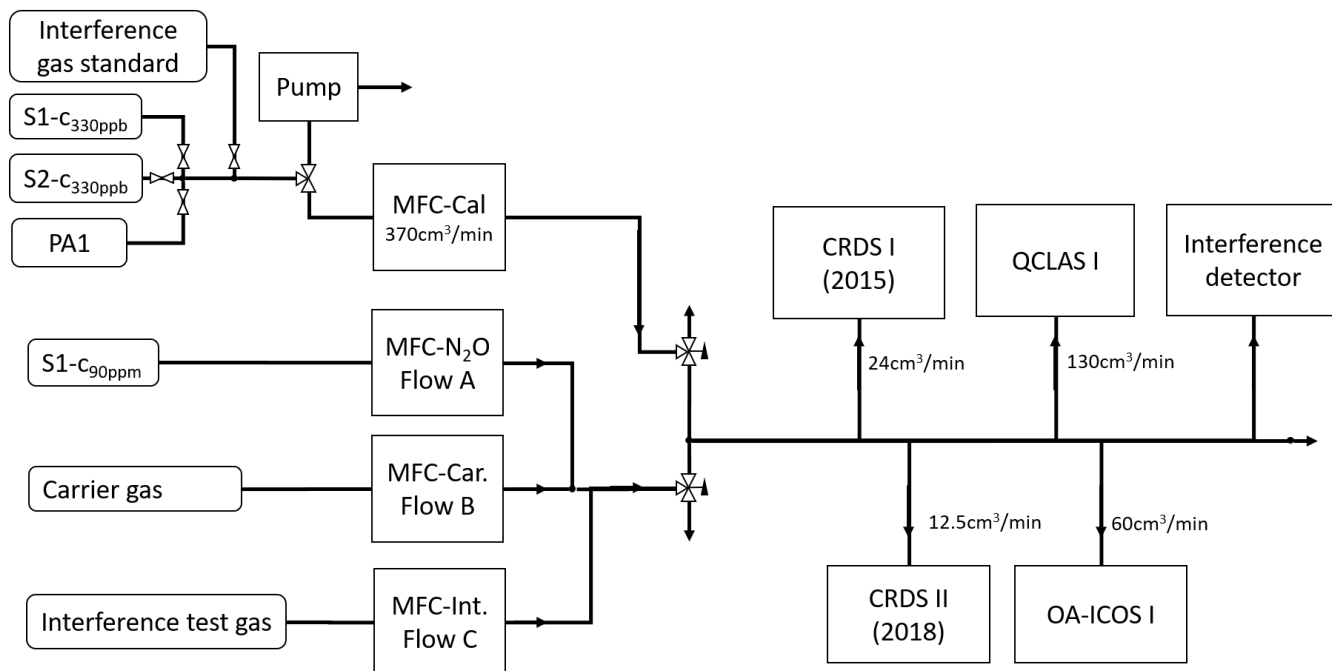
**Fig. 2.** The generalized experimental setup used for all experiments conducted in this study.

### 2.3.2 Measurement procedures, data processing and calibration

With the exception of Allan variance experiments performed in Sect. 2.4.1, all gas mixtures analyzed during this study were measured by the laser spectrometers for a period of 15 minutes, with the last 5 minutes used for data processing. Customized R-scripts (R Core Team, 2017) were used to extract the 5 min averaged data for each analyzer. Whilst the OA-ICOS and QCLAS instruments provide individual $^{14}N^{14}N^{16}O$, $^{14}N^{15}N^{16}O$, $^{15}N^{14}N^{16}O$ and $^{14}N^{14}N^{18}O$ mole fractions, the default data output generated by the CRDS analyzers are δ values, with underlying calculation schemes inaccessible to the user.

Therefore, to remain consistent across analyzers, uncalibrated δ values were calculated for OA-ICOS and QCLAS instruments first, using literature values for the $^{15}N/^{14}N$ (0.0036782) and $^{18}O/^{16}O$ (0.0020052) isotope ratios of AIR-N2 and VSMOW (Werner and Brand, 2001).

5   Each experiment was performed over the course of one day, and consisted of three phases: (1) an initial calibration phase; (2) an experimental phase; and (3) a final calibration phase. During phases (1) and (3), references gases S1-c$_{330ppb}$ and S2-c$_{330ppb}$ were analyzed. On each occasion (i.e. twice a day), this was followed by the analysis of PA1, which was used to determine the long-term (day-to-day) repeatability of the analyzers. Phase (2) experiments are outlined in Sect. 2.4. Throughout all three

10   phases, all measurements were systematically alternated with an Anchor gas measurement, the purpose of which was twofold: (1) to enable drift correction; and (2) as a means of quantifying deviations of the measured [N$_2$O] and δ values caused by increasing [N$_2$O] (Sect. 2.4.4), the removal of matrix gases (O$_2$ and Ar in Sect. 2.4.5) or addition of trace gases (CO$_2$, CH$_4$ and CO in Sect 2.4.6). Accordingly, the composition of the Anchor gas varied across experiments (see Sect. 2.4), but remained consistent

15   throughout each experiment. A drift correction was applied to the data if a linear or non-linear model fitted to the Anchor gas measurement over the course of an experiment was statistically significant at $p < 0.05$. Otherwise, no drift correction was applied.

In Sects. 2.4.3 (repeatability experiments) and 2.4.8 (two end-member mixing experiments), trace gas

20   effects were corrected according to Eqs. (1), (2) and (3) using derived analyzer-specific correction functions because the CO$_2$, CH$_4$ and CO composition of PA1 in Sect. 2.4.3 and the gas mixtures in Sect. 2.4.8 varied from those of the calibration gases S1-c$_{330ppb}$ (S1) and S2-c$_{330ppb}$ (S2):

$$[N_2O]_{tc,G} = [N_2O]_{meas,G} - \sum_x \left( \Delta[N_2O] \left( \Delta[x]_G, [N_2O]_{meas,G} \right) \right) \tag{1}$$

$$\delta_{tc,G} = \delta_{meas,G} - \sum_x \left( \Delta\delta \left( \Delta[x]_G, \delta_{meas,G} \right) \right) \tag{2}$$

25   and,

$$\Delta[x]_G = [x]_G - \frac{[x]_{S1} + [x]_{S2}}{2} \tag{3}$$

where $[N_2O]_{tc,G}$ and $\delta_{tc,G}$ refer to the trace gas-corrected $[N_2O]$ and $\delta$ values ($\delta^{15}N^{\alpha}$, $\delta^{15}N^{\beta}$ or $\delta^{18}O$) of sample gas G, respectively; $[N_2O]_{meas,G}$ and $\delta_{meas,G}$ are the raw uncorrected $[N_2O]$ and $\delta$ values measured by the analyzer for sample gas G, respectively; $\Delta[N_2O]$ and $\Delta\delta$ refer to the offset on the $[N_2O]$ or $\delta$ values, respectively, resulting from the difference in trace gas mole fraction between sample gas G and reference gases, denoted $\Delta[x]_G$; $[x]_G$ is the mole fraction of trace gas $x$ ($CO_2$, $CH_4$ or CO) in sample gas G; and $[x]_{S1}$ and $[x]_{S2}$ are the mole fractions of trace gas $x$ in reference gases S1-c$_{330ppb}$ and S2-c$_{330ppb}$. It is important to note that the differences in $CO_2$ and $CH_4$ mole fractions in S1-c$_{330ppb}$ and S2-c$_{330ppb}$ are two orders of magnitude smaller than the differences to PA1.

Thereafter, $\delta$ values of trace gas-corrected, mole fraction-corrected (Sect.2.4.8 only) and drift-corrected measurements from the analyzers were normalized to $\delta$ values on the international isotope ratio scales using a two-point linear calibration procedure derived from values of S1-c$_{330ppb}$ (S1) and S2-c$_{330ppb}$ (S2) calculated using Eq. (4) (Gröning, 2018):

$$\delta_{Cal,G} = \frac{\delta_{true,S1} - \delta_{true,S2}}{\delta_{meas,S1} - \delta_{meas,S2}} * \left( \delta_{Uncal,G} - \delta_{meas,S1} \right) + \delta_{true,S1} \tag{4}$$

where $\delta_{Cal,G}$ is the calibrated $\delta$ value for sample gas G normalized to international isotope ratio scales; $\delta_{true,S1}$ and $\delta_{true,S2}$ are the respective $\delta$ values assigned to reference gases S1-c$_{330ppb}$ and S2-c$_{330ppb}$; $\delta_{meas,S1}$ and $\delta_{meas,S2}$ are the respective $\delta$ values of reference gases S1-c$_{330ppb}$ and S2-c$_{330ppb}$ measured by the analyzer; and $\delta_{Uncal,G}$ is the trace gas-corrected, mole fraction-corrected (Sect.2.4.8 only) and drift-corrected measurement of sample gas G acquired by the analyzer. In Eq. (4), the calibration span is given by the difference in $\delta$ values between S1 and S2.

**2.4 Testing of instruments**

An overview of all experiments performed in this study, including applied corrections and instruments tested, is provided in Table 4.

**Table 4.** Overview of the experiments performed in this study.

| Experiment | Sections | Aims | Corrections applied | Instruments tested | Comments |
|---|---|---|---|---|---|
| Instrumental precision (Allan deviation) | 2.4.1 3.1 | Short-term precision, optimal integration time/maximum precision and drift | None | OA-ICOS I CRDS I & II QCLAS I QCLAS II & III (ambient only) TREX-QCLAS I | Conducted at $N_2O$ concentrations ~326, 1000, 10000 ppb |
| Temperature effects | 2.4.2 3.2 | Temperature effects on $[N_2O]$ and isotope deltas | None | OA-ICOS I CRDS I & II QCLAS I | |
| Repeatability (short-term, ~2 hour) | 2.4.3 3.3 | Repeatability | Drift | OA-ICOS I CRDS I & II QCLAS I TREX-QCLAS I | Conducted at $N_2O$ concentrations ~326, 1000, 10000 ppb |
| Repeatability (long-term, ~2 week) | 2.4.3 3.3 | Repeatability | Drift, delta calibration, trace gas effect[a)] | OA-ICOS I CRDS I & II QCLAS I TREX-QCLAS I | Conducted at ~326 ppb $N_2O$ using PA1 |
| $N_2O$ mole fraction effects | 2.4.4 3.4 | $[N_2O]$ effects on isotope deltas, and derive correction functions | Drift | OA-ICOS I CRDS I & II QCLAS I | CRDS: 300 to 1500 ppb $N_2O$, OA-ICOS, QCLAS: 300 to 90000 ppb |
| Gas matrix effects ($N_2$, $O_2$ and Ar) | 2.4.5 3.5 | Gas matrix effects on $[N_2O]$ and isotope deltas, and derive correction functions | Drift | OA-ICOS I CRDS I & II QCLAS I TREX-QCLAS I | Conducted at $N_2O$ concentrations ~330, 660, 990 ppb |
| Trace gas effects ($H_2O$, $CO_2$, $CH_4$, CO) | 2.4.6 3.6 | Trace gas effects on $[N_2O]$ and isotope deltas, and derive correction functions | Drift | OA-ICOS I CRDS I & II QCLAS I TREX-QCLAS I (except $H_2O$) | Conducted at $N_2O$ concentrations ~330, 660, 990 ppb |
| $CO_2$ and CO removal | 2.4.7 3.6 | Effects of removal of $CO_2$ (Ascarite) and CO (Sofnocat) on $[N_2O]$ and isotope deltas | Drift | OA-ICOS I CRDS I & II QCLAS I | Conducted at $N_2O$ concentrations ~330 ppb |
| Two end-member mixing | 2.4.8 3.7 | Test the ability of the instruments to extrapolate a $N_2O$ source using a Keeling plot approach | Drift, 3-point concentration dependence, delta calibration, trace gas effect[a)], and scaled with $N_2O$[b)] | OA-ICOS I (exp. 1-6) CRDS I & II (exp. 1-4) QCLAS I (exp. 1-6) TREX-QCLAS I (exp. 1-2) GC $[N_2O]$, IRMS [δ] (exp. 1-6) | The workflow provided in Sect. 4.3 was applied |

### 2.4.1 Allan precision

The precision of the laser spectrometers was determined using the Allan variance technique (Allan,
5   1966; Werle et al., 1993). Experiments were conducted at different [$N_2O$]: ambient, 1000 ppb, and
10000 ppb. For the Allan variance testing conducted at ambient [$N_2O$], a continuous flow of PA1 was
measured continuously for 30 h. For testing conducted at 1000 and 10000 ppb [$N_2O$], S1-$c_{90ppm}$ was
dynamically diluted to 1000 or 10000 ppb [$N_2O$] with matrix gas c for 10 h. CRDS I and II were
disconnected for the 10000 ppb measurement because [$N_2O$] exceeded the specified measurement
10   range. Daily drifts were estimated using the slope of the linear regression over the measurement period
normalized to 24 h (i.e. ppb $d^{-1}$ and ‰ $d^{-1}$).

### 2.4.2 Temperature effects

To investigate instrumental sensitivities to variations in ambient temperature, PA1 was simultaneously
and continuously measured by all analyzers in flow-through mode for a period of 24 h while the air
15   conditioning of the laboratory was turned off for over 30 h, which led to a rise in room temperature
from 21 °C to 30 °C. Thereafter, the air conditioning was restarted and the laboratory temperature
returned to 21ºC.

### 2.4.3 Repeatability

Measurements of PA1 were taken twice daily over ~2 weeks prior to and following the experimental
20   measurement period to test the long-term repeatability of the analyzers. Measurements were
sequentially corrected for differences in trace gas concentrations (Eqs. 1 – 3), drift (if required), and
then δ-calibrated (Eq. 4). No matrix gas corrections were applied because the $N_2$, $O_2$ and Ar
composition of PA1 was identical to that of S1-$c_{330ppb}$ and S2-$c_{330ppb}$. TREX-QCLAS I measurements
for long-term repeatability were collected separately from other instruments over a period of six-
25   months. Repeatability over shorter time periods (2.5 h) was also tested for each analyzer by acquiring

10 repeated 15 min measurements at different $N_2O$ mole fractions: ambient (PA1), 1000 ppb and 10000 ppb $N_2O$.

### 2.4.4 $N_2O$ mole fraction dependence

To determine the effect of changing $[N_2O]$ on the measured $\delta$ values, S1-c$_{90ppm}$ was dynamically diluted
5   with matrix c to various $[N_2O]$ spanning the operational ranges of the instruments. For both CRDS
analyzers mole fractions between 300 to 1500 ppb were tested, while for the OA-ICOS I and QCLAS I
mixing ratios ranged from 300 to 90000 ppb. Between each $[N_2O]$ step change, the dilution ratio was
systematically set to 330 ppb $N_2O$ to perform an Anchor gas measurement. For each instrument, the
effect of increasing $[N_2O]$ on $\delta$ values was quantified by comparing the measured $\delta$ values at each step
10   change to the mean measured $\delta$ values of the Anchor gas, and was denoted $\Delta\delta$ such that $\Delta\delta = \delta_{measured}$ -
$\delta_{Anchor}$ and $\Delta\delta_{Anchor} = 0$. The experiment was repeated on three consecutive days to test day-to-day
variability.

### 2.4.5 Gas matrix effects ($O_2$ and Ar)

Gas matrix effects were investigated by determining the dependence of $[N_2O]$ and isotope $\delta$ values on
15   the $O_2$ or Ar mixing ratio of a gas mixture. For $O_2$ testing, Gas 1, 2 and 3 ($N_2$) were mixed to
incrementally change mixing ratios of $O_2$ (0–20.5 % $O_2$) while maintaining a consistent $[N_2O]$ of 330
ppb. As an Anchor gas, Gas 1 (S1-a$_{90ppm}$) was dynamically diluted with Gas 2 (matrix a) to produce 330
ppb $N_2O$ in matrix a (Table 5). $O_2$ mole fractions in the various gas mixtures were analyzed with a
paramagnetic $O_2$ analyzer (Servomex, UK) and agreed with expected values to within 0.3 % (relative).
20   For Ar testing, Gas 1 (S1-b$_{90ppm}$) was dynamically diluted with Gas 2 (matrix b) to produce an Anchor
gas with ~330 ppb $N_2O$ in matrix b. Gas 1, 2 and 3 ($N_2 + O_2$) were then mixed to incrementally change
mixing ratios of Ar (0.003–0.95 % Ar), while a consistent $[N_2O]$ of 330 ppb was maintained. Ar
compositional differences were estimated based on gas cylinder manufacturer specifications and
selected gas flows. The effects of decreasing $O_2$ and Ar on $[N_2O]$ and $\delta$ values were quantified by
25   comparing the measured $[N_2O]$ and $\delta$ values at each step change to the mean measured $[N_2O]$ and $\delta$
values of the Anchor gas, and were denoted $\Delta[N_2O]$ and $\Delta\delta$, similar to Sect. 2.4.4. Deviations in $O_2$ and

Ar mixing ratios were quantified by comparing the $[O_2]$ and $[Ar]$ at each step change to the mean $[O_2]$ and $[Ar]$ of the Anchor gas, and were denoted $\Delta O_2$ and $\Delta Ar$ such that, for example, $\Delta O_2 = O_{2\ measured} - O_{2\ Anchor}$ and $\Delta O_{2\ Anchor} = 0$. Both $O_2$ and Ar experiments were triplicated.

5   In addition, $O_2$ and Ar effects were derived for $N_2O$ mole fractions of ~660 ppb and ~990 ppb. These experiments were undertaken in a way similar to those described above, except Anchor gas measurements were conducted once (not triplicated).

**Table 5.** Gas mixtures used to test effects of gas matrix ($O_2$, Ar) or trace gases ($CO_2$, $CH_4$, CO) on
10 $[N_2O]$ and isotope deltas. Gas 1 was dynamically diluted with Gas 2 to make up an Anchor gas with $[N_2O]$ of ~330 ppb which was systematically measured throughout the experiments to (1) enable drift correction, and (2) quantify deviations of the measured $[N_2O]$ and $\delta$ values caused by the removal of matrix gases ($O_2$ and Ar in Sect. 2.4.5) or addition of trace gases ($CO_2$, $CH_4$ and CO in Sect 2.4.6). Gas 1, 2 and 3 were combined in different fractions to make up sample gas with identical $[N_2O]$ but varying
15 mixing ratio of the target compound.

| Target compound | Gas 1 | Gas 2 | Gas 3 | Mixing range |
|---|---|---|---|---|
| $O_2$ | S1-a$_{90ppm}$ ($N_2O + N_2 + O_2$) | $N_2 + O_2$[a] | $N_2$ | 0-20.5 % $O_2$ |
| Ar | S1-b$_{90ppm}$ ($N_2O + N_2 + O_2 + Ar$) | $N_2 + O_2 + Ar$[b] | $N_2 + O_2$[a] | 0.003-0.95 % Ar |
| $CO_2$ | S1-b$_{90ppm}$ ($N_2O + N_2 + O_2 + Ar$) | $N_2 + O_2 + Ar$[b] | $CO_2$ in $N_2 + O_2 + Ar$[b] | 1.72-2030 ppm $CO_2$ |
| $CH_4$ | S1-b$_{90ppm}$ ($N_2O + N_2 + O_2 + Ar$) | $N_2 + O_2 + Ar$[b] | $CH_4$ in $N_2 + O_2 + Ar$[b] | 0.014-10.25 ppm $CH_4$ |
| CO | S1-b$_{90ppm}$ ($N_2O + N_2 + O_2 + Ar$) | $N_2 + O_2 + Ar$[b] | CO in $N_2 + O_2 + Ar$[b] | 0.14-2.13 ppm CO |

[a] matrix a: 20.5 % $O_2$ in $N_2$

[b] matrix b: 20.95 % $O_2$, 0.95 % Ar in $N_2$

**2.4.6 Trace gas effects ($CO_2$, $CH_4$, CO and $H_2O$)**

The sensitivity of $[N_2O]$ and $\delta$ values on changing trace gas concentrations was tested in a similar way
20 to those described in Sect. 2.4.5. In short, Gas 1 (S1-b$_{90ppm}$) was dynamically diluted with Gas 2 (matrix b) to create an Anchor gas with 330 ppb $N_2O$ in matrix b. Gas 1, 2 and 3 (either $CO_2$, $CH_4$ or CO in matrix gas b) were mixed to incrementally change the mixing ratios of the target substances (1.7 – 2030 ppm $CO_2$, 0.01 – 10.25 ppm $CH_4$ and 0.14 – 2.14 ppm CO) while maintaining a consistent gas matrix and $[N_2O]$ of 330 ppb (Table 5). Trace gas mole fractions in the produced gas mixtures were analyzed
25 with a Picarro G2401 (Picarro Inc., USA) and agreed with predictions within better than 2–3 %

(relative). Similar to Sect. 2.4.4, the effects of increasing $CO_2$, $CH_4$ and CO on $[N_2O]$ and δ values were quantified by comparing the measured $[N_2O]$ and δ values at each step change to the mean measured $[N_2O]$ and δ values of the Anchor gas, and were denoted $\Delta[N_2O]$ and $\Delta\delta$. Similar to Sect. 2.4.5, deviations in $CO_2$ $CH_4$ and CO mixing ratios were quantified by comparing the measured $[CO_2]$, $[CH_4]$ and [CO] at each step change to the mean measured $[CO_2]$, $[CH_4]$ and [CO] of the Anchor gas. Each experiment was triplicated. The interference effects were also tested at ~660 ppb and ~990 ppb $N_2O$.

The sensitivity of the analyzers to water vapor was tested by firstly diluting Gas 1 (S1-$c_{90ppm}$) with Gas 2 (matrix c) to produce an Anchor gas with 330 ppb $N_2O$. This mixture was then combined with Gas 3 (also matrix c) which had been passed through a humidifier (customized setup by Glasbläserei Möller, Switzerland) set to 15°C (F20 Julabo GmbH, Germany) dew point. By varying the flows of Gas 2 and 3, different mixing ratios of water vapor ranging from 0 – 13800 ppm were produced and measured using a dewpoint meter (model 973, MBW, Switzerland). $H_2O$ effects were quantified as described above, but $[N_2O]$ results were additionally corrected for dilution effects caused by the addition of water vapor into the gas stream. Water vapor dependence testing was not performed on the TREX-QCLAS I as the instrument is equipped with a permeation dryer at the inlet.

### 2.4.7 $CO_2$ and CO removal using NaOH (Ascarite) and Sofnocat

The efficiency of NaOH and Sofnocat for removing spectral effects caused by $CO_2$ and CO was assessed by repeating $CO_2$ and CO interference tests (Sect. 2.4.6), but with the respective traps connected in-line. These experiments were triplicated but only undertaken at ~330 ppb $N_2O$. NaOH traps were prepared using stainless steel tubing (OD 2.54 cm, length 20 cm) filled with 14 g Ascarite (0-30 mesh, Sigma Aldrich, Switzerland) bracketed by 3g $Mg(ClO_4)_2$ (Alfa Aesar, Germany) each separated by glass wool. The Sofnocat trap was prepared similarly using stainless steel tubing (OD 2.54 cm, length 20 cm) filled with 50 g Sofnocat (Sofnocat 423, Molecular Products Limited, GB) and capped on each side with glass wool.

## 2.4.8 Two end-member mixing

The ability of the instruments to accurately extrapolate $N_2O$ source compositions was tested using a simulated two end-member mixing scenario in which a gas with high $N_2O$ concentration, considered to be a $N_2O$ *source* gas (SG), was dynamically diluted into a gas with ambient $N_2O$ concentration (PA2), considered to be *background* air. $N_2O$ mole fractions were raised above ambient levels (denoted as $\Delta N_2O$) in three different scenarios ranging from: (1) 0–30 ppb; (2) 0–700 ppb and (3) 0–10000 ppb. In each scenario, two isotopically different *source* gases with high $N_2O$ concentration were used; one *source* gas (SG1-a90ppm) $^{15}N$ depleted compared to PA2; and a second *source* gas (SG2-a90ppm) $^{15}N$ enriched compared to PA2 (Table 3). The three different mixing scenarios and two different *source* gases resulted in a total of six mixing scenarios (referred to as Exp. 1–6). During each experiment, PA2 was alternated with PA2 + SG in four different mixing ratios to give a span of $N_2O$ concentrations and isotopic compositions required for Keeling plot analysis. Each experiment was triplicated. OA-ICOS I and QCLAS I were used in all experiments (Exp. 1–6), CRDS was used for $\Delta N_2O$ 0–30 ppb and 0–700 ppb (Exp. 1–4) and TREX-QCLAS was only used for $\Delta N_2O$ 0–30 ppb (Exp. 1–2).

To test the robustness of trace gas correction equations derived for each analyzer in Sect. 3.6, NaOH and Sofnocat traps were placed in-line between the PA2 + SG mixtures and the analyzers such that we could ensure a difference in $CO_2$ and CO mole fractions between the measured gas mixture and reference gases (S1-c330ppb, S2-c330ppb). The experiments were also bracketed by two calibration phases (S1-c330ppb, S2-c330ppb) to allow for δ calibration, followed by two phases where the $N_2O$ concentration dependence was determined.

Gas samples for GC-IRMS analysis were taken in the same phase (last five min of 15 min interval) used during the minute prior to the final five minutes used for averaging by the laser-based analyzers. The gas was collected at the common overflow port of the laser spectrometers using a 60 mL syringe connected via a Luer lock three-way valve to needle and port. 200 mL samples were taken at each concentration step. 180 mL of gas sample was stored in pre-evacuated 110 mL serum crimp vials for

isotopic analysis using IRMS. IRMS analyses were conducted at ETH Zürich using a gas preparation unit (Trace Gas, Elementar, Manchester, UK) coupled to an IsoPrime100 IRMS (Elementar, Manchester, UK). The remaining 20 mL were injected in a pre-evacuated 12 mL Labco exetainer for [$N_2O$] analysis using gas chromatography equipped with Electron Capture Detector (ECD) performed at ETH Zürich (Bruker, 456-GC, Scion Instruments, Livingston, UK). After injection, samples were separated on HayeSep D packed columns with a 5% $CH_4$ in Ar mixture (P5) as carrier and make-up gas. The GC was calibrated using a suite of calibration gases at $N_2O$ concentrations of 0.393 (Carbagas AG, Switzerland), 1.02 (PanGas AG, Switzerland) and 3.17 ppm (Carbagas AG, Switzerland). For further analytical details see Verhoeven et al. (2019) and Supplementary Material 1.

For the laser-based analyzers, data was processed as described in Sect. 2.3.2 using the following sequential order: (1) analyzer-specific correction functions, determined in Sect 3.6, were applied to correct for differences in trace gas concentrations ($CO_2$, CO) between sample gas and calibration gases; (2) the effect of [$N_2O$] changes was corrected using a three-point correction; (3) a drift-correction based on repeated measurements of PA2 was applied if necessary; and (4) a δ-calibration (Eq. 4) using S1-$c_{330ppb}$ and S2-$c_{330ppb}$ was applied.

## 3 Results

### 3.1 Allan precision

Allan deviations (square root of Allan variance) for 5 min and 10 min averaging times, often reported in manufacturer specifications, at ~327 ppb, 1000 ppb and 10000 ppb [$N_2O$] are shown in Table 6.

At near-atmospheric $N_2O$ mole fractions of ~326.5 ppb, both CRDS analyzers showed the greatest precision and stability for the measurement of $\delta^{15}N^{\alpha}$, $\delta^{15}N^{\beta}$ and $\delta^{18}O$ (0.32 – 0.41 ‰, 0.41 – 0.45 ‰, 0.41 – 0.46 ‰ at 300 s averaging time, respectively), while for the precision of [$N_2O$], the OA-ICOS I and the CRDS II showed best performance ($1.7 \cdot 10^{-2}$ ppb at 300 s averaging time) (Fig. 3; Table 6). The Allan precision of CRDS and OA-ICOS analyzers further improved with increasing averaging times

and optimal averaging times typically exceeded 1.5-3 h. The precision and daily drift of the OA-ICOS I and both CRDS analyzers were in agreement with manufacturer specifications (ABB-Los Gatos Research Inc., 2019; Picarro Inc., 2019). The CRDS II outperformed the CRDS I for precision, presumably due to manufacturer upgrades/improvements in the newer model. The QCLAS spectrometers exhibited significant differences between instruments, which might be due to differences in the instrument hardware / design, as instruments were manufactured between 2012 – 2016, or in the parameter setting (such as cell pressure and tuning parameters) of different analyzers. Generally, short-term (approx. up to 100 s) precision of QCLAS instruments was compatible or superior to CRDS or OA-ICOS, but data quality was decreased for longer averaging times due to drift effects. Nonetheless, the performance of QCLAS I, II and III generally agrees with Allan precision measurements executed by Yamamoto et al. (2014), who reported 1.9 – 2.6 ‰ precision for δ values at ambient $N_2O$ mole fractions and 0.4 – 0.7 ‰ at 1000 ppb $N_2O$. QCLAS I, which was tested further in Sects. 3.2 – 3.7, displayed the poorest performance of all QCLAS analyzers, in particular for $\delta^{15}N^\beta$. The primary cause of the observed excess drift in QCLAS I was fluctuating spectral baseline structure (pers. comm. ARI), which can be significantly reduced by applying an automatic spectral correction method developed by ARI. This methodology is currently in trial phase and, thus, not yet implemented in the software that controls the QCLAS instruments. A brief overview of the methodology is provided in Supplementary Material 3, and corrected results for QCLAS I provided in Table 6. This methodology is not discussed in detail here as it is beyond the scope of this work. Nonetheless, QCLAS I achieved Allan deviations of ~0.4 ‰ at 300 s averaging time for $\delta^{15}N^\alpha$ and $\delta^{15}N^\beta$ at ambient $N_2O$ mole fractions when this correction method was applied by ARI.

At [$N_2O$] of 1000 ppb, the precision of δ values measured by all analyzers, except CRDS I, significantly improved due to greater signal-to-noise ratios. Whilst the performance of OA-ICOS I was similar to that of CRDS II for $\delta^{15}N^\alpha$ and $\delta^{15}N^\beta$ (0.24‰ and 0.24‰ for CRDS II; 0.28‰ and 0.37‰ for OA-ICOS I at 300 s averaging time), CRDS II displayed the best precision for $\delta^{18}O$ (0.21‰ at 300 s averaging time). Also notable was the improved performance of the 2018 model (CRDS II) compared to the 2015 model (CRDS I). QCLAS analyzers showed the best 1 s precision for δ values, but beyond 100 s, δ-

measurements were still heavily affected by instrumental drift resulting in lower precision, especially for QCLAS I. When the spectral correction method described in Supplementary Material 3 was applied, QCLAS I achieved Allan deviations of ~0.2 ‰ at 300 s averaging time for $\delta^{15}N^{\alpha}$ and $\delta^{15}N^{\beta}$ at 1000 ppb $N_2O$.

At [$N_2O$] of 10000 ppb all analyzers showed excellent precision, with QCLAS I, II and III outperforming OA-ICOS I for precision of $\delta^{15}N^{\alpha}$ and $\delta^{15}N^{\beta}$ (collectively better than 0.10 ‰ at 300 s averaging time for both $\delta^{15}N^{\alpha}$ and $\delta^{15}N^{\beta}$). QCLAS II had the best precision for [$N_2O$] (1.2 ppb at 300 s averaging time). OA-ICOS I and QCLAS III were the only analyzers tested in this study that could be

10 used to measure $\delta^{18}O$ at 10000 ppb $N_2O$. OA-ICOS I attained a precision of 0.17 ‰, while QCLAS III attained a precision of 0.48 ‰, both with 300 s averaging time. QCLAS I achieved Allan deviations of ~0.02 – 0.03 ‰ at 300 s averaging time for $\delta^{15}N^{\alpha}$ and $\delta^{15}N^{\beta}$ at 10000 ppb $N_2O$ when the spectral correction method (Supplementary Material 3) was applied.

15 The precision of instruments on [$N_2O$] measurements at 1000 and 10000 ppb $N_2O$ might not be representative because of small fluctuations in the final gas mixture produced by the MFCs, which were likely amplified due to the small dilution ratios. Therefore, the indicated [$N_2O$] precisions should be considered as a pessimistic estimate. This was most apparent for the QCLAS and the OA-ICOS analyzers, which showed the highest short-term precision, although this likely applies to all analyzers.

20 Accordingly, the deviation of the Allan variance of mole fraction measurements by QCLAS II and III as well as OA-ICOS I at elevated [$N_2O$] from instrumental white (Gaussian) noise was likely due to uncertainty contributions from MFCs. Therefore, it is likely that the precision of all analyzers for [$N_2O$] measurements is better than shown in Fig. 3 and Table 6. Nonetheless, at 1000 ppb $N_2O$, QCLAS III showed the best precision for [$N_2O$] ($1.0 \cdot 10^{-1}$ ppb at 300 s averaging time), which was almost one order

25 of magnitude greater than at atmospheric $N_2O$ mole fractions.

**Table 6.** Key parameters for instrument stability retrieved from Allan variance experiments for [$N_2O$], $\delta^{15}N^{\alpha}$, $\delta^{15}N^{\beta}$ and $\delta^{18}O$: precision (1σ) at 300s and 600s averaging times, and daily drift at various $N_2O$ concentrations. 1σ data refers to Allan deviation (square root of Allan variance).

| Instrument | 1σ $N_2O$ (300 s) | 1σ $N_2O$ (600 s) | $N_2O$ drift (ppb day$^{-1}$) | 1σ $\delta^{15}N^{\alpha}$ (300s) | 1σ $\delta^{15}N^{\alpha}$ (600s) | $\delta^{15}N^{\alpha}$ drift (‰ day$^{-1}$) | 1σ $\delta^{15}N^{\beta}$ (300s) | 1σ $\delta^{15}N^{\beta}$ (600s) | $\delta^{15}N^{\beta}$ drift (‰ day$^{-1}$) | 1σ $\delta^{18}O$ (300s) | 1σ $\delta^{18}O$ (600s) | $\delta^{18}O$ drift (‰ day$^{-1}$) |
|---|---|---|---|---|---|---|---|---|---|---|---|---|
| 326.5 ppb $N_2O$ | | | | | | | | | | | | |
| CRDS I | $3.0 \cdot 10^{-2}$ | $2.3 \cdot 10^{-2}$ | $2.0 \cdot 10^{-2}$ | 0.41 | 0.27 | 0.22 | 0.45 | 0.38 | 0.18 | 0.46 | 0.34 | 0.03 |
| CRDS II | $1.7 \cdot 10^{-2}$ | $1.2 \cdot 10^{-2}$ | $3.2 \cdot 10^{-2}$ | 0.32 | 0.23 | $3.5 \cdot 10^{-3}$ | 0.41 | 0.31 | 0.14 | 0.41 | 0.28 | 0.10 |
| OA-ICOS I | $1.7 \cdot 10^{-2}$ | $1.3 \cdot 10^{-2}$ | $1.5 \cdot 10^{-2}$ | 1.08 | 0.82 | 0.07 | 0.79 | 0.52 | 0.50 | 1.69 | 1.14 | 2.34 |
| QCLAS I | $6.3 \cdot 10^{-2}$ | $4.6 \cdot 10^{-2}$ | $3.7 \cdot 10^{-2}$ | 1.24 | 1.41 | 6.80 | 3.45 | 4.22 | 15.81 | n.d. | n.d. | n.d. |
| QCLAS I[a] | $2.1 \cdot 10^{-2}$ | $2.4 \cdot 10^{-2}$ | 0.12 | 0.39 | 0.37 | 0.71 | 0.42 | 0.55 | 4.83 | n.d. | n.d. | n.d. |
| QCLAS II | $9.5 \cdot 10^{-3}$ | $1.1 \cdot 10^{-2}$ | 1.00 | 1.08 | 1.44 | 0.20 | 0.60 | 0.72 | 0.05 | n.d. | n.d. | n.d. |
| QCLAS III | $2.5 \cdot 10^{-2}$ | $3.6 \cdot 10^{-2}$ | 0.75 | 0.81 | 1.23 | 0.09 | 0.78 | 1.22 | 0.04 | 0.97 | 1.51 | 0.13 |
| ~1000 ppb $N_2O$ | | | | | | | | | | | | |
| CRDS I | $7.7 \cdot 10^{-1}$ | $6.0 \cdot 10^{-1}$ | 0.29 | 0.88 | 0.67 | 0.67 | 0.89 | 0.73 | 1.39 | 0.81 | 0.67 | 0.32 |
| CRDS II | $2.1 \cdot 10^{-1}$ | $1.3 \cdot 10^{-1}$ | 0.54 | 0.24 | 0.20 | 0.36 | 0.24 | 0.18 | 0.23 | 0.21 | 0.13 | 0.86 |
| OA-ICOS I | $1.7 \cdot 10^{-1}$ | $1.2 \cdot 10^{-1}$ | 1.02 | 0.28 | 0.23 | 0.93 | 0.37 | 0.25 | 0.54 | 0.67 | 0.44 | 0.15 |
| QCLAS I | $3.3 \cdot 10^{-1}$ | $2.4 \cdot 10^{-1}$ | 1.03 | 0.47 | 0.61 | 7.25 | 0.83 | 1.11 | 8.01 | n.d. | n.d. | n.d. |
| QCLAS I[a] | $1.4 \cdot 10^{-1}$ | $1.0 \cdot 10^{-1}$ | $1.2 \cdot 10^{-3}$ | 0.19 | 0.23 | 0.61 | 0.20 | 0.22 | 0.11 | n.d. | n.d. | n.d. |
| QCLAS II | $2.0 \cdot 10^{-1}$ | $2.4 \cdot 10^{-1}$ | 4.11 | 0.52 | 0.49 | 0.04 | 0.22 | 0.19 | $4.3 \cdot 10^{-3}$ | n.d. | n.d. | n.d. |
| QCLAS III | $1.0 \cdot 10^{-1}$ | $1.6 \cdot 10^{0}$ | 1.61 | 0.81 | 1.37 | 0.06 | 0.72 | 1.18 | 0.03 | 0.38 | 0.54 | 0.05 |
| ~10000 ppb $N_2O$ | | | | | | | | | | | | |
| OA-ICOS I | $1.7 \cdot 10^{0}$ | $1.3 \cdot 10^{-3}$ | 1.30 | 0.12 | 0.10 | 0.12 | 0.15 | 0.09 | 0.54 | 0.17 | 0.12 | 0.35 |
| QCLAS I | $3.3 \cdot 10^{0}$ | $2.3 \cdot 10^{0}$ | 3.74 | 0.06 | 0.07 | 1.09 | 0.09 | 0.11 | 0.82 | n.d. | n.d. | n.d. |
| QCLAS I[a] | $4.6 \cdot 10^{-1}$ | $3.8 \cdot 10^{-1}$ | 0.10 | 0.03 | 0.03 | 0.02 | 0.02 | 0.03 | 0.10 | n.d. | n.d. | n.d. |
| QCLAS II | $1.2 \cdot 10^{0}$ | $9.9 \cdot 10^{-1}$ | 35.1 | 0.09 | 0.07 | $2.9 \cdot 10^{-3}$ | 0.09 | 0.08 | $7.0 \cdot 10^{-3}$ | n.d. | n.d. | n.d. |
| QCLAS III | $1.3 \cdot 10^{0}$ | $1.6 \cdot 10^{0}$ | 66.1 | 0.10 | 0.17 | $3.4 \cdot 10^{-3}$ | 0.10 | 0.13 | $5.8 \cdot 10^{-3}$ | 0.48 | 0.65 | $2.8 \cdot 10^{-3}$ |

[a] Data re-processed by Aerodyne Research Inc. technicians using an automatic spectral correction method. This method corrects data that was influenced by changing baseline structure. Further information on this method is provided in Supplementary Material 3.

n.d. not determined
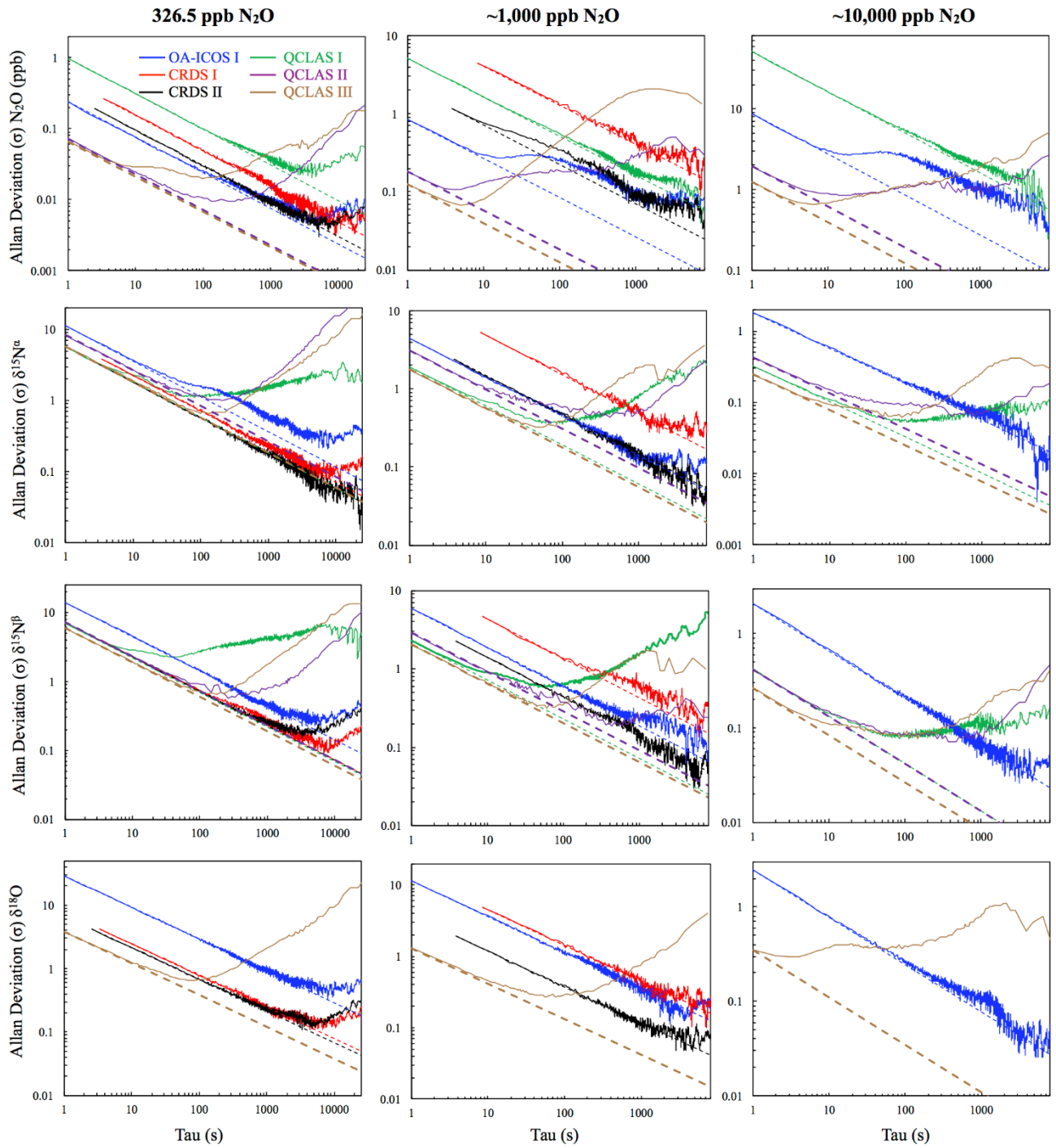
**Fig. 3.** Allan deviation (square root of Allan Variance) plots for the OA-ICOS I (blue), CRDS I (red), CRDS II (black), QCLAS I (green), QCLAS II (purple) and QCLAS III (brown) at different N₂O mole

fractions (~327, 1000 and 10000 ppb). The dashed lines represent a slope of -0.5 (log-log scale) and indicate the expected behavior for Gaussian white noise in each analyzer.

## 3.2 Temperature effects

All instruments tested showed significant effects, albeit to varying degrees, on their measurements due
5   to the change in laboratory temperature (Fig. 4). The OA-ICOS I displayed no clear temperature effects
for [$N_2O$], $\delta^{15}N^\alpha$ and $\delta^{15}N^\beta$, but displayed a moderate temperature dependence for $\delta^{18}O$ measurements
(up to 14‰ deviation from the mean), with measurement drift closely paralleling the laboratory
temperature ($r^2 = 0.78$). Both CRDS instruments displayed smaller shifts in [$N_2O$] (up to 0.14 ppb
deviation from the mean), $\delta^{15}N^\alpha$, $\delta^{15}N^\beta$ and $\delta^{18}O$ that occurred particularly when the laboratory
10   temperature had an acute change. QCLAS I showed a strong temperature dependence on $\delta^{15}N^\alpha$ ($r^2 = 0.85$) and $\delta^{15}N^\beta$ ($r^2 = 0.96$).
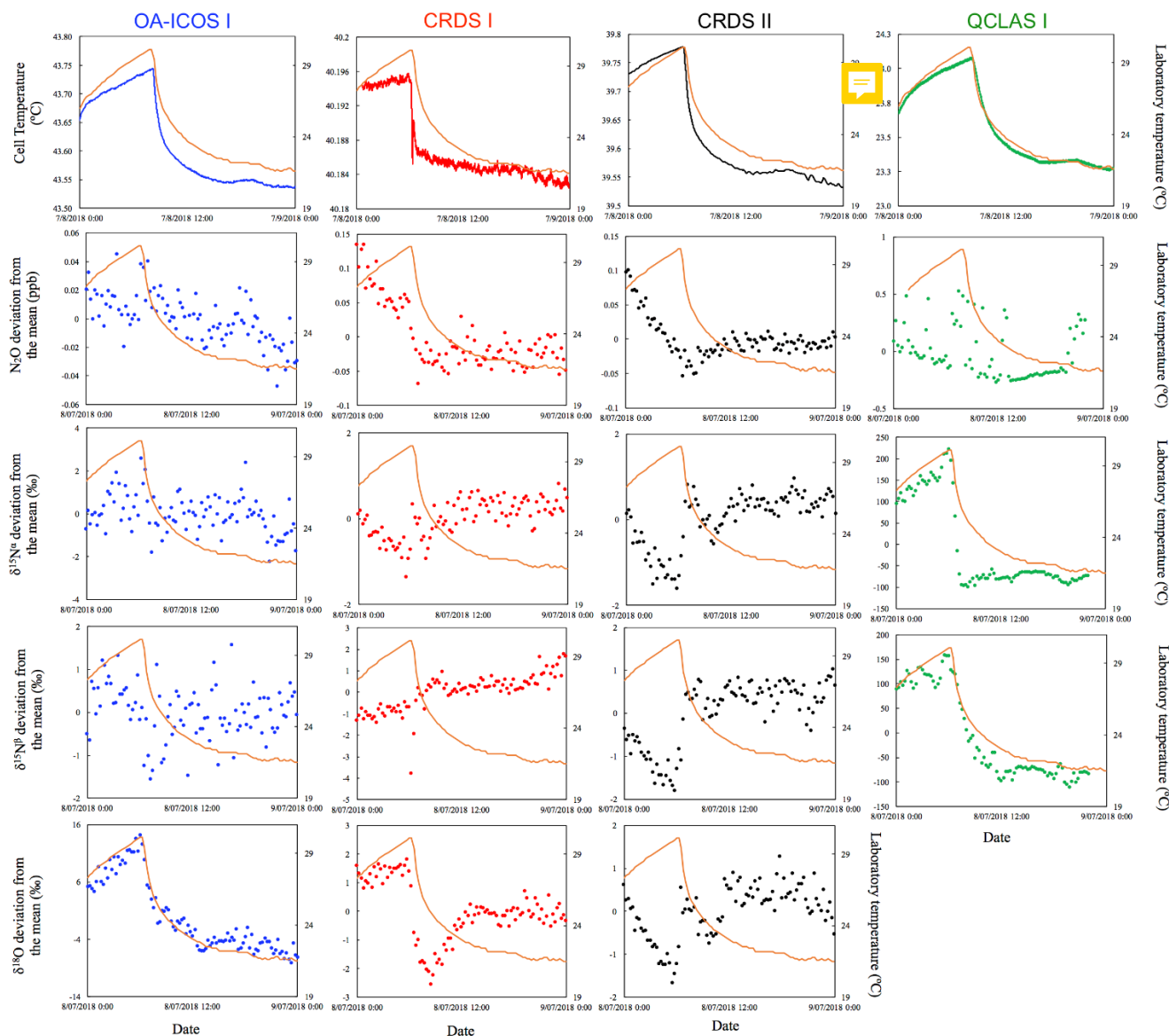
**Fig. 4.** Dependency of the measured [N₂O], $\delta^{15}N^\alpha$, $\delta^{15}N^\beta$ and $\delta^{18}O$ values on laboratory temperature (°C) for OA-ICOS I (blue), CRDS I (red), CRDS II (black) and QCLAS I (green). The laboratory temperature is indicated by a solid orange line and was allowed to vary over time. Cell temperatures for each instrument are also plotted for comparison. Results are plotted as the deviation from the mean, without any anchoring to reference gases.

## 3.3 Repeatability

The best long-term repeatability for δ values was achieved by TREX-QCLAS I with 0.60 ‰ for $\delta^{15}N^{\alpha}$, 0.37 ‰ for $\delta^{15}N^{\beta}$ and 0.46 ‰ for $\delta^{18}O$, even though measurements were taken over a six-month period (Table 7). The best repeatability without preconcentration was achieved by CRDS analyzers with 0.52 –

5 0.75 ‰ for CRDS II and 0.79 – 0.83 ‰ for CRDS I for all δ values. OA-ICOS I achieved repeatability between 1 – 2 ‰ (1.47, 1.19 and 2.17 ‰ for $\delta^{15}N^{\alpha}$, $\delta^{15}N^{\beta}$ and $\delta^{18}O$, respectively). QCLAS I isotopic measurements attained repeatability of 5.4 and 8.6 ‰ for $\delta^{15}N^{\alpha}$ and $\delta^{15}N^{\beta}$, respectively. Short-term repeatability results for 10 repeated 15 min measurements periods over 2.5 h are provided in Supplementary Material 4.

10 **Table 7.** Summary of the measured [$N_2O$], $\delta^{15}N^{\alpha}$, $\delta^{15}N^{\beta}$ and $\delta^{18}O$ and associated 1σ at 300s averaging times based on repeated measurements of PA1.

| Instrument | $n$ | $N_2O$ [ppb] | 1σ $N_2O$ [ppb] | $\delta^{15}N^{\alpha}$ [‰] | 1σ $\delta^{15}N^{\alpha}$ [‰] | $\delta^{15}N^{\beta}$ [‰] | 1σ $\delta^{15}N^{\beta}$ [‰] | $\delta^{18}O$ [‰] | 1σ $\delta^{18}O$ [‰] |
|---|---|---|---|---|---|---|---|---|---|
| CRDS I | 22 | 326.66 | 0.30 | 15.86 | 0.79 | -2.30 | 0.83 | 44.48 | 0.81 |
| CRDS II | 22 | 326.72 | 0.26 | 15.71 | 0.52 | -2.86 | 0.64 | 44.40 | 0.75 |
| OA-ICOS I | 22 | 326.49 | 0.07 | 15.29 | 1.47 | -2.11 | 1.19 | 44.01 | 2.17 |
| QCLAS I | 22 | 326.82 | 0.16 | 13.92 | 5.35 | -2.97 | 8.57 | - | - |
| TREX-QCLAS I | 28 | 326.70 | 1.29 | 15.72 | 0.60 | -2.82 | 0.37 | 44.31 | 0.46 |
| Empa-assigned values | 3 | 326.51 | 0.06 | 15.81 | 0.07 | -3.31 | 0.004 | 44.72 | 0.04 |

## 3.4 Dependence of isotopic measurements on $N_2O$ mole fraction

There was an offset in measured δ values resulting from the change in [$N_2O$] introduced to the analyzers

15 (Fig. 5). A linear relationship between $\Delta\delta^{15}N^{\alpha,\beta}$ and $\Delta\delta^{18}O$ values with [$1/N_2O$] was observed across all analyzers tested, which is characteristic of optical analyzers calibrated using a δ calibration scheme (Griffith et al., 2012; Griffith, 2018). However, examination of the residuals from the linear regression revealed varying degrees of residual curvature, highlighting that further non-linear terms would be required to adequately describe, and correct for, this mole fraction dependence (see Griffith et al.,

20 2012). Repeated analysis of [$N_2O$] dependencies on consecutive days showed similar trends, indicating that the structure of non-linear effects might be stable over short periods of time. Nevertheless, there were small variabilities in δ values at a given $N_2O$ mole fraction, which could be due to the inherent

uncertainty of the measurement and/or day–to–day variations in the mole fraction dependence. The standard deviation of individual 5 min averages of $\delta^{15}N^{\alpha,\beta}$ and $\delta^{18}O$ also varied according to the [N$_2$O] measured by each analyzer due to variations in the signal:noise ratio (Supplementary Material 5).
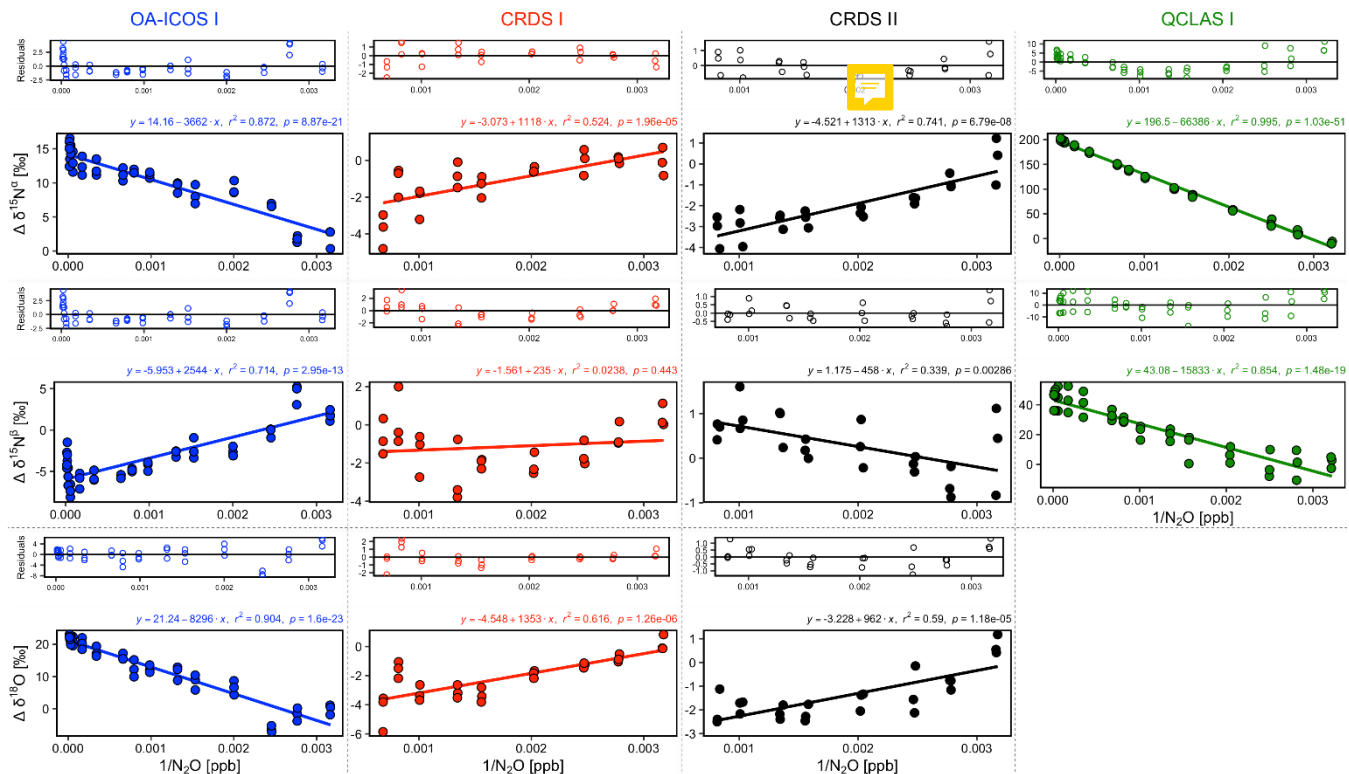
**Fig. 5.** Deviations of the measured $\delta^{15}N^{\alpha}$, $\delta^{15}N^{\beta}$ and $\delta^{18}O$ values according to 1/[N$_2$O] for the OA-ICOS I (blue), CRDS I (red), CRDS II (black) and QCLAS I (green). Measurements span the manufacturer-specified operational ranges of the analyzers. The experiment was repeated on three separate days. A linear regression is indicated by the solid line, and a residual plot is provided above each plot. Individual linear equations, coefficients of determination ($r^2$) and $p$-values are indicated above each plot.

### 3.5 Gas matrix effects (O$_2$ and Ar)

### 3.5.1 Gas matrix effects at ambient N$_2$O mole fractions

With the exception of TREX-QCLAS I, all instruments displayed strong O$_2$ dependencies for [N$_2$O] and $\delta$ values (Fig. 6). For these instruments, linear regressions best described the offset of measured [N$_2$O] and $\delta$ values resulting from the change in O$_2$ composition of the matrix gas. Importantly, CRDS I and II

displayed different degrees of $O_2$ interference on $[N_2O]$ and $\delta$ values, suggesting that these dependencies were either analyzer-specific or differences were due to hardware/software modifications between different production years. Preconcentration prior to analysis, as performed in TREX–QCLAS I, eliminated $O_2$ dependencies as the gas matrix was normalized to synthetic air (20.5 % $O_2$).

The change in Ar composition of the matrix gas caused minor, yet measurable, interferences on $[N_2O]$ and $\delta$ measurements (Fig. 7). The range investigated was between approximately 0 % and 0.95 % Ar, and as such the effects were significantly smaller than that observed for $O_2$. The interference effects were found to be best described by second-order polynomial functions, though we expect that a linear fit would serve equally well if a wider range of effects were investigated. Whilst most functions to describe the dependence on Ar across all instruments were statistically significant ($p < 0.05$), maximum effects were typically only one-tenth of maximum $O_2$ effects, and did not transgress the repeatability ($1\sigma$) of the Anchor gas measurements. TREX-QCLAS I measurements were not impaired by gas matrix effects.
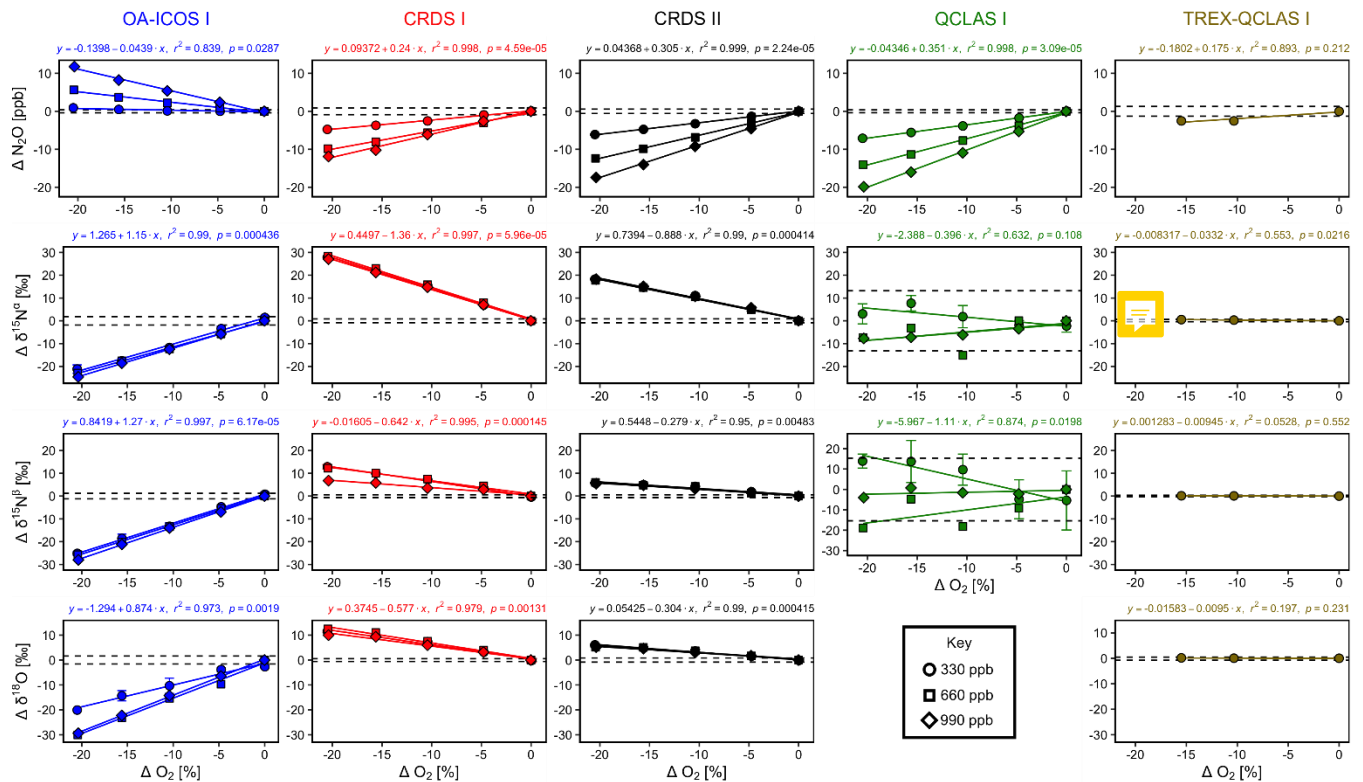
**Fig. 6.** Deviations of the measured [$N_2O$], $\delta^{15}N^\alpha$, $\delta^{15}N^\beta$ and $\delta^{18}O$ values according to $\Delta O_2$ (%) at different $N_2O$ mole fractions (330, 660 and 990 ppb) for the OA-ICOS I (blue), CRDS I (red), CRDS II (black), QCLAS I (green) and TREX-QCLAS I (brown). The standard deviation of the Anchor gas (±1σ) is indicated by dashed lines. Data points represent the mean and standard deviation (1σ) of triplicate measurements. Dependencies are best-described using linear regression, which are indicated by a solid line. Individual equations, coefficients of determination ($r^2$) and $p$-values are indicated above each plot for the 330 ppb $N_2O$ data only.
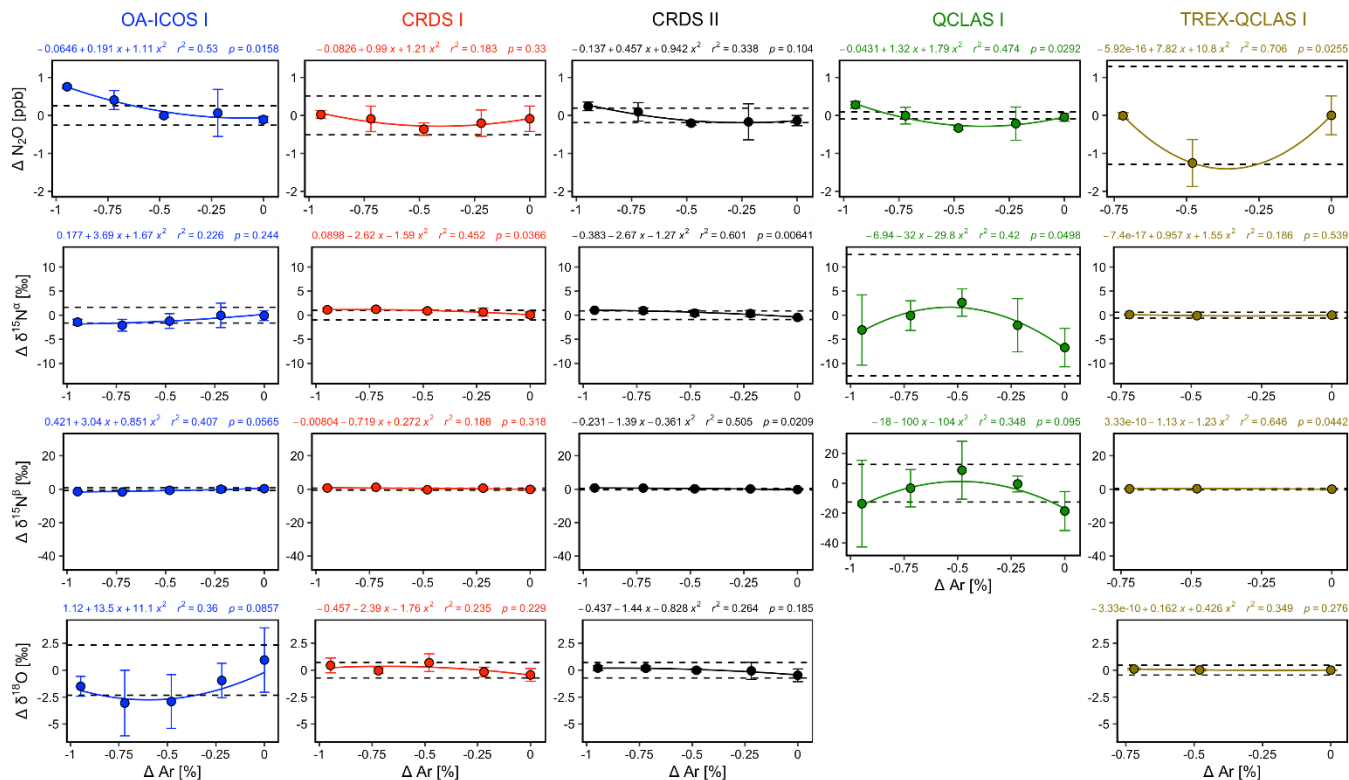
**Fig. 7.** Deviations of the measured $[N_2O]$, $\delta^{15}N^\alpha$, $\delta^{15}N^\beta$ and $\delta^{18}O$ values according to $\Delta Ar$ (%) for the OA-ICOS I (blue), CRDS I (red), CRDS II (black), QCLAS I (green) and TREX-QCLAS I (brown). Data points represent the mean and standard deviation (1$\sigma$) of triplicate measurements. Dependencies are best-described by polynomial fits, which are indicated by solid lines. Individual equations, coefficients of determination ($r^2$) and $p$-values are indicated above each plot.

### 3.5.2 Continuity of gas matrix corrections at higher $N_2O$ mole fractions

When mole fractions of 660 and 990 ppb $N_2O$ were measured by the laser spectrometers, $O_2$ interference effects on $[N_2O]$ and $\delta$ values were well-described using linear regression, albeit with different slopes to those obtained for 330 ppb $N_2O$ (Fig. 6; Table 8).

**Table 8.** Summary of regression slopes and coefficients of determination ($r^2$) for $O_2$ interferences performed at different $N_2O$ mole fractions (330, 660 and 990 ppb) for OA-ICOS I, CRDS I and II, and QCLAS I.

| $\Delta O_2$ [%] | Co-measured $N_2O$ [ppb] | OA-ICOS I | | CRDS I | | CRDS II | | QCLAS I | |
|---|---|---|---|---|---|---|---|---|---|
| | | Slope | $r^2$ | Slope | $r^2$ | Slope | $r^2$ | Slope | $r^2$ |
| $N_2O$ [ppb] | 330 | -0.044 | 0.84 | 0.24 | 1.00 | 0.305 | 1.00 | 0.351 | 1.00 |
| | 660 | -0.273 | 0.98 | 0.478 | 0.99 | 0.608 | 1.00 | 0.690 | 1.00 |
| | 990 | -0.570 | 0.99 | 0.61 | 0.99 | 0.859 | 1.00 | 0.979 | 1.00 |
| $\delta^{15}N^{\alpha}$ [‰] | 330 | 1.146 | 0.99 | -1.364 | 1.00 | -0.888 | 0.99 | n.s. | n.s. |
| | 660 | 1.116 | 1.00 | -1.387 | 1.00 | -0.874 | 0.99 | n.s. | n.s. |
| | 990 | 1.204 | 1.00 | -1.326 | 1.00 | -0.891 | 0.99 | 0.374 | 0.90 |
| $\delta^{15}N^{\beta}$ [‰] | 330 | 1.270 | 1.00 | -0.642 | 1.00 | -0.279 | 0.95 | -1.111 | 0.87 |
| | 660 | 1.282 | 1.00 | -0.580 | 0.98 | -0.303 | 0.96 | n.s. | n.s. |
| | 990 | 1.361 | 1.00 | -0.319 | 0.96 | -0.273 | 0.99 | n.s. | n.s. |
| $\delta^{18}O$ [‰] | 330 | 0.874 | 0.97 | -0.577 | 0.98 | -0.304 | 0.99 | n.d. | n.d. |
| | 660 | 1.419 | 0.99 | -0.621 | 0.98 | -0.267 | 0.94 | n.d. | n.d. |
| | 990 | 1.446 | 1.00 | -0.507 | 0.97 | -0.256 | 0.98 | n.d. | n.d. |

n.d. not determined

n.s. not statistically significant at $p < 0.05$

We could not adequately predict the nature in which the slopes of the interference effects scaled with $N_2O$ mole fractions. Overall, this suggests that interference effects were analyzer-specific and varied according to instrumental-specific parameters, rather than due to *bona fide* scaling of the pressure broadening effect. Therefore, to account for combined effects of [$O_2$] and [$N_2O$] changes on measurements, a user would be required to perform a series of laboratory tests across the range of expected [$O_2$] and [$N_2O$]. In an exemplary approach, we applied a series of empirical equations (Eqs. 5 – 6) to predict the offset of measured [$N_2O$] and δ values caused by changes in [$O_2$] as a function of [$N_2O$] introduced to the analyzers in this study:

$$\Delta[N_2O]_{meas,mix}\left(\Delta[O_2]_A, [N_2O]_{exp,mix}\right) = \left(A \cdot [N_2O]_{exp,mix}^2 + B \cdot [N_2O]_{exp,mix}\right) \cdot \Delta[O_2]_A \qquad (5)$$

$$\Delta\delta_{meas,mix}\left(\Delta[O_2]_A, [N_2O]_{exp,mix}\right) = \left(a \cdot [N_2O]_{exp,mix}^2 + b \cdot [N_2O]_{exp,mix} + c\right) \cdot \Delta[O_2]_A \qquad (6)$$

where $\Delta[N_2O]_{meas,mix}$ and $\Delta\delta_{meas,mix}$ are the measured offsets on [N$_2$O] and $\delta$ values for the gas mixtures introduced to the analyzers as reported in Sect. 3.5.1, respectively; $\Delta[O_2]_A$ is the difference in O$_2$ mole fraction between the gas mixture and Anchor gas as reported in Sect. 3.5.1; $[N_2O]_{exp,mix}$ is the expected [N$_2$O] of gas mixtures introduced to the analyzer, calculated based on gas flows and cylinder compositions of Gases 1, 2 and 3 as reported in Sect. 2.4.5; A and B, and a, b and c are analyzer-specific constants.

Using Eqs. (5) and (6) to fit values for the constants A and B for $\Delta[N_2O]_{meas,mix}$, and a, b and c for $\Delta\delta_{meas,mix}$ resulted in a total of 11 analyzer-specific values (Supplementary Material 6). With gas-specific constants established, interferences on [N$_2$O] and $\delta$ measurements for a sample gas G for a given analyzer can be corrected using Eqs. (7–8):

$$[N_2O]_{mc,G} = \frac{-(1+B\cdot\Delta[O_2]_G)+\sqrt{(1+B\cdot\Delta[O_2]_G)^2+4\cdot A\cdot\Delta[O_2]_G\cdot[N_2O]_{meas,G}}}{2\cdot A\cdot\Delta[O_2]_G} \qquad (7)$$

$$\delta_{mc,G} = \delta_{meas,G} - \left(a \cdot [N_2O]_{mc,G}^2 + b \cdot [N_2O]_{mc,G} + c\right) \cdot \Delta[O_2]_G \qquad (8)$$

where $[N_2O]_{mc,G}$ and $\delta_{mc,G}$ are the matrix-corrected [N$_2$O] and $\delta$ values of sample gas G, respectively; $\Delta[O_2]_G$ is the difference in O$_2$ mole fraction between sample gas G and reference gases. Correction using Eqs. (7–8) removes the O$_2$ effect to a degree that corrected measurements from Sect. 3.5.1 are typically within the uncertainty bounds of the anchor (Supplementary Material 6).

Although Ar effects seemingly scaled with increased N$_2$O mole fractions (not shown in Fig. 7 for clarity), we did not derive scaling coefficients for Ar because the derived Ar correction equations at 330, 660 and 990 ppb N$_2$O were typically not statistically significant at $p < 0.05$. These interferences also did not always exceed the repeatability of Anchor gas measurements. While the effects could be more fully investigated with higher levels of Ar, we limited the investigated to Ar levels close to ambient conditions.

### 3.6 Trace gas effects ($H_2O$, $CO_2$, $CH_4$ and CO)

### 3.6.1 Trace gas effects at ambient $N_2O$ mole fractions

The apparent offset of [$N_2O$] and $\delta$ values resulting from the change in $CO_2$ composition of the matrix gas were best described by linear functions (Fig. 8). OA-ICOS I exhibited discrete and well-defined linear interference effects of $CO_2$ on [$N_2O$], $\delta^{15}N^{\alpha}$, $\delta^{15}N^{\beta}$ and $\delta^{18}O$ (all $r^2 > 0.95$), likely due to crosstalk between $CO_2$ absorption lines situated near 2192.46 $cm^{-1}$ and 2192.33 $cm^{-1}$. Both CRDS instruments showed $CO_2$ interference effects of smaller magnitude for [$N_2O$], $\delta^{15}N^{\alpha}$ and $\delta^{18}O$, presumably due to $CO_2$ absorption lines at 2196.21 $cm^{-1}$, 2195.72 $cm^{-1}$ and 2196.02 $cm^{-1}$. QCLAS I displayed less well-defined $CO_2$ interference effects for $\delta^{15}N^{\beta}$, which was possibly due to several overlapping absorption lines of $CO_2$ located near 2187.85 $cm^{-1}$. All linear functions derived for the TREX-QCLAS I were not statistically significant at $p < 0.05$. As shown in Fig. 8, the NaOH trap was effective in removing the $CO_2$ effect (if present) across the mole fraction ranges tested for all instruments.

Similarly, $CH_4$ effects on apparent [$N_2O$] and $\delta$ values were well-described by linear functions (Fig. 9). The largest effects were for CRDS I and II, which both displayed strong $CH_4$ dependencies for $\delta^{15}N^{\alpha}$ and $\delta^{18}O$ of similar magnitude. This might be due to crosstalk of $^{14}N^{15}N^{16}O$ and $^{14}N^{14}N^{18}O$ absorption lines with the respective $CH_4$ lines located at 2195.76 $cm^{-1}$ and 2195.95 $cm^{-1}$. For OA-ICOS I, minor $CH_4$ effects were observed for $\delta^{15}N^{\beta}$, due to absorption line overlap at 2192.33 $cm^{-1}$. QCLAS I did not display any $CH_4$ interference effect over the tested [$CH_4$] range. Linear functions derived for the TREX-QCLAS I were not statistically significant at $p < 0.05$. The similarity between the [$N_2O$] dependencies on $CH_4$ mole fractions for OA-ICOS I, CRDS I, II and QCLAS I suggests that the apparent effects may be due to small fluctuations in the gas mixtures produced by the MFCs, rather than a discrete spectral interference effect.

The CRDS analyzers showed minor interference effects for $\delta^{15}N^{\alpha}$ and $\delta^{15}N^{\beta}$ on [CO] (0.14 – 2.14 ppm) (Fig. 10), likely due to crosstalk with CO absorption lines located at 2195.69 $cm^{-1}$ and 2195.83 $cm^{-1}$. The magnitude of these effects was similar for both models. QCLAS I displayed interference effects for

$\delta^{15}N^\alpha$ and $\delta^{15}N^\beta$ caused by a CO absorption line located near 2187.9 cm$^{-1}$, although this effect did not exceed the repeatability of the Anchor gas (containing no CO) over the measurement range. The effects of [CO] on $\delta$ values acquired using OA-ICOS I and TREX-QCLAS I were not statistically significant at $p < 0.05$. Similar to $CH_4$, the resemblance of [CO] effects on [$N_2O$] measurements for OA-ICOS I, CRDS I, II and QCLAS I suggests that the apparent effects may be due to inaccuracies in the dynamic dilution process, rather than a discrete spectral interference effect. As shown in Fig. 10, the Sofnocat trap was effective in removing CO (if present) across the mole fraction ranges tested for all instruments.

OA-ICOS I exhibited large effects of [$H_2O$] (0 – 13800 ppm) on $\delta^{15}N^\beta$ (up to -10 ‰) and $\delta^{18}O$ (up to -15 ‰), and minor dependencies for $\delta^{15}N^\alpha$ (up to 4 ‰) and [$N_2O$] (up to 1 ppb) across the range tested (Fig. 11). For QCLAS I, the $H_2O$ effect was largest for $\delta^{15}N^\alpha$ (up to 20 ‰), whilst minor effects for [$N_2O$] (up to 2 ppb) were observed in relation to the Anchor gas (no $H_2O$). In contrast, both CRDS instruments showed no significant effects across the range tested, which is attributable to the installation of permeation dryers inside the analyzers by the manufacturer.
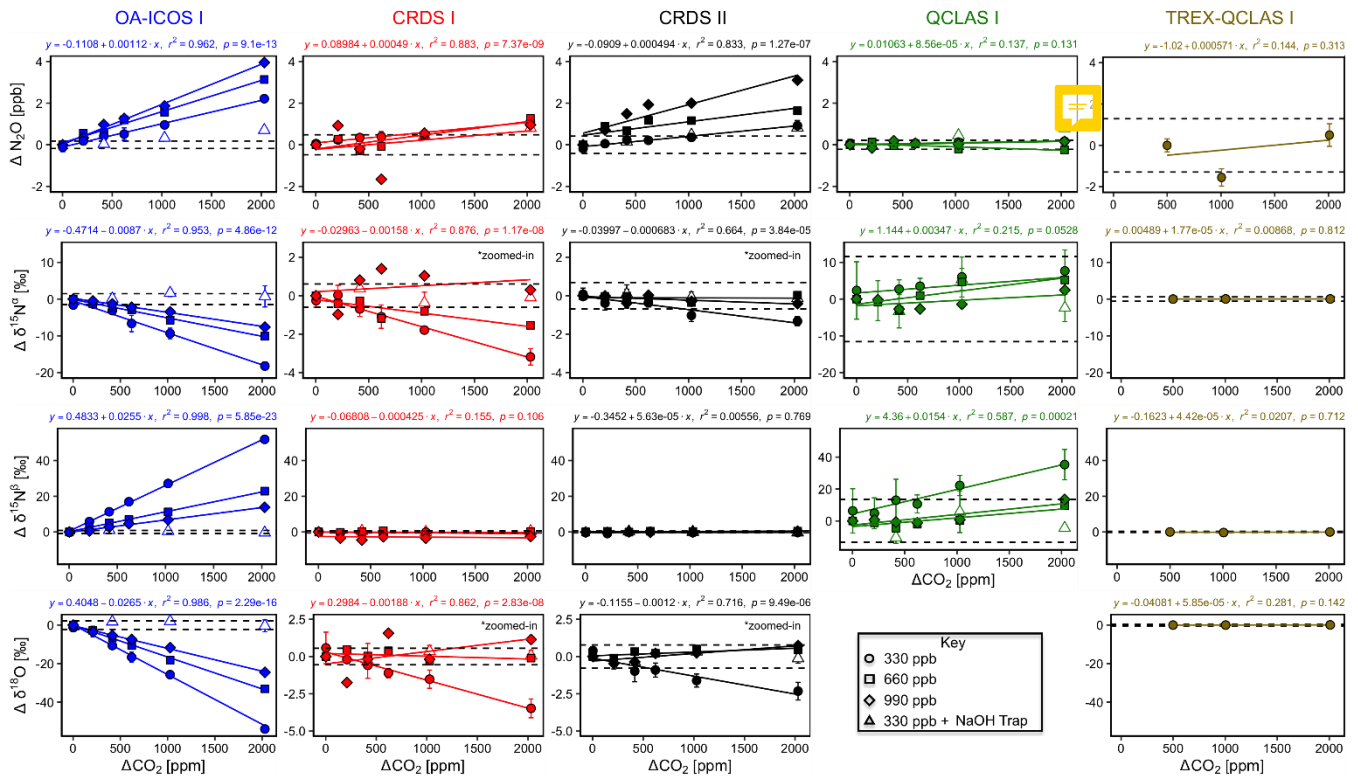
**Fig. 8.** Deviations of the measured [N₂O], $\delta^{15}N^{\alpha}$, $\delta^{15}N^{\beta}$ and $\delta^{18}O$ values according to $\Delta CO_2$ (ppm) at different N₂O mole fractions (330, 660 and 990 ppb) for the OA-ICOS I (blue), CRDS I (red), CRDS II (black), QCLAS I (green) and TREX-QCLAS I (brown). The standard deviation of the Anchor gas ($\pm 1\sigma$) is indicated by dashed lines. Data points represent the mean and standard deviation ($1\sigma$) of triplicate measurements. Dependencies are best-described by linear fits, which are indicated by solid lines. Individual equations, coefficients of determination ($r^2$) and $p$-values are indicated above each plot for the 330 ppb N₂O data only.
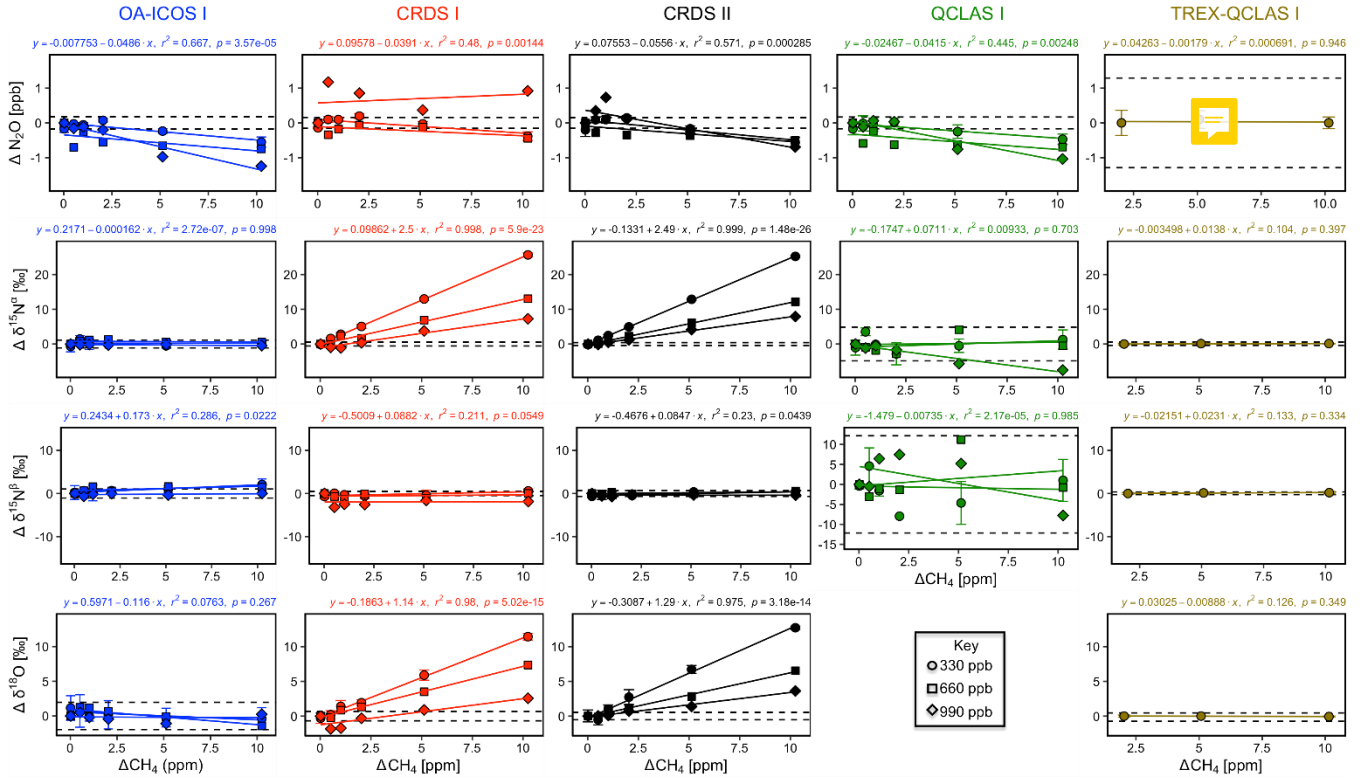
**Fig. 9.** Deviations of the measured [$N_2O$], $\delta^{15}N^\alpha$, $\delta^{15}N^\beta$ and $\delta^{18}O$ values according to $\Delta CH_4$ (ppm) at different $N_2O$ mole fractions (330, 660 and 990 ppb) for the OA-ICOS I (blue), CRDS I (red), CRDS II (black), QCLAS I (green) and TREX-QCLAS I (brown). Data points represent the mean and standard deviation (1σ) of triplicate measurements. Dependencies are best-described by linear fits, which are indicated by solid lines. Individual equations, coefficients of determination ($r^2$) and $p$-values are indicated above each plot for the 330 ppb $N_2O$ data only.
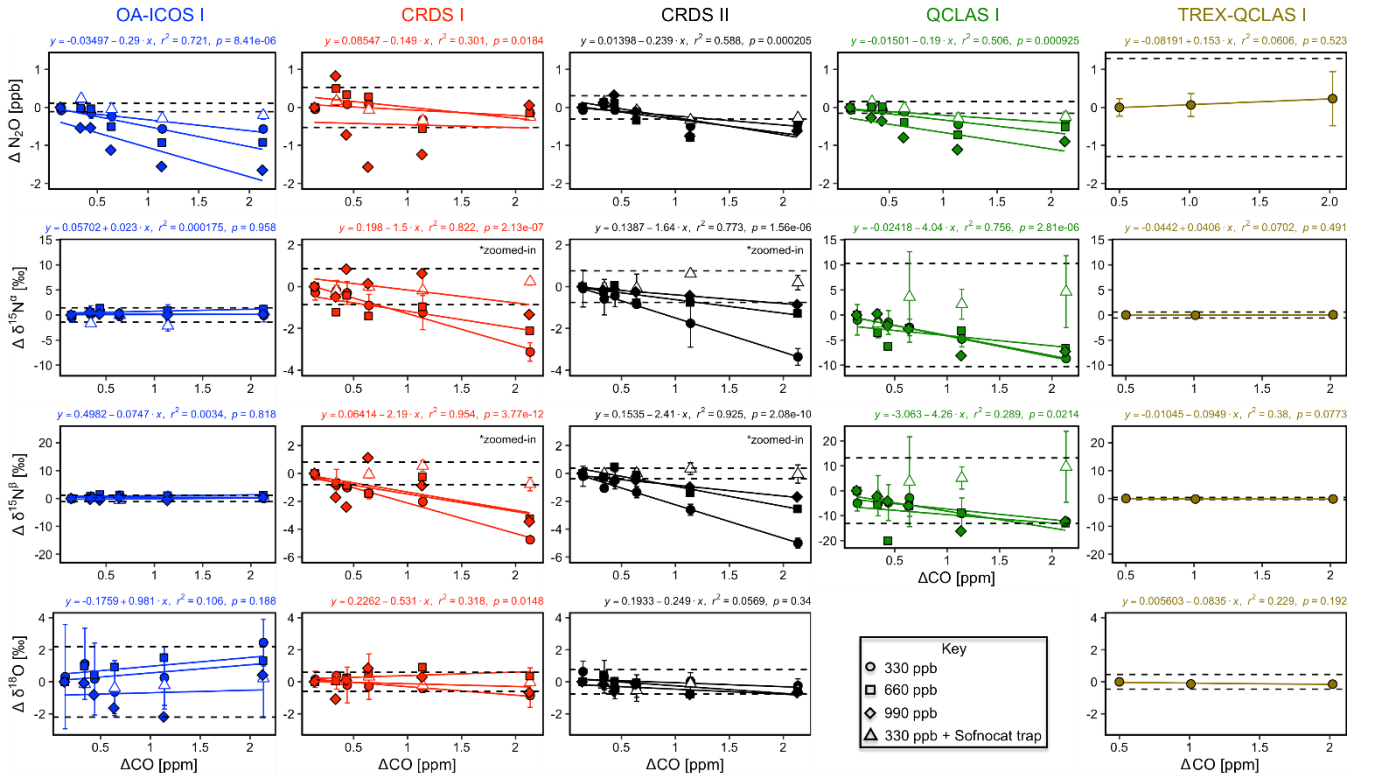
**Fig. 10.** Deviations of the measured [N₂O], δ¹⁵Nᵅ, δ¹⁵Nᵝ and δ¹⁸O values according to ΔCO (ppm) at different N₂O mole fractions (330, 660 and 990 ppb) for OA-ICOS I (blue), CRDS I (red), CRDS II (black), QCLAS I (green) and TREX-QCLAS I (brown). The standard deviation of the Anchor gas (±1σ) is indicated by dashed lines. Data points represent the mean and standard deviation (1σ) of triplicate measurements. Dependencies are best-described by linear fits, which are indicated by solid lines. Individual equations, coefficients of determination (*r²*) and *p*-values are indicated above each plot for the 330 ppb N₂O data only.

**Fig. 11.** Deviations of the measured [N₂O], $\delta^{15}N^\alpha$, $\delta^{15}N^\beta$ and $\delta^{18}O$ values according to $\Delta H_2O$ (ppm) for OA-ICOS I (blue), CRDS I (red), CRDS II (black) and QCLAS I (green). The standard deviation of the Anchor gas (±1σ) is indicated by dashed lines. Data points represent the mean and standard deviation (1σ) of triplicate measurements. Dependencies are best-described by either linear or polynomial fits, which are indicated by solid lines. Individual equations, coefficients of determination ($r^2$) and $p$-values are indicated above each plot.

### 3.6.2 Continuity of trace gas corrections at higher N₂O mole fractions

Interference effects from $CO_2$, $CH_4$ and $CO$ on apparent δ values, where significant, inversely scaled with increasing [N₂O] (Figs. 8, 9 and 10; Table 9). The scaling of trace gas effects can be explained by simple spectral overlap of the $^{14}N^{15}N^{16}O$, $^{15}N^{14}N^{16}O$ and $^{14}N^{14}N^{18}O$ lines with those of the trace gas, which results in the interference effects being inversely proportional to the mixing ratio of N₂O. However, there may be additional spectral overlap between the trace gas and the $^{14}N^{14}N^{16}O$ peak resulting in an offset for the measured [N₂O], which introduces a further shift in the δ values (as shown in Sect. 3.4). The effect on the apparent [N₂O] was less clear and was possibly confounded by

inaccuracies during dynamic gas mixing. In this study, the scaling of interference effects from trace gases as a function of the $[N_2O]$ introduced to the analyzers could be described using Eqs. (9) and (10):

$$\Delta[N_2O]_{meas,mix}\big(\Delta[x]_A, [N_2O]_{exp,mix}\big) = \left(A_x \frac{1}{[N_2O]_{exp,mix}} + B_x\right) \cdot \Delta[x]_A \tag{9}$$

$$\Delta\delta_{meas,mix}\big(\Delta[x]_A, [N_2O]_{exp,mix}\big) = \left(a_x * \frac{1}{[N_2O]_{exp,mix}} + b_x\right) \cdot \Delta[x]_A \tag{10}$$

5   where $\Delta[N_2O]_{meas,mix}$ and $\Delta\delta_{meas,mix}$ are the measured offsets on $[N_2O]$ and δ values for the gas mixtures introduced to the analyzers as reported in Sect. 3.6.1, respectively; $\Delta[x]_A$ is the difference in trace gas mole fraction between the gas mixture and Anchor gas as reported in Sect. 3.6.1; and $A_x$, $B_x$, $a_x$ and $b_x$ are constants that are trace gas and instrument specific. The constant $b_x$ only occurs when there is spectral overlap from the trace gas and $^{14}N^{14}N^{16}O$ absorption lines.

For a sample gas G, the effect can then be corrected by using Eq. (11) and Eq. (12):

$$[N_2O]_{tc,G} = [N_2O]_{meas,G} - \Sigma_x\left(\left(A_x \frac{1}{[N_2O]_{meas,G}} + B_x\right) \cdot \Delta[x]_G\right) \tag{11}$$

$$\delta_{tc,G} = \delta_{meas,G} - \Sigma_x\left(\left(a_x \frac{1}{[N_2O]_{meas,G}} + b_x\right) \cdot \Delta[x]_G\right) \tag{12}$$

In Eqs. (11–12), the sum of the effect of all interfering gases with overlapping absorption lines is taken
15   into account. Similar to Section 3.5.2, correction using Eqs. (11–12) removes the trace gas interference effects to the extent that corrected measurements from Sect. 3.6.1 are within the repeatability bounds of the Anchor gas (Supplementary Material 6). Similar inverse relationships have been described by Malowany et al. (2015) for $H_2S$ interferences on $\delta^{13}C$-$CO_2$.

**Table 9.** Summary of regression slopes and coefficients of determination ($r^2$) for trace gas interferences ($CO_2$, $CH_4$ and CO) performed at different $N_2O$ mole fractions (330, 660 and 990 ppb) for OA-ICOS I, CRDS I and II, and QCLAS I.

| | | OA-ICOS I | | CRDS I | | CRDS II | | QCLAS I | |
|---|---|---|---|---|---|---|---|---|---|
| $\Delta CO_2$ [ppm] | Co-measured $N_2O$ [ppb] | Slope | $r^2$ | Slope | $r^2$ | Slope | $r^2$ | Slope | $r^2$ |
| | 330 | $1.12 \cdot 10^{-3}$ | 0.96 | $4.90 \cdot 10^{-4}$ | 0.88 | $4.94 \cdot 10^{-4}$ | 0.83 | n.s. | n.s. |
| $N_2O$ [ppb] | 660 | $1.50 \cdot 10^{-3}$ | 0.99 | $6.57 \cdot 10^{-4}$ | 0.75 | $6.45 \cdot 10^{-4}$ | 0.73 | $-1.64 \cdot 10^{-4}$ | 0.70 |
| | 990 | $1.92 \cdot 10^{-3}$ | 0.99 | n.s. | n.s. | $1.37 \cdot 10^{-3}$ | 0.87 | n.s. | n.s. |
| | 330 | $-8.70 \cdot 10^{-3}$ | 0.95 | $-1.58 \cdot 10^{-3}$ | 0.88 | $-6.83 \cdot 10^{-4}$ | 0.66 | n.s. | n.s. |
| $\delta^{15}N^\alpha$ [‰] | 660 | $-5.01 \cdot 10^{-3}$ | 0.99 | $-6.95 \cdot 10^{-4}$ | 0.76 | n.s. | n.s. | n.s. | n.s. |
| | 990 | $-3.80 \cdot 10^{-3}$ | 1.00 | n.s. | n.s. | n.s. | n.s. | n.s. | n.s. |
| | 330 | $2.55 \cdot 10^{-2}$ | 1.00 | n.s. | n.s. | n.s. | n.s. | $1.54 \cdot 10^{-2}$ | 0.59 |
| $\delta^{15}N^\beta$ [‰] | 660 | $1.11 \cdot 10^{-2}$ | 1.00 | n.s. | n.s. | n.s. | n.s. | $5.50 \cdot 10^{-3}$ | 0.70 |
| | 990 | $6.94 \cdot 10^{-3}$ | 0.99 | n.s. | n.s. | n.s. | n.s. | $6.64 \cdot 10^{-3}$ | 0.76 |
| | 330 | $-2.65 \cdot 10^{-2}$ | 0.99 | $-1.88 \cdot 10^{-3}$ | 0.86 | $-1.20 \cdot 10^{-3}$ | 0.72 | n.d. | n.d. |
| $\delta^{18}O$ [‰] | 660 | $-1.66 \cdot 10^{-2}$ | 1.00 | n.s. | n.s. | n.s. | n.s. | n.d. | n.d. |
| | 990 | $-1.18 \cdot 10^{-2}$ | 1.00 | n.s. | n.s. | $5.09 \cdot 10^{-4}$ | 0.72 | n.d. | n.d. |
| $\Delta CH_4$ [ppm] | | | | | | | | | |
| | 330 | $-4.86 \cdot 10^{-2}$ | 0.67 | $-3.91 \cdot 10^{-2}$ | 0.48 | $-5.56 \cdot 10^{-2}$ | 0.57 | $-4.15 \cdot 10^{-2}$ | 0.45 |
| $N_2O$ [ppb] | 660 | n.s. | n.s. | n.s. | n.s. | n.s. | n.s. | n.s. | n.s. |
| | 990 | $-1.28 \cdot 10^{-1}$ | 0.92 | n.s. | n.s. | $-1.06 \cdot 10^{-1}$ | 0.69 | $-1.14 \cdot 10^{-1}$ | 0.88 |
| | 330 | n.s. | n.s. | $2.50 \cdot 10^{0}$ | 1.00 | $2.49 \cdot 10^{0}$ | 1.00 | n.s. | n.s. |
| $\delta^{15}N^\alpha$ [‰] | 660 | n.s. | n.s. | $1.29 \cdot 10^{0}$ | 0.98 | $1.22 \cdot 10^{0}$ | 1.00 | n.s. | n.s. |
| | 990 | n.s. | n.s. | $8.26 \cdot 10^{-1}$ | 0.95 | $8.13 \cdot 10^{-1}$ | 0.99 | $-7.59 \cdot 10^{-1}$ | 0.93 |
| $\delta^{15}N^\beta$ [‰] | 330 | $1.73 \cdot 10^{-1}$ | 0.29 | n.s. | n.s. | $8.47 \cdot 10^{-2}$ | 0.23 | n.s. | n.s. |
| | 660 | n.s. | n.s. | n.s. | n.s. | n.s. | n.s. | n.s. | n.s. |

| | | | | | | | | |
|---|---|---|---|---|---|---|---|---|
| | 990 | n.s. | n.s. | n.s. | n.s. | n.s. | n.s. | n.s. | n.s. |
| $\delta^{18}O$ [‰] | 330 | n.s. | n.s. | $1.14\cdot10^{0}$ | 0.98 | $1.29\cdot10^{-1}$ | 0.97 | n.d. | n.d. |
| | 660 | $-2.21\cdot10^{-1}$ | 0.74 | $7.34\cdot10^{-1}$ | 0.99 | $6.36\cdot10^{-1}$ | 0.99 | n.d. | n.d. |
| | 990 | n.s. | n.s. | $3.76\cdot10^{-1}$ | 0.79 | $3.55\cdot10^{-1}$ | 0.98 | n.d. | n.d. |
| $\Delta CO$ [ppm] | | | | | | | | | |
| $N_2O$ [ppb] | 330 | $-2.90\cdot10^{-1}$ | 0.72 | $-1.49\cdot10^{-1}$ | 0.30 | $-2.39\cdot10^{-1}$ | 0.59 | $-1.90\cdot10^{-1}$ | 0.51 |
| | 660 | $-5.29\cdot10^{-1}$ | 0.76 | n.s. | n.s. | n.s. | n.s. | n.s. | n.s. |
| | 990 | $-7.72\cdot10^{-1}$ | 0.76 | n.s. | n.s. | n.s. | n.s. | n.s. | n.s. |
| $\delta^{15}N^{\alpha}$ [‰] | 330 | n.s. | n.s. | $-1.50\cdot10^{0}$ | 0.82 | $-1.64\cdot10^{0}$ | 0.77 | $-4.04\cdot10^{0}$ | 0.76 |
| | 660 | n.s. | n.s. | n.s. | n.s. | $-6.49\cdot10^{-1}$ | 0.81 | n.s. | n.s. |
| | 990 | n.s. | n.s. | n.s. | n.s. | $-4.16\cdot10^{-1}$ | 0.98 | $-4.17\cdot10^{0}$ | 0.73 |
| $\delta^{15}N^{\beta}$ [‰] | 330 | n.s. | n.s. | $-2.19\cdot10^{0}$ | 0.95 | $-2.41\cdot10^{0}$ | 0.92 | $-4.26\cdot10^{0}$ | 0.29 |
| | 660 | n.s. | n.s. | $-1.31\cdot10^{0}$ | 0.67 | $-1.44\cdot10^{0}$ | 0.89 | n.s. | n.s. |
| | 990 | n.s. | n.s. | n.s. | n.s. | $-7.86\cdot10^{-1}$ | 0.95 | n.s. | n.s. |
| $\delta^{18}O$ [‰] | 330 | n.s. | n.s. | $-5.31\cdot10^{-1}$ | 0.32 | | n.s. | n.d. | n.d. |
| | 660 | n.s. | n.s. | n.s. | n.s. | n.s. | n.s. | n.d. | n.d. |
| | 990 | n.s. | n.s. | n.s. | n.s. | n.s. | n.s. | n.d. | n.d. |

n.d. not determined

n.s. not statistically significant at $p < 0.05$

### 3.7 Two end-member mixing

Results for the two end-member mixing experiment were evaluated in two different ways. First, results for individual gas mixtures acquired by laser spectroscopy and GC-IRMS were compared to expected [$N_2O$] and $\delta$ values calculated from $N_2O$ mole fractions and isotopic composition of end-members and mixing fractions. Second, source values were extrapolated using a weighted total least squares regression analysis, known as Keeling plot analysis (Keeling, 1958), and compared to assigned $\delta$ values of the *source* gas used in each experiment.

### 3.7.1 Comparison with expected [$N_2O$] and δ values

Triplicate measurements (mean ± 1σ) obtained using the laser spectrometers and GC-IRMS were plotted against expected [$N_2O$] and δ values calculated using MFC flow rates, $N_2O$ mole fractions and isotopic composition of *background* and *source* gases (Figs. 12-15). Comparisons between individual laser spectrometer measurements and GC-IRMS are plotted in Supplementary Material 7, and are discussed only briefly below.

OA-ICOS I

Generally, there was good agreement of [$N_2O$] between the OA-ICOS I and expected values, although the analyzer over-estimated mole fractions at higher $\Delta N_2O$ during experiments 5 and 6 (Fig. 12). There was excellent agreement between the OA-ICOS I and calculated expected δ values (all $r^2 > 0.95$). Measurements for $\delta^{15}N^{\alpha}$ were mostly within ± 2.4 ‰ of expected values, while $\delta^{15}N^{\beta}$, $\delta^{15}N^{bulk}$ and SP were all within ± 2 ‰ of expected values. $\delta^{18}O$ measurements were the poorest performing, but were typically within ± 3.6 ‰ of expected values. Similarly, there was excellent agreement between OA-ICOS I and IRMS isotope values (all $r^2 > 0.95$), which agreed within 1.7–2.4 ‰ (Fig. S6-2). The standard deviations of triplicate isotope measurements decreased dramatically with increasing $\Delta N_2O$, improving from 1 – 2 ‰ during experiments 1 and 2 to typically better than 0.1 ‰ during experiments 5 and 6. Conversely, the standard deviations of triplicate sample measurements for [$N_2O$] increased with increasing $\Delta N_2O$, rising from < 0.1 ppb during experiments 1 through 4, to > 1 ppb during experiments 5 and 6. Nonetheless, all OA-ICOS I [$N_2O$] measurements had better 1σ repeatability than those acquired using GC. The repeatability of the triplicate isotope measurements with OA-ICOS I was typically better than IRMS exclusively at higher $\Delta N_2O$ (> 700 ppb).
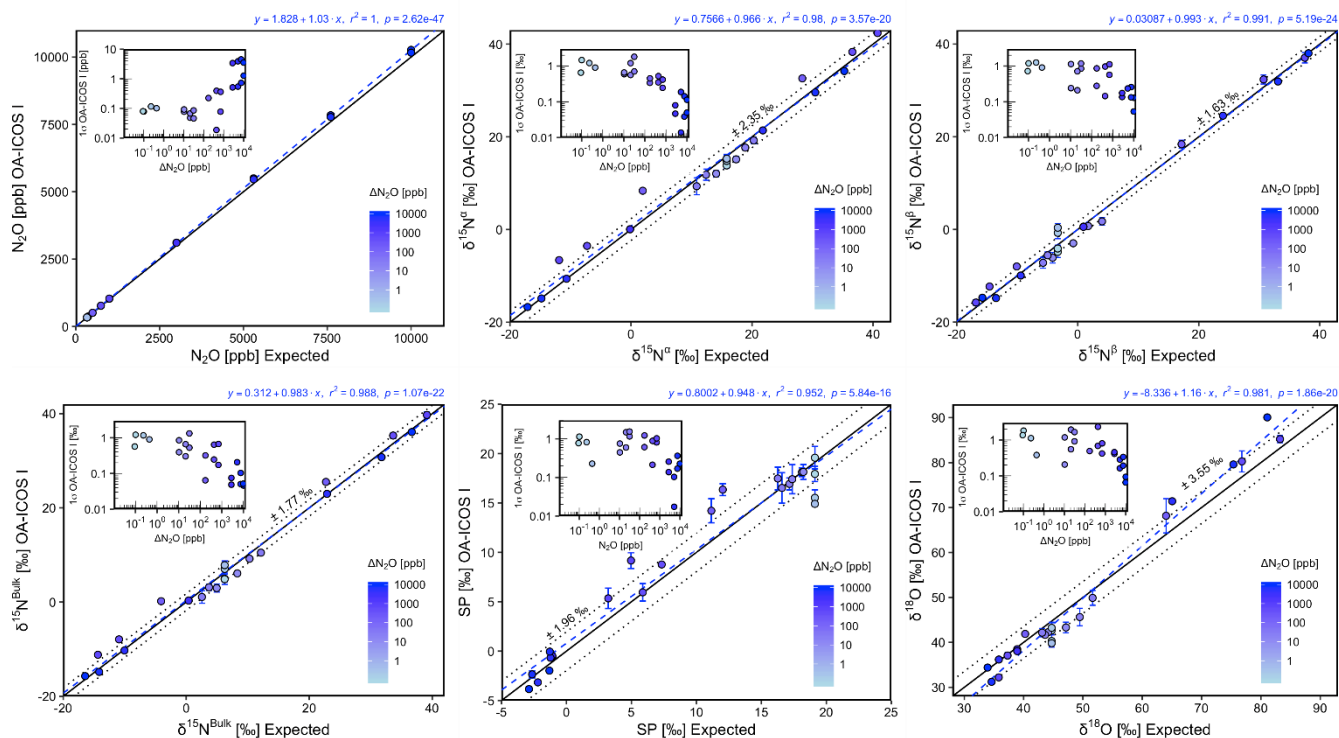
**Fig. 12.** Correlation diagrams for [N₂O], $\delta^{15}N^\alpha$, $\delta^{15}N^\beta$, $\delta^{15}N^{bulk}$, SP and $\delta^{18}O$ measurements at various $\Delta N_2O$ mole fractions analyzed by the OA-ICOS I plotted against expected values. The solid black line denotes the 1:1 line, while the dotted line indicates ±1σ of the residuals from the 1:1 line. The dashed blue line represents a linear fit to the data. Individual equations, coefficients of determination ($r^2$) and p-values are indicated above each plot. Each data point represents the mean and standard deviation (1σ) of triplicate measurements. The inset plots indicate the standard deviation (1σ) of the triplicate measurements achieved at different $\Delta N_2O$ mole fractions, and the 1:1 line is similarly a solid line.

CRDS I

[N₂O] acquired by CRDS I were in good agreement with expected values, although the analyzer slightly under-estimated mole fractions at higher $\Delta N_2O$ during experiments 3 and 4 (Fig. 13). There was excellent agreement between the CRDS I and calculated expected isotope values (all $r^2 > 0.95$). Measurements for $\delta^{15}N^\alpha$ and $\delta^{15}N^\beta$ were mostly better than ± 1.1 ‰ of expected values, while $\delta^{15}N^{bulk}$ was within ± 0.5 ‰ of expected values. SP and $\delta^{18}O$ measurements were typically within ± 1.5 ‰ of expected values. There was excellent agreement between CRDS I and IRMS isotope values (all $r^2 > 0.93$), which agreed to within 0.5 – 1.9 ‰ (Fig. S6-3). In general, the standard deviations of triplicate isotope measurements increased as a function of $\Delta N_2O$, with the lowest deviations of 0.1–1 ‰

occurring when $\Delta N_2O$ < 100 ppb. However, two triplicated measurements for $\delta^{15}N^{bulk}$ had standard deviations better than 0.1 ‰. The standard deviations of triplicate measurements for [$N_2O$] also increased with increasing $\Delta N_2O$ mole fractions, rising from 0.03–0.07 ppb when $\Delta N_2O$ = ~0 ppb (i.e. ambient conditions) to ~1 ppb when $\Delta N_2O$ = ~700 ppb. With the exception of one triplicate

5      measurement, all CRDS I [$N_2O$] measurements had better $1\sigma$ repeatability than those acquired using GC. Overall, IRMS had slightly better repeatability (most ranging from 0.1 – 1 ‰) than CRDS I (most ranging from 0.1 – 2 ‰) for isotopic measurements.
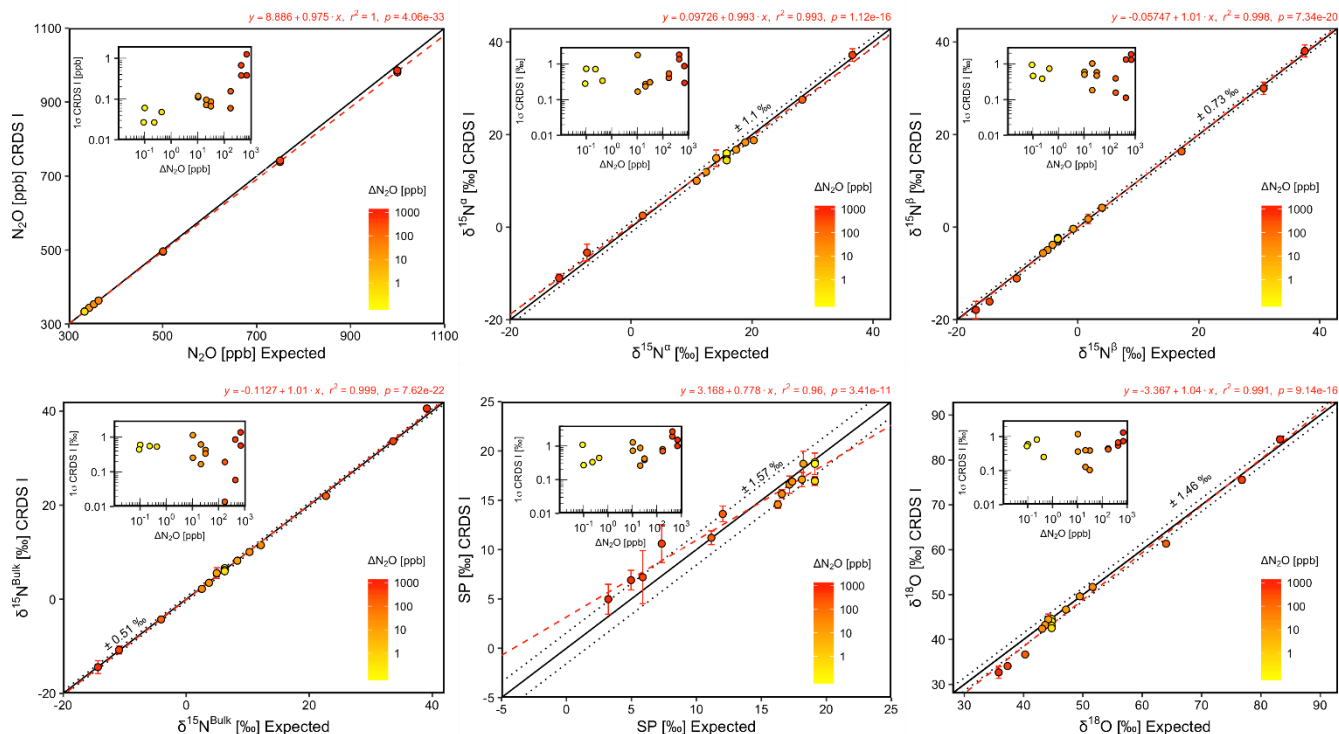
**Fig. 13.** Correlation diagrams for [$N_2O$], $\delta^{15}N^{\alpha}$, $\delta^{15}N^{\beta}$, $\delta^{15}N^{bulk}$, SP and $\delta^{18}O$ measurements at various

10      $\Delta N_2O$ mole fractions analyzed by the CRDS I plotted against expected values. The solid black line denotes the 1:1 line, while the dotted line indicates $\pm 1\sigma$ of the residuals from the 1:1 line. The dashed red line represents a linear fit to the data. Individual equations, coefficients of determination ($r^2$) and $p$-values are indicated above each plot. Each data point represents the mean and standard deviation ($1\sigma$) of triplicate measurements. The inset plots indicate the standard deviation ($1\sigma$) of the triplicate

15      measurements achieved at different $\Delta N_2O$ mole fractions, and the 1:1 line is similarly a solid line.

CRDS II

Similar to results for CRDS I, [$N_2O$] acquired by CRDS II were in good agreement with expected values but slightly under-estimated mole fractions at higher $\Delta N_2O$ during experiments 3 and 4 (Fig. 14). There was excellent agreement between the CRDS II and calculated expected isotope values (all $r^2 >$ 0.99). Measurements for $\delta^{15}N^\alpha$ and SP were typically better than $\pm$ 0.8 ‰ of expected values, while $\delta^{15}N^\beta$, $\delta^{15}N^{bulk}$ measurements were all within $\pm$ 0.4 ‰ of expected values. $\delta^{18}O$ measurements were within $\pm$ 1.0 ‰ of expected values. There was excellent agreement between CRDS II and IRMS isotope values (all $r^2 > 0.98$), which agreed within $\pm$ 0.6–1.4 ‰ (Fig. S6-4). The standard deviations of triplicate isotope measurements typically decreased as a function of $\Delta N_2O$, with the lowest deviations of <0.1–0.3 ‰ occurring when $\Delta N_2O$ = ~700 ppb. Conversely, the standard deviations of triplicate sample measurements for [$N_2O$] increased with increasing $\Delta N_2O$, rising from 0.04–0.09 ppb when $\Delta N_2O$ = ~0 ppb (i.e. ambient conditions) to ~0.4 ppb when $\Delta N_2O$ = ~700 ppb. All CRDS II [$N_2O$] measurements had better $1\sigma$ repeatability than those acquired using GC. There was no clear distinction between CRDS II and IRMS triplicate repeatability, with both achieving triplicate repeatability ranging from 0.1 to 1 ‰ for most isotopic measurements. However, the repeatability of SP CRDS II measurements was mostly better than IRMS, achieving triplicate repeatability between 0.1–0.6 ‰, compared to 0.2–1 ‰ for IRMS.
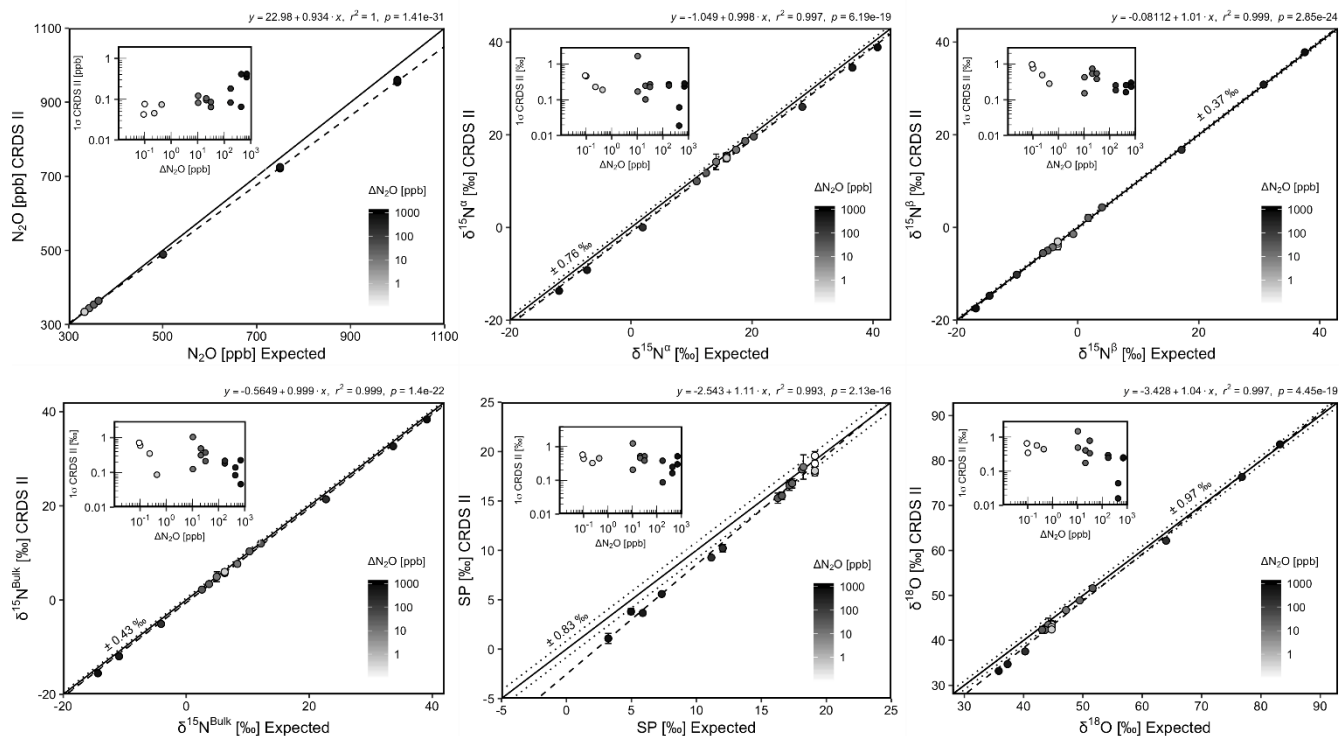
**Fig. 14.** Correlation diagrams for [N₂O], $\delta^{15}N^{\alpha}$, $\delta^{15}N^{\beta}$, $\delta^{15}N^{bulk}$, SP and $\delta^{18}O$ measurements at various $\Delta N_2O$ mole fractions analyzed by the CRDS II plotted against expected values. The solid black line denotes the 1:1 line, while the dotted line indicates $\pm 1\sigma$ of the residuals from the 1:1 line. The dashed black line represents a linear fit to the data. Individual equations, coefficients of determination ($r^2$) and $p$-values are indicated above each plot. Each data point represents the mean and standard deviation ($1\sigma$) of triplicate measurements. The inset plots indicate the standard deviation ($1\sigma$) of the triplicate measurements achieved at different $\Delta N_2O$ mole fractions, and the 1:1 line is similarly a solid line.

QCLAS I

There was good agreement of [N₂O] between QCLAS I and expected values, however the analyzer under-estimated mole fractions at higher $\Delta N_2O$ during experiments 5 and 6 (Fig. 15). Unfortunately, it is clear from the large spread of isotope values depicted in Fig. 15 that the standardized calibration scheme selected for the two end-member mixing tests was insufficient for acquiring accurate and precise isotopic measurements using QCLAS I. For this reason, we urge researchers not to over-interpret such results, as the implementation of a QCLAS-specific calibration procedure (in-line with results from Sects. 3.1 and 3.3) would improve results dramatically. Nonetheless, QCLAS I obtained accurate results at higher N₂O mole fractions (indicated in red in Fig. 15), such that when $\Delta N_2O < 700$

ppb measurements were excluded, $\delta^{15}N^{\alpha}$, $\delta^{15}N^{\beta}$, $\delta^{15}N^{bulk}$ and SP were within ± 3.0 ‰, 1.4 ‰, 1.4 ‰ and 3.8 ‰ of calculated expected values, respectively. Similarly, QCLAS I showed good agreement with IRMS only at higher $\Delta N_2O$ (> 700 ppb; Fig. S6-5). Similar to OA-ICOS I, the standard deviations of QCLAS I triplicate isotope measurements decreased dramatically with increasing $\Delta N_2O$, improving

5   from ~10 ‰ during experiments 1 and 2 to typically between 0.1–1 ‰ during experiments 5 and 6. Conversely, the standard deviations of triplicate sample measurements for [$N_2O$] increased with increasing $\Delta N_2O$, rising from < 0.1 ppb during experiments 1 through 4, to > 1 ppb during experiments 5 and 6. All QCLAS I [$N_2O$] measurements had better $1\sigma$ repeatability than those acquired using GC. QCLAS I had triplicate isotope measurement standard deviations comparable to IRMS only at higher

10   $\Delta N_2O$ (>700 ppb).
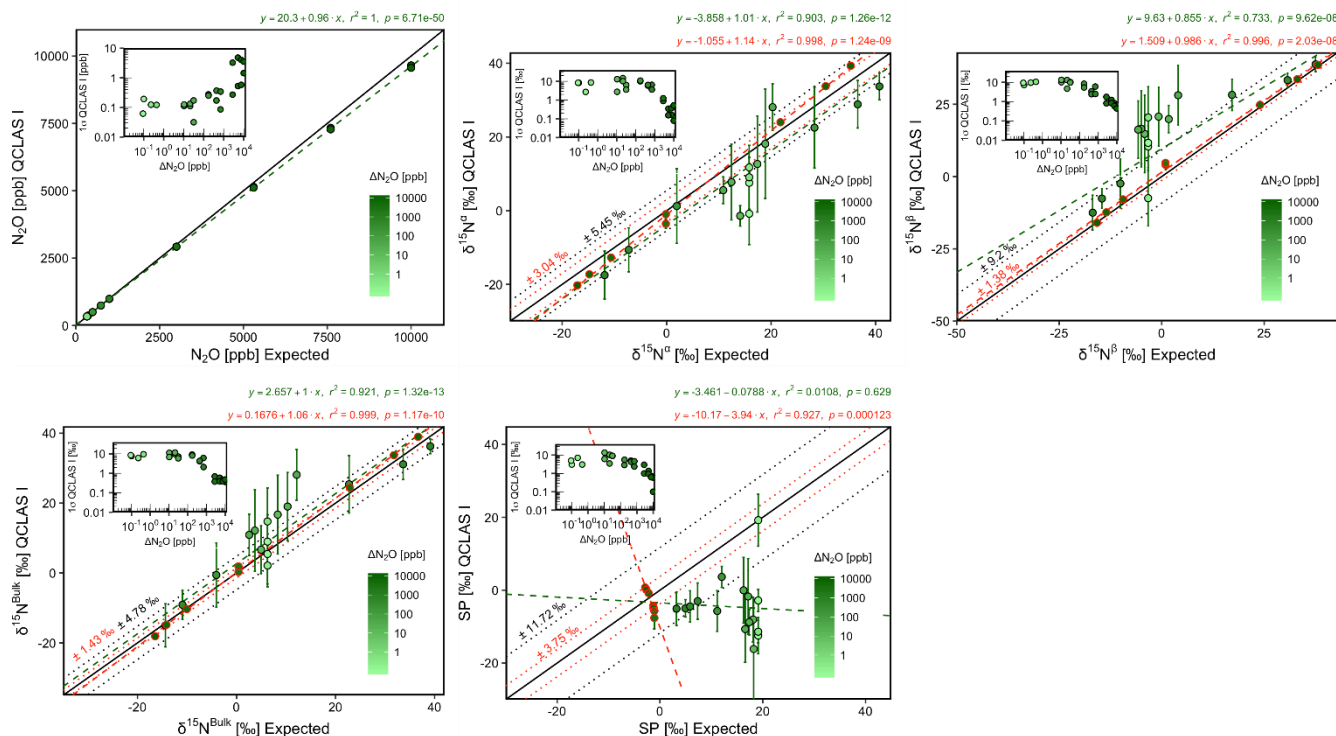
**Fig. 15.** Correlation diagrams for $N_2O$ mole fractions, $\delta^{15}N^{\alpha}$, $\delta^{15}N^{\beta}$, $\delta^{15}N^{bulk}$ and SP measurements at various $\Delta N_2O$ mole fractions analyzed by the QCLAS I plotted against expected values. The solid black line denotes the 1:1 line, while the dotted line indicates $\pm 1\sigma$ of the residuals from the 1:1 line. The

15   dashed green line represents a linear fit to the data. Individual equations, coefficients of determination ($r^2$) and $p$-values are indicated above each plot. Each data point represents the mean and standard deviation ($1\sigma$) of triplicate measurements. The inset plots indicate the standard deviation ($1\sigma$) of the

triplicate measurements achieved at different $\Delta N_2O$ mole fractions, and the 1:1 line is similarly a solid line. Results for Exp. 5-6 are highlighted in red, with the dashed red line indicating a linear fit to this data.

## 5 TREX-QCLAS I

There was good agreement of $N_2O$ mixing ratios between the TREX-QCLAS I and expected values (Fig. 16). Similarly, there was excellent agreement between the TREX-QCLAS I and calculated expected isotope values (all $r^2 > 0.97$). Measurements for $\delta^{15}N^\alpha$, $\delta^{15}N^\beta$, $\delta^{15}N^{bulk}$ and SP were within $\pm$ 0.29 ‰, 0.32 ‰, 0.23 ‰ and 0.41 ‰ of expected values, respectively. $\delta^{18}O$ measurements were 
10 typically within $\pm$ 0.24 ‰ of expected values. Generally, the standard deviations of triplicate isotope measurements decreased with increasing $\Delta N_2O$, improving from typically 0.2–0.3 ‰ at low $\Delta N_2O$ mole fractions (ambient) to close to or better than 0.1 ‰ when $\Delta N_2O$ reached 30 ppb. Conversely, the standard deviations of triplicate sample measurements for [$N_2O$] increased with increasing $\Delta N_2O$, rising from < 0.3 ppb to ~1 ppb. No comparison could be made between TREX-QCLAS I and IRMS 
15 measurements because TREX-QCLAS measurements were undertaken separately from the other instruments.
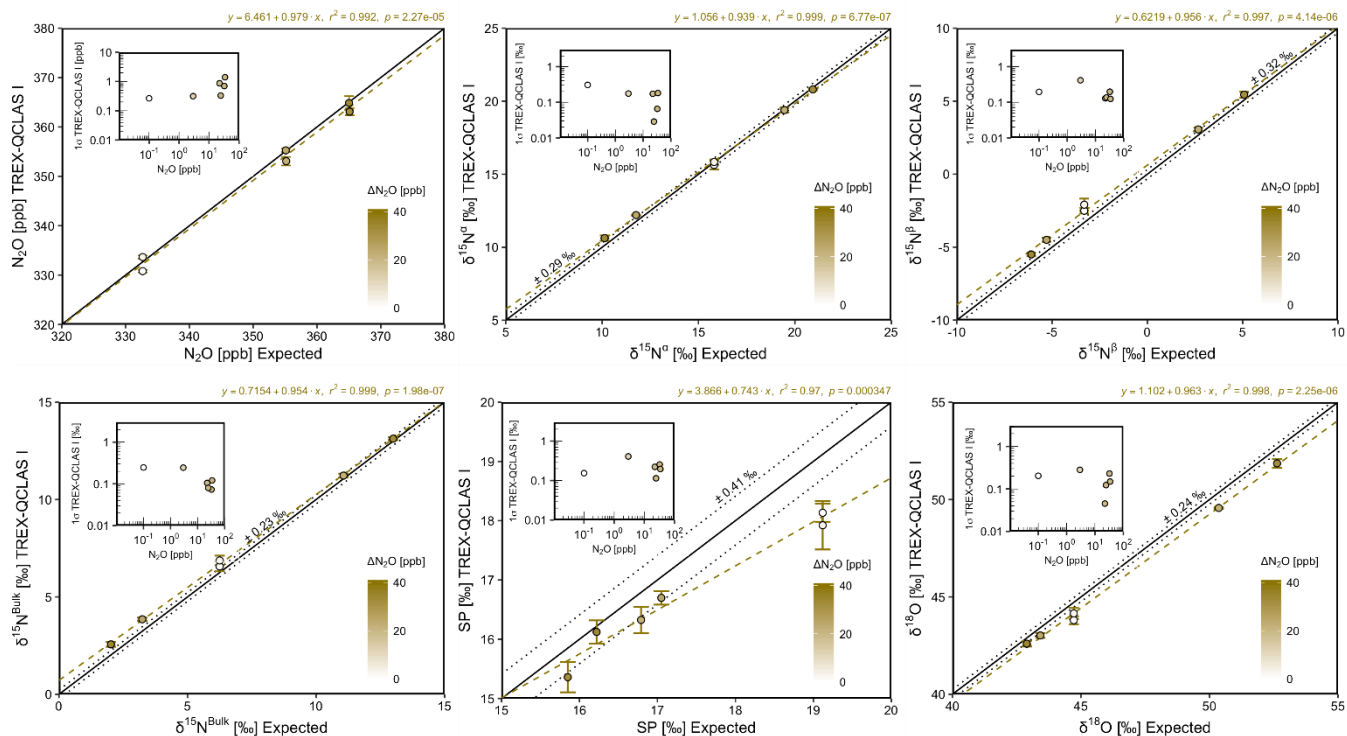
**Fig. 16.** Correlation diagrams for [N₂O], $\delta^{15}N^{\alpha}$, $\delta^{15}N^{\beta}$, $\delta^{15}N^{bulk}$, SP and $\delta^{18}O$ measurements at various $\Delta N_2O$ mole fractions analyzed by the TREX-QCLAS I plotted against expected values. The solid black line denotes the 1:1 line, while the dotted line indicates $\pm 1\sigma$ of the residuals from the 1:1 line. The dashed green line represents a linear fit to the data. Individual equations, coefficients of determination ($r^2$) and p-values are indicated above each plot. Each data point represents the mean and standard deviation ($1\sigma$) of triplicate measurements. The inset plots indicate the standard deviation ($1\sigma$) of the triplicate measurements achieved at different $\Delta N_2O$ mole fractions, and the 1:1 line is similarly a solid line.

### 3.7.2 Source identification using Keeling analysis

Despite the excellent agreement between expected and measured values across all experiments for OA-ICOS I, CRDS I and II, and TREX-QCLAS I, the extrapolated *source* intercept values acquired using Keeling analysis showed large standard errors, especially for Experiments 1 and 2 ($\Delta N_2O = 30$ ppb) (Fig. 17; Table 10). This was mostly due to the small mole fraction range (i.e. large inverse mole fraction range) over which the regression line was extrapolated in order to acquire the intercept value. The cause of the erroneous intercepts values was likely two-fold: (1) the extrapolated source was highly susceptible to measurements acquired at background levels, and due to the inherent greater uncertainty

associated with measurements acquired at ambient $N_2O$ mole fractions, intercepts can be skewed accordingly; and (2) any further non-linearity that could not be taken into account in the three-point concentration dependence correction applied. Overall, this implies that $N_2O$ isotope source studies using laser spectroscopy focusing on near-ambient $N_2O$ variations remain a challenging undertaking, and one

5 should expect large uncertainty in source estimates over small mole fraction changes.

For Experiments 3 through 6, however, the accuracy of the source intercept and its standard error improved dramatically for all analyzers on account of the decreasing uncertainty in measurement. OA-ICOS I and both CRDS analyzers typically achieved within ± 2–5 ‰ of the assigned values for $\delta^{15}N^{\alpha}$,

10 $\delta^{15}N^{\beta}$, $\delta^{15}N^{bulk}$, SP and $\delta^{18}O$, and had performance comparable to or better than the GC-IRMS approach (Fig. 17). Similarly, the standard error of all intercepts decreased dramatically for Experiments 3 through 6, and all analyzers typically achieved better than ± 1 ‰ standard error on derived intercepts in Experiments 5 and 6.
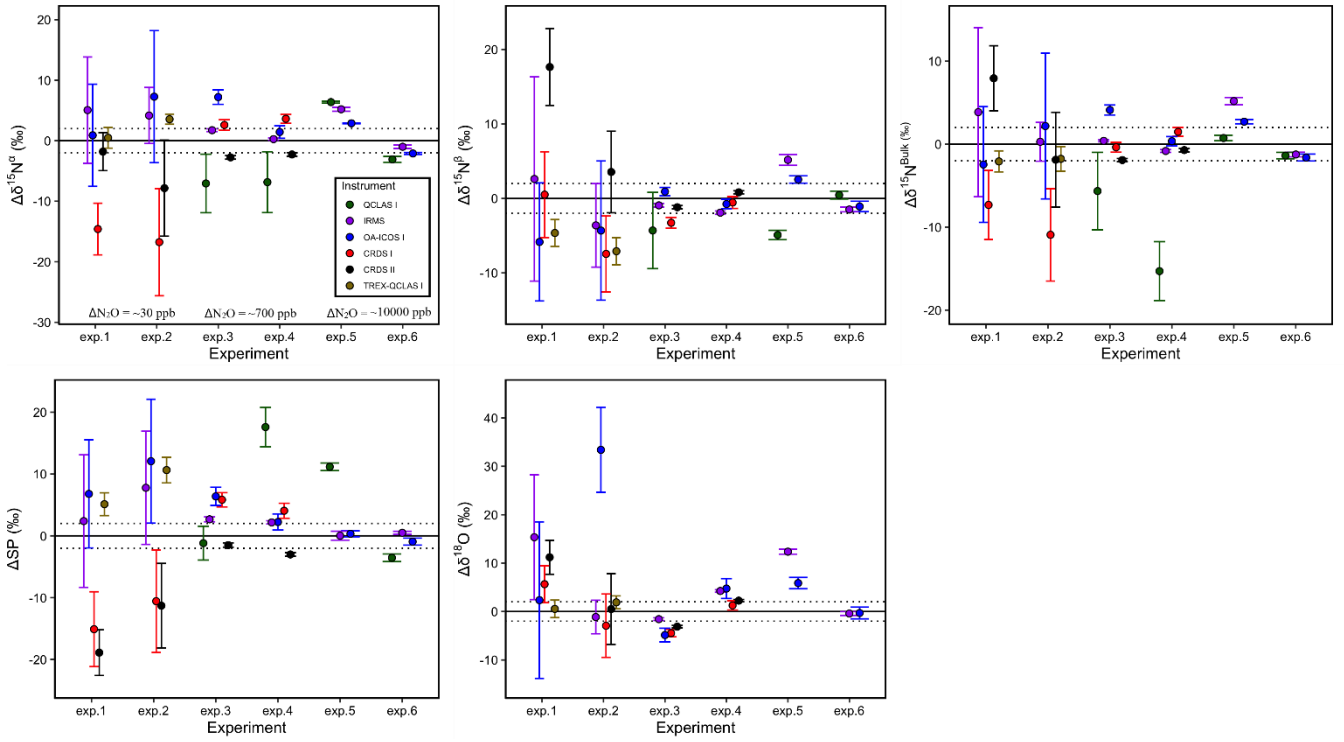
**Fig. 17.** $\Delta\delta^{15}N^{\alpha}$, $\Delta\delta^{15}N^{\beta}$, $\Delta\delta^{15}N^{bulk}$, $\Delta SP$ and $\Delta\delta^{18}O$ (Estimated$_{Source}$ – True$_{Source}$) values derived from the OA-ICOS I (blue), CRDS I (red), CRDS II (black), QCLAS I (green) and IRMS (purple) via Keeling analysis of the two end-member mixing scenario. Estimated$_{Source}$ = True$_{Source}$ is indicated by a solid black line at y = 0, and the dotted lines indicated ± 2‰ deviation from y = 0. The change in concentration exceeding that of the background gas is indicated for experiments 1-2 ($\Delta N_2O$ = ~30 ppb), 3-4 ($\Delta N_2O$ = ~700 ppb) and 5-6 ($\Delta N_2O$ = ~10000 ppb). Note: the QCLAS I results for experiments 1 and 2 are not depicted to maintain clarity, as they exceed the selected y-axis scale.

**Table 10.** Intercept values obtained by the four analyzers from the Keeling analysis. The error reported is 1 standard error. A 3-point concentration correction was applied to the data. Error (Source$_{Estimated}$ − Source$_{True}$) represents the error (‰) between the *estimated* source values and the *true* source values. $\Delta N_2O$ represents the average concentration difference (ppb) between the highest concentration in each experiment and the *background* based on the measurements recorded by each analyzer.

| Experiment sequence | ΔN$_2$O [ppb] | Instrument | | | | | Error (Source$_{Estimated}$ − Source$_{True}$) | | | | |
|---|---|---|---|---|---|---|---|---|---|---|---|
| | | δ$^{15}$N$^\alpha$ [‰] | δ$^{15}$N$^\beta$ [‰] | δ$^{15}$N$^{bulk}$ [‰] | SP [‰] | δ$^{18}$O [‰] | δ$^{15}$N$^\alpha$ [‰] | δ$^{15}$N$^\beta$ [‰] | δ$^{15}$N$^{bulk}$ [‰] | SP [‰] | δ$^{18}$O [‰] |
| | | OA-ICOS I | | | | | | | | | |
| 1 – Enriched | 31.42 | 71.15 ± 8.44 | 80.04 ± 7.93 | 75.62 ± 6.97 | -8.84 ± 8.74 | 131.2 ± 16.16 | 0.89 | -5.84 | -2.45 | 6.79 | 2.35 |
| 2 – Depleted | 31.26 | -37.4 ± 10.91 | -37.19 ± 9.34 | -36.59 ± 8.78 | 0.28 ± 10.02 | 58.65 ± 8.78 | 7.27 | -4.32 | 2.18 | 12.08 | 33.40 |
| 3 – Depleted | 694.22 | -18.53 ± 1.19 | -22.7 ± 0.56 | -20.56 ± 0.60 | 4.27 ± 1.46 | 26.49 ± 1.41 | 7.21 | 0.92 | 4.12 | 6.39 | -4.85 |
| 4 – Enriched | 701.46 | 54.64 ± 1.03 | 57.21 ± 0.63 | 55.94 ± 0.56 | -2.51 ± 1.30 | 107.3 ± 2.06 | 1.43 | -0.75 | 0.35 | 2.24 | 4.75 |
| 5 – Enriched | 9831.51 | 53.3 ± 0.07 | 56.62 ± 0.49 | 54.96 ± 0.26 | -3.33 ± 0.48 | 105.1 ± 1.17 | 2.88 | 2.54 | 2.71 | 0.33 | 5.88 |
| 6 – Depleted | 9933.59 | -26.46 ± 0.16 | -24.02 ± 0.70 | -25.26 ± 0.42 | -2.35 ± 0.56 | 31.49 ± 1.21 | -2.11 | -1.08 | -1.62 | -0.94 | -0.30 |
| | | CRDS I | | | | | | | | | |
| 1 – Enriched | 29.37 | 55.66 ± 4.27 | 86.39 ± 5.76 | 70.75 ± 4.15 | -30.73 ± 6.05 | 134.5 ± 3.81 | -14.60 | 0.51 | -7.32 | -15.10 | 5.65 |
| 2 – Depleted | 29.21 | -61.43 ± 8.86 | -40.32 ± 5.10 | -49.69 ± 5.57 | -22.37 ± 8.29 | 22.32 ± 6.54 | -16.76 | -7.45 | -10.92 | -10.57 | -2.93 |
| 3 – Depleted | 646.99 | -23.14 ± 0.86 | -26.89 ± 0.73 | -25.05 ± 0.59 | 3.72 ± 1.15 | 26.89 ± 0.78 | 2.60 | -3.27 | -0.37 | 5.84 | -4.45 |
| 4 – Enriched | 651.93 | 56.83 ± 0.74 | 57.41 ± 0.8 | 57.07 ± 0.53 | -0.69 ± 1.21 | 103.8 ± 0.95 | 3.62 | -0.55 | 1.48 | 4.06 | 1.27 |
| | | CRDS II | | | | | | | | | |
| 1 – Enriched | 29.55 | 68.45 ± 3.15 | 103.53 ± 5.16 | 86.01 ± 3.92 | -34.52 ± 3.7 | 140.05 ± 3.52 | -1.81 | 17.65 | 7.94 | -18.89 | 11.21 |
| 2 – Depleted | 29.41 | -52.51 ± 7.94 | -29.32 ± 5.47 | -40.65 ± 5.72 | -23.1 ± 6.84 | 25.76 ± 7.31 | -7.84 | 3.55 | -1.88 | -11.30 | 0.51 |
| 3 – Depleted | 620.28 | -28.49 ± 0.30 | -24.8 ± 0.22 | -26.59 ± 0.19 | -3.61 ± 0.35 | 28.23 ± 0.24 | -2.76 | -1.18 | -1.91 | -1.49 | -3.11 |
| 4 – Enriched | 626.24 | 50.94 ± 0.30 | 58.78 ± 0.21 | 54.87 ± 0.21 | -7.76 ± 0.29 | 104.75 ± 0.25 | -2.27 | 0.82 | -0.72 | -3.01 | 2.25 |
| | | QCLAS I | | | | | | | | | |
| 1 – Enriched | 30.52 | 185.3 ± 84.81 | 157.7 ± 74.91 | 172.3 ± 68.04 | 26.11 ± 59.38 | - | 115.0 | 71.81 | 94.27 | 41.74 | - |
| 2 – Depleted | 30.48 | 106.5 ± 68.41 | 103.3 ± 111.5 | 102.7 ± 82.67 | 2.23 ± 76.5 | - | 151.1 | 136.2 | 141.5 | 14.03 | - |
| 3 – Depleted | 648.35 | -32.8 ± 4.83 | -27.92 ± 5.12 | -30.33 ± 4.67 | -3.3 ± 2.74 | - | -7.07 | -4.30 | -5.65 | -1.18 | - |
| 4 – Enriched | 654.63 | 46.36 ± 5.03 | 34.08 ± 2.84 | 40.29 ± 3.55 | 12.85 ± 3.19 | - | -6.85 | -23.88 | -15.30 | 17.60 | - |
| 5 – Enriched | 9231.17 | 56.8 ± 0.17 | 49.17 ± 0.63 | 52.99 ± 0.33 | 7.51 ± 0.61 | - | 6.38 | -4.91 | 0.74 | 11.17 | - |
| 6 – Depleted | 9323.02 | -27.44 ± 0.48 | -22.49 ± 0.53 | -25.02 ± 0.39 | -4.96 ± 0.61 | - | -3.09 | 0.45 | -1.38 | -3.55 | - |
| | | TREX-QCLAS I | | | | | | | | | |
| 1 – Enriched | 32.38 | 73.95 ± 1.71 | 86.49 ± 1.80 | 80.20 ± 1.27 | -12.54 ± 1.85 | 134.3 ± 1.81 | 0.48 | -4.64 | -2.10 | 5.12 | 0.55 |
| 2 – Depleted | 34.14 | -44.84 ± 0.83 | -41.78 ± 1.83 | -43.31 ± 1.47 | -3.02 ± 2.08 | 25.96 ± 1.33 | 3.55 | -7.09 | -1.79 | 10.64 | 1.90 |
| | | GC-IRMS | | | | | | | | | |
| 1 – Enriched | 30.14 | 75.31 ± 8.78 | 88.49 ± 13.71 | 81.93 ± 10.19 | -13.24 ± 10.73 | 144.2 ± 12.88 | 5.06 | 2.61 | 3.86 | 2.39 | 15.35 |
| 2 – Depleted | 30.43 | -40.50 ± 4.63 | -36.49 ± 5.61 | -38.48 ± 2.34 | -4.02 ± 9.17 | 24.12 ± 3.46 | 4.17 | -3.62 | 0.27 | 7.77 | -1.13 |
| 3 – Depleted | 668.62 | -24.00 ± 0.23 | -24.55 ± 0.25 | -24.28 ± 0.12 | 0.55 ± 0.40 | 29.77 ± 0.27 | 1.74 | -0.93 | 0.40 | 2.67 | -1.57 |
| 4 – Enriched | 674.33 | 53.48 ± 0.19 | 56.05 ± 0.23 | 54.76 ± 0.16 | -2.57 ± 0.27 | 106.7 ± 0.26 | 0.26 | -1.91 | -0.82 | 2.17 | 4.24 |
| 5 – Enriched | 8540.91 | 55.62 ± 0.33 | 59.25 ± 0.73 | 57.44 ± 0.44 | -3.63 ± 0.72 | 111.5 ± 0.51 | 5.20 | 5.17 | 5.19 | 0.03 | 12.37 |
| 6 – Depleted | 8958.53 | -25.35 ± 0.29 | -24.43 ± 0.32 | -24.89 ± 0.28 | -0.92 ± 0.24 | 31.38 ± 0.39 | -1.00 | -1.49 | -1.24 | 0.49 | -0.41 |

# 4 Discussion

## 4.1 Factors affecting the precision and accuracy of $N_2O$ isotopocule measurements using laser spectroscopy

Our results highlight that the precision at which laser-based analyzers acquire $N_2O$ isotopocule measurements is a function of $N_2O$ mole fraction, the selected measuring and averaging times and calibration frequency according to measurement stability. The temperature sensitivities of all analyzers tested necessitates that, especially when such instruments are deployed in the field, laser spectrometers in general be operated under temperature-controlled conditions (such as in maintained field stations), and/or their dependence adequately characterized and corrected. The degree of accuracy obtained using different laser spectrometers is ultimately a function of the robustness of corrections aimed at removing matrix and trace gas effects, and the selected calibration procedure aimed at standardizing the data to international scales.

The experiments performed in this study were undertaken using a standardized protocol, including a two-point $\delta$ calibration, with which we could compare instrument performance. In cases where calibrations are performed on the derived isotope ratios or $\delta$ values, $[N_2O]$ dependence corrections should span the range of expected $N_2O$ mole fractions and account for non-linear effects (e.g. Winther et al. 2018). Alternative calibration approaches based on isotopocule concentrations or ratio calibration procedures were not included in our study, but have the potential to remove the need for this correction (e.g. Wen et al., 2013; Flores et al., 2017; Griffith, 2018). Isotopocule calibration approaches would require a set of $N_2O$ standard gases with high accuracy mole fractions in addition to assigned $\delta$ values.

All analyzers tested in this study showed significant effects from changing $O_2$ composition of the gas matrix. Similar $O_2$ dependencies have been reported by Erler et al. (2015) for CRDS $N_2O$ isotope laser spectrometers, as well as for CRDS $H_2O$ isotope analyzers (Johnson and Rella, 2017). Notably, the magnitude of effects reported for the CRDS analyzers in this study varied across CRDS I (a 2015 model) and CRDS II (a 2018 model), as well as from those reported by Erler et al. (2015). Therefore,

we recommended that in applications where $O_2$ concentrations vary, such as groundwater, estuaries, stratified waterbodies, and incubation studies, researchers test individual analyzers for their specific dependencies to allow for correction. This is especially important given that $N_2O$ production and reduction processes in such environments are strongly controlled by $O_2$ availability. Although the Ar effects characterized in this study were not large, it is nonetheless recommended as a precautionary measure that researchers ensure, where possible, the standard calibration gas Ar composition is similar to that of the sample gas.

The $CO_2$ effects for OA-ICOS and $CH_4$ effects for CRDS analyzers must be considered for applications of these analyzers where $CO_2$ and $CH_4$ may also co-vary, such as during diel atmospheric monitoring, in soil-flux chamber measurements, incubation studies and even waterbodies (e.g. Erler et al. 2015). These effects need to be either characterized and corrected for by the user, or the interfering gas quantitatively removed. To our knowledge, there is currently no commercially-available technique to remove $CH_4$ from a gas stream without affecting $N_2O$, and therefore independent co-analysis of $CH_4$ is ultimately required to correct for these effects post-measurement. Similarly, while water vapor effects can in theory be characterized and corrected for all instruments, we recommend that researchers remove water vapor from the gas stream prior to analysis. Although not tested here, other studies have highlighted possible spectral interference effects associated with elevated $H_2S$ and volatile organic compounds (Erler et al., 2015; Ostrom and Ostrom, 2017), but these may also be removed from gas streams using chemical traps (e.g. Cu and activated carbon traps, respectively).

The scaling of gas matrix and trace gas effects with [$N_2O$] has important implications for any measurement setup that relies on post-measurement correction equations. An equation developed to correct for $CH_4$ effects that was derived using a [$N_2O$] of 330 ppb should not be implemented for a sample gas containing 990 ppb $N_2O$. For example, as highlighted in Table 9, the measured interference effect on $\delta^{15}N^{\alpha}$ measurements acquired using CRDS II for 10 ppm [$CH_4$] at 330 ppb $N_2O$ was 24.9 ‰, while at 990 ppb $N_2O$ it was 8.1 ‰, resulting in a 16.8 ‰ difference. The scaling of interference effects from trace gases has been reported previously for $CO_2$/$CH_4$ laser spectrometers (Assan et al., 2017;

Malowany et al., 2015). This underlines the usefulness of removing $H_2O$, $CO_2$ and CO with scrubbers prior to measurement, as this removes the need for correction equations to begin with and the scaling of corrections that can ensue. We are unaware of any studies that have shown that $O_2$ interferences caused by pressure broadening linewidth effects change as a function of $N_2O$ mole fraction. While we were

5   unable to describe the scaling of the $O_2$ effect sufficiently using correction functions based on theoretical deductions, empirical equations based on experimental testing such as those developed in Sects. 3.5.2 and 3.6.2, could be implemented by researchers when co-variation in both $O_2$ and $N_2O$ in the sample gas is expected. Alternatively, as shown in this study, matrix and/or trace gas effects can be removed by automated $N_2O$ preconcentration devices such as TREX (Ibraim et al., 2018; Mohn et al.,

10  2010), similar to IRMS. However, such devices are not commercially available, complex to build and operate, and restrict sample frequency.

## 4.2 Pre-measurement considerations

Our study clearly shows that knowledge/estimation of the matrix and trace gas composition of both reference standards and sample gases, and the differences between them, are critical for accurate $N_2O$

15  isotopocule analysis using laser spectroscopy. We acknowledge, however, that this may be difficult to predict in certain applications without prior testing of the sample gas, and therefore researchers should err on the side of caution.

As a pre-requisite to acquiring measurements using $N_2O$ isotope laser spectrometers, researchers will be

20  required to consider the accessory gas mixtures required to characterize their instrument. For applications with significant variations in matrix ($O_2$, Ar) or trace gas ($CO_2$, $CH_4$, CO) compositions, researchers will require gas mixtures containing the gas of interest in order to characterize the associated interference effects for their laser spectrometer. This also necessitates that appropriate interference detectors are implemented, especially $O_2$ and $CH_4$ analyzers given that these effects cannot

25  be mitigated using chemical traps.

In this study, interference effects, and the associated scaling of these effects according to the co-measured $N_2O$ mole fraction, were derived via dynamic dilution with various gas mixtures using MFCs. This allowed for the introduction of a wide range of gas mixtures to the analyzers for interference testing, and consequently only a small amount of gas mixtures were required for all of the experiments

5   outlined in Sect. 2.4. In comparison, a much larger number of individual gas mixtures would have been required had they been prepared using static dilution techniques (see Erler et al. 2015). The scaling of interference effects were sufficiently distinguished by undertaking testing at three different $N_2O$ mole fractions ($N_2O$ = 330, 660 and 990 ppb), and we therefore recommend this as a minimum criterion for researchers wishing to characterize this effect.

Researchers should also consider the sample gas volume required for a given measurement application using a specific laser spectrometer. In our experience, ensuring that five laser cavity cell volumes have been flushed prior to measurement is *best practice* to negate any memory effects during a measurement run. By following this procedure and using the operating parameters selected in this study, the sample

15   gas volume required for a single 300 s measurement is approximately 84 mL for CRDS II, 147 mL for CRDS I, 603 mL for OA-ICOS I and 1170 mL for QCLAS I. The different sample volumes required for CRDS I and CRDS II is due to the different selected flow rates. By comparison, TREX-QCLAS I requires approximately 5 L of sample gas to allow for $N_2O$ preconcentration. Thus, users should carefully consider the available volume of the sample gas, although the possibility exists to dilute high

20   concentration samples to increase gas volume. Researchers should also ensure that gas samples contain $N_2O$ within the operational ranges of the different laser spectrometers (Table 1).

**4.3 Measurement workflow**

In-line with our results, we propose a step-by-step workflow that can be followed by researchers to acquire $N_2O$ isotopocule measurements. For specific applications, such as incubation experiments with

25   He, accessory injection units and setups using TREX, related actions have to be taken. Depending on the desired precision, users may vary the measurement and averaging times, and calibration frequency.

1. Prior to any measurement, consider the expected $N_2O$ range, desired precision, volume of sample gas required and temperature stability, and evaluate whether the preceding is implementable with the desired laser spectrometer.

2. Implement $H_2O$, $CO_2$ and CO scrubbers into the measurement setup.

3. Consider whether the $O_2$, Ar and/or $CH_4$ composition of the sample gas is likely to differ to that of the reference gas. If no, proceed to Step 5.

4. Co-analyze $O_2$ and $CH_4$ in the sample gas so that post-measurement correction can be made. Appropriate calibration of $O_2$ and $CH_4$ analyzers should be undertaken. Ar compositional differences can be estimated based on the reference standard gas matrix composition.

5. During the measurement run, analyze a minimum of two reference gases whose isotopic composition span the expected isotope compositions. Systemic measurement of a gas cylinder can be used to account for drift. If measurements are to be calibrated on derived ratio or δ values, mole fraction dependence must be characterized using a minimum three-point procedure, although more points may be required to account for non-linear effects. The frequency at which this step is implemented should be in-line with the analyzer stability.

6. Analyze the sample gas. Best precision can be gained with optimized analysis time and replication of analysis.

7. Quantify the difference in $[O_2]$, $[Ar]$ and/or $[CH_4]$ between the sample and reference gas. If $[N_2O] = \sim 330$ ppb, go to step 8. If $[N_2O] > \sim 330$ ppb, go to Step 9. If there is no difference in $[O_2]$, $[Ar]$ and/or $[CH_4]$ between the sample and reference gas, go to Step 10.

8. Apply analyzer-specific matrix and/or trace gas corrections derived when the co-measured $[N_2O] = \sim 330$ ppb. Interference effect equations may be derived prior to or post sample gas measurement.

9. Apply analyzer-specific matrix and/or trace gas coefficients to scale correction equations according to $[N_2O]$. Interference effect equations may be derived prior to or post sample gas measurement, and effects should be derived at a minimum three $N_2O$ mole fractions (for example, when $N_2O = 330$, 660 and 990 ppb).

10. Correct data, if applicable, for $[N_2O]$ dependence.

11. If required, apply drift correction.

12. Standardize δ values to international scales using desired method (e.g. Gröning, 2018; Wen et al. 2013).

## 4.4 What degree of accuracy can be achieved using this workflow?

5    The simulated two end-member mixing experiments conducted in this study show that, when the workflow proposed above is applied, accuracy within ± 0.5‰ can be achieved for TREX-QCLAS, ± 0.4–1.6 ‰ for CRDS analyzers, and ± 1.6–3.6 ‰ for OA-ICOS analyzers. Likewise, the comparison between the laser spectrometers and IRMS highlights that cross-technique compatibility within ± 1–2.5 ‰ can be achieved for most $N_2O$ isotopocule measurements. However, it is clear that the balanced (i.e.

10    non analyzer-specific) approach applied for the purpose of this comparative study did not cater to QCLAS I. Therefore, a more specific calibration protocol for the QCLAS I will likely yield better performance, as shown in Supplementary Material 3.

Whilst the laboratory-simulated mixing experiment is not fully representative of naturally-occurring two

15    end-member mixing *per se*, the results are useful in comparing intercept accuracy and uncertainty amongst analyzers and against IRMS. Our results show that large uncertainties exist for $N_2O$ source apportionment using Keeling analysis performed at near-ambient $N_2O$ mole fractions. Given the amount of corrections that are required in the experiment, we have not detailed individual analyzer uncertainty budgets to quantify individual sources of error on the intercept, as it is beyond the scope of this study.

20    Nonetheless, the reduction of uncertainty with increasing $\Delta N_2O$ shown in experiments 1–6 in Sect. 3.7 has also been shown in previous studies (e.g. Wolf et al., 2015). Therefore, by extension, it is reasonable to assume that the current largest source of uncertainty for ambient $N_2O$ measurements using laser spectroscopy is the inherent signal-to-noise ratio of the measurement.

## 5 Conclusions

In this study, we characterized and compared $N_2O$ isotope laser-based analyzers with the three most common detection schemes, including OA-ICOS, CRDS and QCLAS. Our results show a number of factors that need to be carefully considered to ensure precise and accurate measurements of $N_2O$ isotopocules using laser spectroscopy. The performance of $N_2O$ isotope laser spectrometers depends on a complex interplay between instrumental precision, drift, matrix gas composition and associated spectral interferences that ultimately vary as a function of $N_2O$ mole fraction. On this basis, we echo recommendations from Ostrom and Ostrom (2017), who cautioned not to underestimate the need for the careful consideration of analyzer-specific corrections. These analyzers clearly do not represent "plug and play" devices – instead, one needs to carefully consider the desired application, precision and accuracy, and develop appropriate calibration strategies to achieve these outcomes.

Consequently, we recommend calibration schemes that have: (1) a calibration frequency that is adequate for constraining instrument drift over experimental period/long-term measurements; (2) temperature stability during measurement, or the temperature effect adequately characterized and corrected; (3) a three-point or higher [$N_2O$] effect correction that spans the range of expected [$N_2O$] (if calibration relies on ratio or δ values, rather than isotopocule abundance); and (4) accounted for the differences in matrix and trace gas composition between the sample gas and reference gases, whereby either analyzer-specific interference corrections have been carefully characterized and applied, or where possible interfering substances ($CO_2$, $CO$, $H_2O$) removed using chemical traps. Correcting for interference effects becomes significantly more complicated once [$N_2O$] exceed ambient levels, requiring a multitude of analyzer- and gas-specific constants that inevitably increase the number of gas mixtures required by the user, as well as the uncertainty of the measurement. Researchers should therefore strive to implement measurement setups that require as few corrections as possible, and this will inherently decrease the combined uncertainty in the measurement.

It is important to note that the results of this study should be interpreted for these analyzer models only, and results are likely to vary slightly across the same make. Newer analyzers and models may yield

better performance than reported here. As illustrated by the noticeable improvement between the CRDS I (2015 model) and CRDS II (2018 model), it is foreseeable that the performance of $N_2O$ isotope laser spectrometers will continue to improve into the future. Future studies should focus on quantifying the error contributions to $N_2O$ isotopocule analysis using laser spectroscopy.

*Author contributions.* SH and JL, guided by JM, designed the study, established the setup and coordinated the experiments. Responsibilities on the analyzers were as follows: SH, BK and DC OA-ICOS; JL and TB CRDS I; LX and BW QCLAS I and CRDS II; JW and KZ TREX-QCLAS I; MB and JS QCLAS II, QCLAS III and GC-IRMS. JM prepared the non-commercial gas mixtures used in this study. LY referenced the δ values of applied gas mixtures to international scales. SH and JL performed the main data analysis and together with JM developed correction algorithms. SH and JL wrote the manuscript with input from all co-authors.

*Data availability.* All data are available from the corresponding author upon request.

*Competing interests*. The authors declare that they have no conflict of interest.

*Acknowledgements.* We extend our thanks to Doug Baer, Rob Provencal and Frederick Despagne from ABB Los Gatos Research Inc., Renato Winkler, Magdalena Hofmann and Paulos Getachew from Picarro Inc., and Dave Nelson and Barry McManus from Aerodyne Research Inc. for their helpful discussions and assistance concerning the analyzers. We thank Christoph Zellweger for his assistance analysing matrix gas cylinders and providing the Picarro G2401 for matrix interference testing, and the NABEL laboratory at Empa for providing the dew point generator for water vapor testing. We want to thank Kristýna Kantnerová from Empa and Daniel Zindel from ETH for the synthesis of ^{18}O-labelled $N_2O$.

This study was supported by the European Metrology Programme for Innovation and Research (EMPIR) 16ENV06 project "Metrology for Stable Isotope Reference Standards (SIRS)". The EMPIR

initiative is co-funded by the European Union's Horizon 2020 research and innovation programme and the EMPIR Participating States. Furthermore, this research was supported by grants from the Cotton Research and Development Corporation (CRDC), and was facilitated by an Endeavour Research Fellowship acquired by Stephen Harris from the Australian Government. Stephen Harris is supported by PhD scholarships from the Australian Government, the Australian Institute of Nuclear Science and Engineering (AINSE), Australian Nuclear Science and Technology Organisation (ANSTO) and CRDC. The UNSW Sydney $N_2OIA$-30e-EP was purchased using funds from the Australian National Groundwater Infrastructure Scheme. Jing Wei and Longfei Yu were supported by the EMPAPOSTDOCS-II programme, which received funding from the European Union's Horizon 2020 research and innovation programme under the Marie Skłodowska-Curie grant agreement number 754364.

## References

ABB-Los Gatos Research Inc.: Off-Axis Integrated Cavity Output Spectroscopy (OA-ICOS), available at http://www.lgrinc.com/advantages/, 2019.

Allan, D.: Statistics of atomic frequency standards, Proc. IEEE, 54, 221–230, 1966.

Anderson, B., Bartlett, K., Frolking, S., Hayhoe, K., Jenkins, J., and Salas, W.: Methane and Nitrous Oxide Emissions from Natural Sources, Office of Atmospheric Programs, US EPA, EPA 430-R-10-001, Washington DC, 2010.

Assan, S., Baudic, A., Guemri, A., Ciais, P., Gros, V., and Vogel, F.R.: Characterization of interferences to in situ observations of $\delta^{13}CH_4$ and $C_2H_6$ when using a cavity ring-down spectrometer at industrial sites, Atmos. Meas. Tech., 10, 2077–2091, doi: 10.5194/amt-10-2077-2017, 2017.

Baer, D. S., Paul, J. B., Gupta, M., and O'Keefe, A.: Sensitive absorption measurements in the near-infrared region using off-axis integrated-cavity-output spectroscopy, Appl. Phys. B-Lasers O., 75, 261–265, doi:10.1007/s00340-002-0971-z, 2002.

5 Baggs, E.M.: A review of stable isotope techniques for $N_2O$ source partitioning in soils: recent progress, remaining challenges and future considerations, Rapid Communications in Mass Spectrometry, 22, 1664–1672, doi: 10.1002/rcm.3456, 2008.

Bernard, S., Röckmann, T., Kaiser, J., Barnola, J.-M., Fischer, H., Blunier, T., and Chappellaz, J.:
10 Constraints on $N_2O$ budget changes since pre-industrial time from new firn air and ice core isotope measurements, Atmos. Chem. Phys., 6, 493–503, doi:10.5194/acp-6-493-2006, 2006.

Bouwman, A. F., Boumans, L. J. M., and Batjes N. H.: Modeling global annual $N_2O$ and NO emissions from fertilized fields, Global Biogeochem. Cycles, 16, 1080, doi:10.1029/2001GB001812, 2002.

Bowling, D. R., Burns, S. P., Conway, T. J., Monson, R. K., and White, J. W. C.: Extensive observations of $CO_2$ carbon isotope content in and above a high-elevation subalpine forest, Global Biogeochem. Cy, 19, GB3023, doi:10.1029/2004gb002394, 2005.

20 Bowling, D. R., Sargent, S. D., Tanner, B. D., and Ehleringer, J. R.: Tunable diode laser absorption spectroscopy for stable isotope studies of ecosystem-atmosphere $CO_2$ exchange, Agr. Forest Meteorol., 118, 1–19, doi:10.1016/s0168-1923(03)00074-1, 2003.

Brase, L., Bange, H.W., Lendt, R., Sanders, T., and Dähnke, K.: High Resolution Measurements of
25 Nitrous Oxide ($N_2O$) in the Elbe Estuary, Front. Mar. Sci., 4, 162, doi:10.3389/fmars.2017.00162, 2017.

Buchen, C., Lewicka-Szczebak, D., Flessa, H. and Well, R.: Estimating $N_2O$ processes during grassland renewal and grassland conversion to maize cropping using $N_2O$ isotopocules, Rapid Commun Mass Spectrom, 32, 1053–1067, doi:10.1002/rcm.8132, 2018.

5    Decock, C. and Six, J.: How reliable is the intramolecular distribution of $^{15}N$ in $N_2O$ to source partition $N_2O$ emitted from soil?, Soil Biol. Biochem., 65, 114–127, doi: 10.1016/j.soilbio.2013.05.012, 2013.

Denk, T.R., Mohn, J., Decock, C., Lewicka-Szczebak, D., Harris, E., Butterbach-Bahl, K., Kiese, R., and Wolf, B.: The nitrogen cycle: A review of isotope effects and isotope modeling approaches, Soil 10    Biol Biochem., 105, 121–137, doi:10.1016/j.soilbio.2016.11.015, 2017.

Denman, K. L., Brasseur, G., Chidthaisong, A., Ciais, P., Cox, P. M., Dickinson, R. E., Hauglustaine, D., Heinze, C., Holland, E., Jacob, D., Lohmann, U., Ramachandran, S., da Silva Dias, P. L., Wofsky, S. C., and Zhang, X.: Couplings between changes in the climate system and biogeochemistry, in: 15    Climate change 2007, the physical science basis, contribution of working group I to the Fourth Assessment Report of the Intergovernmental Panel on Climate Change, edited by: Solomon, S., Qin, D., Manning, M., Chen, Z., Marquis, M., Averyt, K. B., Tignor, M., and Miller, H. L., Cambridge University Press, Cambridge, United Kingdom and New York, NY, USA, 499–587, 2007.

20    Erler, D.V., Duncan, T.M., Murray, R., Maher, D.T., Santos, I.R., Gatland, J.R., Mangion, P., and Eyre, B.D.: Applying cavity ring-down spectroscopy for the measurement of dissolved nitrous oxide mole fractions and bulk nitrogen isotopic composition in aquatic systems: Correcting for interferences and field application, Limnol Oceanogr Methods, 13, 391–401, doi:10.1002/lom3.10032, 2015.

25    Eyer, S., Tuzson, B., Popa, M.E., Van Der Veen, C., Röckmann, T., Rothe, M., Brand, W.A., Fisher, R., Lowry, D., Nisbet, E.G., and Brennwald, M.S.: Real-time analysis of $\delta^{13}C$- and $\delta D$-$CH_4$ in ambient air with laser spectroscopy: method development and first intercomparison results, Atmos. Meas. Tech., 9, 263–280, doi:10.5194/amt-9-263-2016, 2016.

Flores, E., Viallon, J., Moussay, P., Griffith, D.W., and Wielgosz, R.I.: Calibration strategies for FT-IR and other isotope ratio infrared spectrometer instruments for accurate $\delta^{13}C$ and $\delta^{18}O$ measurements of $CO_2$ in air, Anal. Chem., 89, 3648–3655, doi:10.1021/acs.analchem.6b05063, 2017.

Forster, P., Ramaswamy, V., Artaxo, P., Berntsen, T., Betts, R., Fahey, D. W., Haywood, J., Lean, J., Lowe, D. C., Myhre, G., Nganga, J., Prinn, R., Raga, G., Schulz, M., and Van Dorland, R.: Climate Change 2007: Changes in Atmospheric Constituents and in Radiative Forcing, The Physical Science Basis: Contribution of Working Group I to the Fourth Assessment Report of the Intergovernmental

10   Panel on Climate Change, edited by: Solomon, S., Qin, D., Manning, M., Chen, Z., Marquis, M., Averyt, K. B., Tignor, M., and Miller, H. S., Cambridge University Press, Cambridge, UK, New York, NY, USA, 2007.

Friedrichs, G., Bock, J., Temps, F., Fietzek, P., Körtzinger, A., and Wallace, D.W.: Toward continuous

15   monitoring of seawater $^{13}CO_2/^{12}CO_2$ isotope ratio and $pCO_2$: Performance of cavity ringdown spectroscopy and gas matrix effects, Limnol Oceanogr–Meth, 8, 539–551, doi: 10.4319/lom.2010.8.539, 2010.

Griffis, T. J., Baker, J. M., Sargent, S. D., Tanner, B. D., and Zhang, J.: Measuring field-scale isotopic

20   $CO_2$ fluxes with tunable diode laser absorption spectroscopy and micrometeorological techniques, Agr. Forest Meteorol., 124, 15–29, doi:10.1016/j.agrformet.2004.01.009, 2004.

Griffith, D. W. T., Deutscher, N. M., Caldow, C., Kettlewell, G., Riggenbach, M., and Hammer, S.: A Fourier transform infrared trace gas and isotope analyser for atmospheric applications, Atmos. Meas.

25   Tech., 5, 2481–2498, doi:10.5194/amt-5-2481-2012, 2012.

Griffith, D. W.: Calibration of isotopologue-specific optical trace gas analysers: a practical guide, Atmos. Meas. Tech., 11, 6189–6201, doi:10.5194/amt-11-6189-2018, 2018.

Gröning, M.: TEL Technical Note No. 01. SICalib User Manual (Stable Isotope Calibration for routine δ-scale measurements) Ver 2.16j, 2018.

5    Harris, E., Henne, S., Hüglin, C., Zellweger, C., Tuzson, B., Ibraim, E., Emmenegger L., and Mohn J.: Tracking nitrous oxide emission processes at a suburban site with semicontinuous, in situ measurements of isotopic composition, J. Geophys. Res. Atmospheres, 122, 1850–1870, doi: 10.1002/2016JD025906, 2017.

10   Harris, E., Joss, A., Emmenegger, L., Kipf, M., Wolf, B., Mohn, J. and Wunderlin, P.: Isotopic evidence for nitrous oxide production pathways in a partial nitritation-anammox reactor, Water Res., 83, 258–270, doi:10.1016/j.watres.2015.06.040, 2015a.

Harris, E., Nelson, D.D., Olszewski, W., Zahniser, M., Potter, K.E., McManus, B.J., Whitehill, A.,
15   Prinn, R.G., and Ono, S.: Development of a spectroscopic technique for continuous online monitoring of oxygen and site-specific nitrogen isotopic composition of atmospheric nitrous oxide, Anal. Chem., 86, 1726–1734, doi:10.1021/ac403606u, 2014.

Harris, E., Zeyer, K., Kegel, R., Müller, B., Emmenegger, L. and Mohn, J.: Nitrous oxide and methane
20   emissions and nitrous oxide isotopic composition from waste incineration in Switzerland, Waste Manage., 35, 135–140, doi:10.1016/j.wasman.2014.10.016, 2015b.

Heil, J., Wolf, B., Brüggemann, N., Emmenegger, L., Tuzson, B., Vereecken, H., and Mohn, J.: Site-specific $^{15}$N isotopic signatures of abiotically produced $N_2O$, Geochim. Cosmochim. Ac., 139, 72–82,
25   doi: 10.1016/j.gca.2014.04.037, 2014.

Ibraim, E., Harris, E., Eyer S., Tuzson, B., Emmenegger, L., Six, J., and Mohn, J.: Development of a field-deployable method for simultaneous, real-time measurements of the four most abundant $N_2O$ isotopocules, Isotopes Environ Health Stud., 54, 1–5, doi: 10.1080/10256016.2017.1345902, 2018.

5 Ibraim, E., Wolf, B., Harris, E., Gasche, R., Wei, J., Yu, L., Kiese, R., Eggleston, S., Butterbach-Bahl, K., Zeeman, M., and Tuzson, B.: Attribution of $N_2O$ sources in a grassland soil with laser spectroscopy based isotopocule analysis, Biogeosci., 16, 3247–3266, doi:10.5194/bg-16-3247-2019, 2019.

Ishijima, K., Sugawara, S., Kawamura, K., Hashida, G., Morimoto, S., Murayama, S., Aoki, S., and 10 Nakazawa, T.: Temporal variations of the atmospheric nitrous oxide mole fraction and its $\delta^{15}N$ and $\delta^{18}O$ for the latter half of the 20th century reconstructed from firn air analyses, J Geophys. Res. Atmos., 112, D3, doi: 10.1029/2006JD007208, 2007.

Ji, Q., Grundle, D.S.: An automated, laser-based measurement system for nitrous oxide isotope and 15 isotopomer ratios at nanomolar levels, Rapid Commun Mass Spectrom., 33, 1553–1564, doi:10.1002/rcm.8502, 2019.

Johnson, J. E. and Rella, C. W.: Effects of variation in background mixing ratios of $N_2$, $O_2$, and Ar on the measurement of δ18O–H2O and δ2H–H2O values by cavity ring-down spectroscopy, Atmos. Meas. 20 Tech., 10, 3073-3091, https://doi.org/10.5194/amt-10-3073-2017, 2017.

Keeling, C. D.: The mole fraction and isotopic abundances of atmospheric carbon dioxide in rural areas, Geochim. Cosmochim. Acta, 13, 322–334, doi:10.1016/0016-7037(58)90033-4, 1958.

25 Koba, K., Osaka, K., Tobari, Y., Toyoda, S., Ohte, N., Katsuyama, M., Suzuki, N., Itoh, M., Yamagishi, H., Kawasaki, M., and Kim, S.J.: Biogeochemistry of nitrous oxide in groundwater in a forested ecosystem elucidated by nitrous oxide isotopomer measurements, Geochim. Cosmochim. Acta, 73, 3115–3133, doi:10.1016/j.gca.2009.03.022, 2009.

Kong, X., Duan, Y., Schramm, A., Eriksen, J., Holmstrup, M., Larsen, T., Bol, R., and Petersen, S.O.: Mitigating $N_2O$ emissions from clover residues by 3, 4-dimethylpyrazole phosphate (DMPP) without adverse effects on the earthworm Lumbricus terrestris, Soil Biol. Biochem., 104, 95–107, doi:10.1016/j.soilbio.2016.10.012, 2017.

Köster, J. R., Cárdenas, L., Senbayram, M., Bol, R., Well, R., Butler, M., Mühling, K. H., and Dittert, K.: Rapid shift from denitrification to nitrification in soil after biogas residue application as indicated by nitrous oxide isotopomers, Soil Biol. Biochem., 43, 1671–1677, doi: 10.1002/rcm.6434, 2011.

Köster, J. R., Well, R., Tuzson, B., Bol, R., Dittert, K., Giesemann, A., Emmenegger, L., Manninen, A., Cárdenas, L., and Mohn, J.: Novel laser spectroscopic technique for continuous analysis of $N_2O$ isotopomers – application and intercomparison with isotope ratio mass spectrometry, Rapid Commun. Mass Spectrom., 27, 216–222, doi:10.1002/rcm.6434, 2013.

Lebegue, B., Schmidt, M., Ramonet, M., Wastine, B., Yver Kwok, C., Laurent, O., Belviso, S., Guemri, A., Philippon, C., Smith, J., and Conil, S.: Comparison of nitrous oxide ($N_2O$) analyzers for high-precision measurements of atmospheric mole fractions, Atmos. Meas. Tech., 9, 1221–1238, doi:10.5194/amt-9-1221-2016, 2016.

Lee, A., Winther, M., Priemé, A., Blunier, T., and Christensen, S.: Hot spots of $N_2O$ emission move with the seasonally mobile oxic-anoxic interface in drained organic soils, Soil Biol. and Biochem., 115, 178–186, doi:10.1016/j.soilbio.2017.08.025, 2017.

Lewicka-Szczebak, D., Well, R., Köster, J. R., Fuß, R., Senbayram, M., Dittert, K., and Flessa, H.: Experimental determinations of isotopic fractionation factors associated with $N_2O$ production and reduction during denitrification in soils, Geochim. Cosmochim. Ac., 134, 55–73, doi: 10.1016/j.gca.2014.03.010, 2014.

Lewicka-Szczebak, D.,Well, R., Bol, R., Gregory, A. S., Matthews, G. P., Misselbrook, T., Whalley,W. R., and Cardenas, L. M.: Isotope fractionation factors controlling isotopocule signatures of soil-emitted $N_2O$ produced by denitrification processes of various rates, Rapid Commun. Mass Spectr., 29, 269–282, doi: 10.1002/rcm.7102, 2015.

Li, X., Sørensen, P., Olesen, J.E., and Petersen, S.O.: Evidence for denitrification as main source of $N_2O$ emission from residue-amended soil, Soil Biol. Biochem., 92, 153–160, doi:10.1016/j.soilbio.2015.10.008, 2016.

Li, P., Wang, S., Peng, Y., Liu, Y., and He, J.: The synergistic effects of dissolved oxygen and pH on $N_2O$ production in biological domestic wastewater treatment under nitrifying conditions, Environ. Technol., 36, 1623–1631, doi: 10.1080/09593330.2014.1002862, 2015.

Malowany, K., Stix, J., Van Pelt, A., and Lucic, G.: $H_2S$ interference on $CO_2$ isotopic measurements using a Picarro G1101-i cavity ring-down spectrometer, Atmos. Meas. Tech., 8, 4075–4082, doi: 10.5194/amt-8-4075-2015, 2015.

Miller, J.B., and Tans, P.P.: Calculating isotopic fractionation from atmospheric measurements at various scales, Tellus, 55, 207–214, doi:10.1034/j.1600-0889.2003.00020.x, 2003.

Minamikawa, K., Nishimura, S., Nakajima, Y., Osaka, K.I., Sawamoto, T., and Yagi, K.: Upward diffusion of nitrous oxide produced by denitrification near shallow groundwater table in the summer: a lysimeter experiment, Soil Sci. Plant Nutr., 57, 719–732, doi: 10.1080/00380768.2011.625556, 2011.

Mohn, J., Guggenheim, C., Tuzson, B., Vollmer, M. K., Toyoda, S., Yoshida, N., and Emmenegger, L.: A liquid nitrogen-free preconcentration unit for measurements of ambient $N_2O$ isotopomers by QCLAS, Atmos. Meas. Tech., 3, 609–618, doi:10.5194/amt- 3-609-2010, 2010.

Mohn, J., Tuzson, B., Manninen, A., Yoshida, N., Toyoda, S., Brand, W. A., and Emmenegger, L.: Site selective real-time measurements of atmospheric $N_2O$ isotopomers by laser spectroscopy, Atmos. Meas. Tech., 5, 1601–1609, doi:10.5194/amt-5-1601-2012, 2012.

Mohn, J., Wolf, B., Toyoda, S., Lin, C. T., Liang, C. M., Brüggemann, N., Wissel, H., Steiker, A. E., Dyckmans, J., Szwek, L., Ostrom, N. E., Casciotti, K. L., Forbes, M., Giesemann, A.,Well, R., Doucett, R. R., Yarnes, C. T., Ridley, A. R., Kaiser, J., and Yoshida, N.: Inter-Laboratory assessment of nitrous oxide isotopomer analysis of isotopomer analysis by isotope ratio mass spectrometry and laser spectroscopy: current status and perspectives, Rapid Commun. Mass Spectr., 28, 1995–2007, doi: 10.1002/rcm.6982, 2014.

Mosier, A., Kroeze, C., Nevison, C., Oenema, O., Seitzinger, S. and Van Cleemput, O.: Closing the global $N_2O$ budget: nitrous oxide emissions through the agricultural nitrogen cycle, Nutr. Cycl. Agroecosys., 52, 225–248, doi:10.1023/A:1009740530221, 1998.

Murray, R., Erler, D., Rosentreter, J., Maher, D., and Eyre, B.: A seasonal source and sink of nitrous oxide in mangroves: Insights from mole fraction, isotope, and isotopomer measurements, Geochim. Cosmochim. Acta, 238, 169–192, doi:10.1016/j.gca.2018.07.003, 2018.

Nara, H., Tanimoto, H., Tohjima, Y., Mukai, H., Nojiri, Y., Katsumata, K., and Rella, C.W.: Effect of air composition ($N_2$, $O_2$, Ar, and $H_2O$) on $CO_2$ and $CH_4$ measurement by wavelength-scanned cavity ring-down spectroscopy: calibration and measurement strategy, Atmos. Meas. Tech., 5, 2689–2701, doi:10.5194/amt-5-2689-2012, 2012.

Nikolenko, O., Orban, P., Jurado, A., Morana, C., Jamin, P., Robert, T., Knöller, K., Borges, A.V., and Brouyère, S.: Dynamics of greenhouse gases in groundwater: hydrogeological and hydrogeochemical controls. Appl Geochem., 105, 31–44, doi:10.1016/j.apgeochem.2019.04.009, 2019.

NOAA/ESRL: Combined Nitrous Oxide data from the NOAA/ESRL Global Monitoring Division, 2019.

5   Ogawa, M., and Yoshida, N.: Intramolecular distribution of stable nitrogen and oxygen isotopes of nitrous oxide emitted during coal combustion, Chemosphere, 61, 877–887, doi: 10.1016/j.chemosphere.2005.04.096, 2005.

Ostrom N., and Ostrom, P.: Mining the isotopic complexity of nitrous oxide: a review of challenges and
10  opportunities, Biogeochemistry, 132, 359–372, doi:10.1007/s10533-017-0301-5, 2017.

Ostrom, N.E. and Ostrom, P.H.: The Isotopomers of Nitrous Oxide: Analytical Considerations and Application to Resolution of Microbial Production Pathways, in: Handbook of Environmental Isotope Geochemistry Volume 1, edited by: Baskaran, M., Springer Berlin Heidelberg, Berlin, Heidelberg, 453–
15  476, 2011.

Ostrom, N.E., Gandhi, H., Coplen, T.B., Toyoda, S., Böhlke, J.K., Brand, W.A., Casciotti, K.L., Dyckmans, J., Giesemann, A., Mohn, J., and Well, R.: Preliminary assessment of stable nitrogen and oxygen isotopic composition of USGS51 and USGS52 nitrous oxide reference gases and perspectives
20  on calibration needs, Rapid Commun Mass Spectrom, 32, 1207–1214, doi:10.1002/rcm.8157, 2018.

Ostrom, N. E., Pitt, A., Sutka, R., Ostrom, P. H., Grandy, A. S., Huizinga, K. M., and Robertson, G. P.: Isotopologue effects during $N_2O$ reduction in soils and in pure cultures of denitrifiers, J. Geophys. Res., 112, G02005, doi:10.1029/2006JG000287, 2007.

Pang, J., Wen, X., Sun, X. and Huang, K.: Intercomparison of two cavity ring-down spectroscopy analyzers for atmospheric $^{13}CO_2/^{12}CO_2$ measurement, Atmos. Meas. Tech., 9, 3879–3891, doi:10.5194/amt-9-3879-2016, 2016.

Park, S., Croteau, P., Boering, K.A., Etheridge, D.M., Ferretti, D., Fraser, P.J., Kim, K.R., Krummel, P.B., Langenfelds, R.L., Van Ommen, T.D. and Steele, L.P.: Trends and seasonal cycles in the isotopic composition of nitrous oxide since 1940, Nat. Geosci., 5, 261, doi:10.1038/NGEO1421, 2012.

Pataki, D. E., Bowling, D. R., Ehleringer, J. R., and Zobitz, J. M.: High resolution atmospheric monitoring of urban carbon dioxide sources, Geophys. Res. Lett., 33, L03813, doi:10.1029/2005gl024822, 2006.

Peng, L., Ni, B.J., Erler, D., Ye, L., and Yuan, Z.: The effect of dissolved oxygen on $N_2O$ production by ammonia-oxidizing bacteria in an enriched nitrifying sludge, Water Res., 66, 12–21, doi:10.1016/j.watres.2014.08.009, 2014.

Picarro Inc.: Cavity Ring-Down Spectroscopy (CRDS), available at https://www.picarro.com/company/technology/crds, 2019.

Potter, K.E., Ono, S., and Prinn, R.G.: Fully automated, high-precision instrumentation for the isotopic analysis of tropospheric $N_2O$ using continuous flow isotope ratio mass spectrometry, Rapid Commun Mass Spectrom, 27, 1723–1738, doi:10.1002/rcm.6623, 2013.

Prokopiou, M., Martinerie, P., Sapart, C.J., Witrant, E., Monteil, G., Ishijima, K., Bernard, S., Kaiser, J., Levin, I., Blunier, T., and Etheridge, D.: Constraining $N_2O$ emissions since 1940 using firn air isotope measurements in both hemispheres, Atmos Chem Phys, 17, 4539–4564, doi:10.5194/acp-17-4539-2017, 2017.

Pérez, T., Garcia-Montiel, D., Trumbore, S., Tyler, S., Camargo, P.D., Moreira, M., Piccolo, M., and Cerri, C.: Nitrous oxide nitrification and denitrification ^{15}N enrichment factors from Amazon forest soils, Ecol Appl, 16, 2153–2167, doi: 10.1890/1051-0761(2006)016[2153:NONADN]2.0.CO;2, 2006.

Pérez, T., Trumbore, S.E., Tyler, S.C., Matson, P.A., Ortiz-Monasterio, I., Rahn, T., and Griffith, D.W.T.: Identifying the agricultural imprint on the global $N_2O$ budget using stable isotopes, J Geophys Res Atmos., 106, 9869–9878, doi:10.1029/2000JD900809, 2001.

R Core Team.: R: A language and environment for statistical computing. R Foundation for Statistical Computing, Vienna, Austria. URL https://www.R-project.org/, 2017.

Ravishankara, A. R., Daniel, J. S., and Portmann, R. W.: Nitrous oxide ($N_2O$): the dominant ozone-
10    depleting substance emitted in the 21st century, Science, 326, 123–125, 2009.

Rella, C. W., Chen, H., Andrews, A. E., Filges, A., Gerbig, C., Hatakka, J., Karion, A., Miles, N. L., Richardson, S. J., Steinbacher, M., Sweeney, C., Wastine, B., and Zellweger, C.: High accuracy measurements of dry mole fractions of carbon dioxide and methane in humid air, Atmos. Meas. Tech.,
15    6, 837–860, doi:10.5194/amt-6-837-2013, 2013.

Röckmann, T., and Levin I.: High-precision determination of the changing isotopic composition of atmospheric $N_2O$ from 1990 to 2002, J. Geophys. Res., 110, D21304, doi:10.1029/2005JD006066, 2015.

Rothman, L.S., Jacquemart, D., Barbe, A., Benner, D.C., Birk, M., Brown, L.R., Carleer, M.R., Chackerian Jr, C., Chance, K., Coudert, L.E.A., and Dana, V.: The HITRAN 2004 molecular spectroscopic database, J Quant Spectrosc Radiat Transf., 96, 139–204, doi:10.1016/j.jqsrt.2004.10.008, 2005.

Soto, D.X., Koehler, G., and Hobson, K.A.: Combining denitrifying bacteria and laser spectroscopy for isotopic analyses ($\delta^{15}N$, $\delta^{18}O$) of dissolved nitrate, Anal. Chem., 87, 7000–7005, doi:10.1021/acs.analchem.5b01119, 2015.

Sutka, R. L., Ostrom, N. E., Ostrom, P. H., Breznak, J. A., Gandhi, H., Pitt, A. J., and Li, F.: Distinguishing nitrous oxide production from nitrification and denitrification on the basis of isotopomer abundances, Appl. Environ. Microb., 72, 638–644, doi:10.1128/AEM.72.1.638-644.2006, 2006.

Sutka, R. L., Ostrom, N. E., Ostrom, P. H., Gandhi, H., and Breznak, J. A.: Nitrogen isotopomer site preference of N$_2$O produced by Nitrosomonas europaea and Methylococcus capsulatus bath, Rapid Commun. Mass Sp., 17, 738–745, doi:10.1002/rcm.968, 2003.

10   Tian, H., Chen, G., Lu, C., Xu, X., Ren, W., Zhang, B., Banger, K., Tao, B., Pan, S., Liu, M., Zhang, C., Bruhwiler, L., and Wofsy, S.: Global methane and nitrous oxide emissions from terrestrial ecosystems due to multiple environmental changes, Ecosyst. Health Sustain., 1, 1–20, doi:10.1890/ehs14-0015.1, 2015.

15   Toyoda S., Yoshida N., and Koba K.: Isotopocule analysis of biologically produced nitrous oxide in various environments, Mass Spectrom. Rev., 36, 135–160, doi: 10.1002/mas.21459, 2017.

Toyoda, S. and Yoshida, N.: Determination of nitrogen isotopomers of nitrous oxide on a modified isotope ratio mass spectrometer, Anal. Chem., 71, 4711–4718, doi:10.1021/ac9904563, 1999.

Toyoda, S., Kuroki, N., Yoshida, N., Ishijima, K., Tohjima, Y., and Machida T.: Decadal time series of tropospheric abundance of N$_2$O isotopomers and isotopologues in the Northern Hemisphere obtained by the long-term observation at Hateruma Island, Japan, J. Geophys. Res. Atmos., 118, 3369–3381, doi:10.1002/jgrd.50221, 2013.

Toyoda, S., Mutobe, H., Yamagishi, H., Yoshida, N., and Tanji, Y.: Fractionation of N$_2$O isotopomers during production by denitrifier, Soil Biol. Biochem., 37, 1535–1545, doi:10.1016/j.soilbio.2005.01.009, 2005.

Toyoda, S., Yano, M., Nishimura, S., Akiyama, H., Hayakawa, A., Koba, K., Sudo, S., Yagi, K., Makabe, A., Tobari, Y., Ogawa, N. O., Ohkouchi, N., Yamada, K., and Yoshida, N.: Characterization and production and consumption processes of $N_2O$ emitted from temperate agricultural soils determined via isotopomer ratio analysis, Glob. Biogeochem. Cy., 25, GB2008, doi: 10.1029/2009GB003769, 2011.

Verhoeven, E., Barthel, M., Yu, L., Celi, L., Said-Pullicino, D., Sleutel, S., Lewicka-Szczebak, D., Six, J., and Decock, C.: Early season $N_2O$ emissions under variable water management in rice systems: source-partitioning emissions using isotope ratios along a depth profile, Biogeosci., 16, 383–408, doi:10.5194/bg-16-383-2019, 2019.

Verhoeven, E., Decock, C., Barthel, M., Bertora, C., Sacco, D., Romani, M., Sleutel, S., and Six, J.: Nitrification and coupled nitrification-denitrification at shallow depths are responsible for early season $N_2O$ emissions under alternate wetting and drying management in an Italian rice paddy system, Soil Biol. Biochem., 120, 58–69, doi:10.1016/j.soilbio.2018.01.032, 2018.

Vogel, F. R., Huang, L., Ernst, D., Giroux, L., Racki, S., and Worthy, D. E. J.: Evaluation of a cavity ring-down spectrometer for in situ observations of $^{13}CO_2$, Atmos. Meas. Tech., 6, 301–308, doi:10.5194/amt-6-301-2013, 2013.

Wächter, H., Mohn, J., Tuzson, B., Emmenegger, L., and Sigrist, M.W.: Determination of $N_2O$ isotopomers with quantum cascade laser based absorption spectroscopy, Optics express, 16, 9239–9244, doi:10.1364/OE.16.009239, 2008.

Wassenaar, L.I., Douence, C., Altabet, M.A., and Aggarwal, P.K.: N and O isotope ($\delta^{15}N^{\alpha}$, $\delta15N^{\beta}$, $\delta^{18}O$, $\delta^{17}O$) analyses of dissolved $NO_3^-$ and $NO_2^-$ by the Cd-azide reduction method and $N_2O$ laser spectrometry, Rapid Commun. Mass Spectr., 32, 184–194, doi:10.1002/rcm.8029, 2018.

Wei J., Zhou M., Vereecken H., and Brüggemann N.: Large variability in $CO_2$ and $N_2O$ emissions and in $^{15}N$ site preference of $N_2O$ from reactions of nitrite with lignin and its derivatives at different pH. Rapid Commun. Mass Sp., 31, 1333–1343, doi:10.1002/rcm.7912, 2017.

Well, R., Eschenbach, W., Flessa, H., von der Heide, C., and Weymann, D.: Are dual isotope and isotopomer ratios of $N_2O$ useful indicators for $N_2O$ turnover during denitrification in nitrate-contaminated aquifers? Geochim. Cosmochim. Acta 90, 265–282, doi:10.1016/j.gca.2012.04.045, 2012.

10  Well, R. and Flessa, H.: Isotopologue signatures of $N_2O$ produced by denitrification in soils, J. Geophys. Res., 114, G02020, doi:10.1029/2008JG000804, 2009.

Well, R., Flessa, H., Jaradat, F., Toyoda, S., and Yoshida, N.: Measurement of isotopomer signatures of $N_2O$ in groundwater, J. Geophys. Res. 110, G02006, doi:10.1029/2005JG000044, 2005.

Well, R., Flessa, H., Xing, L., Xiaotang, J., and Römheld, V.: Isotopologue ratios of $N_2O$ emitted from microcosms with $NH_4^+$ fertilized arable soils under conditions favoring nitrification, Soil Biol. Biochem., 40, 2416–2426, doi:10.1016/j.soilbio.2008.06.003, 2008.

20  Wen, X.-F., Meng, Y., Zhang, X.-Y., Sun, X.-M., and Lee, X.: Evaluating calibration strategies for isotope ratio infrared spectroscopy for atmospheric $^{13}CO_2/^{12}CO_2$ measurement, Atmos. Meas. Tech., 6, 1491–1501, doi:10.5194/amt-6-1491-2013, 2013.

Werle, P.O., Mücke, R., and Slemr, F.: The limits of signal averaging in atmospheric trace-gas
25  monitoring by tunable diode-laser absorption spectroscopy (TDLAS), Applied Physics B, 57, 131–139, doi:10.1007/BF00425997, 1993.

Werner, R. A. and Brand, W. A.: Referencing strategies and techniques in stable isotope ratio analysis, Rapid Commun. Mass Spectrom., 15, 501–519, doi:10.1002/rcm.258, 2001.

Winther, M., Balslev-Harder, D., Christensen, S., Priemé, A., Elberling, B., Crosson, E., & Blunier, T.: Continuous measurements of nitrous oxide isotopomers during incubation experiments, Biogeosciences, 15, 767-780, doi:10.5194/bg-15-767-2018, 2018.

Wolf, B., Merbold, L., Decock, C., Tuzson, B., Harris, E., Six, J., Emmenegger L., and Mohn J.: First on-line isotopic characterization of $N_2O$ above intensively managed grassland, Biogeosciences, 12, 2517–2531, doi: 10.5194/bg-12-2517-2015, 2015.

Wunderlin, P., Lehmann, M. F., Siegrist, H., Tuzson, B., Joss, A., Emmenegger, L., and Mohn, J.: Isotope signatures of $N_2O$ in a mixed microbial population system: constraints on $N_2O$ producing pathways in wastewater treatment, Environ. Sci. Technol., 47, 1339–1348, doi: 10.1021/es303174x, 2013.

Wunderlin, P., Mohn, J., Joss, A., Emmenegger, L., and Siegrist, H.: Mechanisms of $N_2O$ production in biological wastewater treatment under nitrifying and denitrifying conditions, Water Res., 46, 1027–37, doi: 10.1016/j.watres.2011.11.080, 2012.

Yamamoto, A., Uchida, Y., Akiyama, H., and Nakajima, Y.: Continuous and unattended measurements of the site preference of nitrous oxide emitted from an agricultural soil using quantum cascade laser spectrometry with intercomparison with isotope ratio mass spectrometry, Rapid Commun. Mass Spectr., 28, 1444 –1452, doi:10.1002/rcm.6916, 2014.

Yoshida, N. and Toyoda, S.: Constraining the atmospheric $N_2O$ budget from intramolecular site preference in $N_2O$ isotopomers, Nature, 405, 330–334, doi:10.1038/35012558, 2000.

Yue, F.J., Li, S.L., Liu, C.Q., Mostofa, K.M., Yoshida, N., Toyoda, S., Wang, S.L., Hattori, S., and Liu, X.L.: Spatial variation of nitrogen cycling in a subtropical stratified impoundment in southwest China, elucidated by nitrous oxide isotopomer and nitrate isotopes, Inland Waters, 8, 186–195, doi: 10.1080/20442041.2018.1457847, 2018.